Increase in Liposome Production: From Microfluidics to Milli-fluidics

Elie Nasr

A Thesis

in

The Department

of

Mechanical, Industrial and Aerospace Engineering (MIAE)

Presented in Partial Fulfillment of the Requirements

for the Degree of Master of Applied Sciences (Mechanical Engineering) at

Concordia University

Montreal, Quebec, Canada

August 2024

CONCORDIA UNIVERSITY
School of Graduate Studies

This is to certify that the thesis prepared

By: Elie Nasr

Entitled: Increase in Liposome Production: From Microfluidics to Milli-fluidics

and submitted in partial fulfillment of the requirements for the degree of

Master of Applied Sciences (Mechanical Engineering)

complies with the regulations of the University and meets the accepted standards with respect to originality and quality.

Signed by the final examining committee:

_____ Chair
Dr. Muthukumaran Packirisamy

_____ Examiner
Dr. Maria Elektorowicz

_____ Examiner
Dr. Mingyuan Chen

_____ Thesis Supervisor(s)
Dr. Ion Stiharu

_____ Thesis Supervisor(s)
Dr. Vahé Nerguizian

Approved by _____
Chair of Department or Graduate Program Director

August 8th 2024 Dean of Faculty

ABSTRACT

Increase in Liposome Production: From Microfluidics to Milli-fluidics

Elie Nasr

Liposomes are tiny vesicles of lipid layers enclosing medication for drug delivery, mostly used in cancer treatment, gene therapy and mRNA vaccines. One of the production technologies implies the use of microfluidic mixers, which produce liposomes at a very low yield. Previous research proved the viability of liposome production but at a very low yield. Based on the successful results of the liposome production at micro-scale, the assumption that scaling up the channel size may lead to an increased production of similar-sized liposomes. To begin evaluating its feasibility, simulations of the mixing of two fluids within scaled up channels were carried out. The objective of the simulations are to evaluate the mixing potential prior to experimental trials. Same linear velocity values and mixing ratio were considered in simulations. However, from the mathematical model, the resulting size of the liposomes cannot be predicted. It may be possible that along with larger channels, larger liposomes might be produced. The same fluid properties will be used during the mixing of a solution containing lipids and alcohol with water, which will result in liposomes formation in both micro and milli channels. The hypothesis behind this experiment states that the size of the liposome depends on the speed of mixing, which is bounded by fluid flow properties, such as velocity, pressure and concentration, that will need to remain similar in values in the enlarged microfluidic device. During simulation, similar mixing results were obtained as the base research, which indicate good mixing efficiency when scaling up the cross-section area by 10 and 25 times.. It seems that it may be possible to increase production of liposomes through larger

devices if the pressure inside the channels is increased due to higher flow rate, which is also scaled by a factor corresponding to the dimension increase. A larger production rate could be a game changer in the pharma industry. Preliminary experiments yield liposomes of increased size - by 20 to 50% in diameter at a significant increase in productivity.

Acknowledgments

I would like to first thank my thesis supervisors Prof. Ion Stiharu and Prof. Vahe Nerguizian (ETS) for their great guidance in a domain which was new to me. It was a real pleasure working with such knowledgeable mentors.

I am also grateful for the work of my peers at Concordia University. Thank you to the following students for their contribution in the experimental work: Jesse Bisbee, Darius Csiky, Connor Lynch-Staunton, Ahmad Ajmal Sharifi, Nicholaos Stounos and Luis Mariano Trujillo Galarza.

From ÉTS, I would like to thank Fatemeh Behrouz for her continuous support throughout the entire project.

Finally, I would like to thank Famic Technologies for their financial support.

Table of Contents

List of Figures

List of Tables

List of Abbreviations

CFD	Computational Fluid Dynamics
DLS	Dynamic Light Scattering
FRR	Flow Rate Ratio
ILV	Intraluminal Vesicles
LUV	Large Unilamellar Vesicles
mRNA	Messenger RNA
MLV	Multilamellar Vesicles
MVV	Multivesicular Vesicles
PDMS	Polydimethylsiloxane
siRNA	Small Interfering RNA
SLA	Stereolithography
SUV	Small Unilamellar Vesicles
TFR	Total Flow Rate

List of Symbols

μ	Dynamic viscosity
A	Area
D	Diffusion coefficient
De	Dean number
D_H	Hydraulic diameter
j	Diffusion flux
k	Boltzmann constant
p	Pressure
Q	Total flow rate
Re	Reynolds number
T	Temperature
u	Flow velocity
η	Viscosity
ν	Kinematic viscosity
ρ	Fluid density
σ	Standard deviation
x	Scaling factor

INTRODUCTION

Delivering goods from producers to consumers is a process that is continuously being optimized. Increasing efficiency means recognizing the importance of packaging at a higher rate before reaching the targeted recipient through an organized transportation network. The same principle applies to delivering drugs within the human body, which is the main purpose behind the production of liposomes (Samad, Sultana, & Aqil, 2007). To reach the same standards as the packaging industry, there must be rapid and consistent production of liposomes at nominal sizes, which are two important limitations in its microfabrication. In microfluidic liposome production, a compromise is made between these two (2) showstoppers to produce these tiny spherical vesicles composed of phospholipid molecules.

It was not before the 1980s that liposomes began to be explored in drug delivery. At this point, researchers had discovered that they could transport the required medicine at the designated location by controlling its size, whether the final destination was a tissue or a cell. Since then, various medical conditions were aimed to be treated with liposome-based therapies. Today, innovative methods are continuously being explored to increase overall productivity.

Controlling the size of liposomes depends on the speed of mixing when injecting the solvent, in this case ethanol, to the lipid solution. When studying the increase in production rate, it is important to match the size of the liposome with the design requirements. To increase the rate of production, the surface area of the microchannels' cross-section will be increased. This will cause a slower velocity in the inlet channels containing the concentrated mixture or water and will directly influence (increase) the liposome size. A solution would be to increase the flow rate and pressure within the microfluidic devices while also maintaining the lipid concentration when scaling to a larger channel. Theoretically, the liposome diameter will be maintained by controlling the mixing

speed. However, upscaling to millifluidics from microfluidics usually entails less precision due to more variability in liposome sizes and encapsulation efficiency (Yanar, Mosayyebi, Nastruzzi, Carugo, & Zhang, 2020).

0.1 Rationale

Medical practices evolved over time to continuously provide safer and more effective treatments of a wide range of health conditions. With new clinical trials of different treatments being tested and delivered to patients worldwide, side effects were always an ethical and legal concern for pharmaceutical companies. From early vaccine adoption to surgical procedures, one's body may react differently when exposed to certain substances. An advantage of using drug delivery using liposomes is the risk reduction in side effect developments associated with certain medications

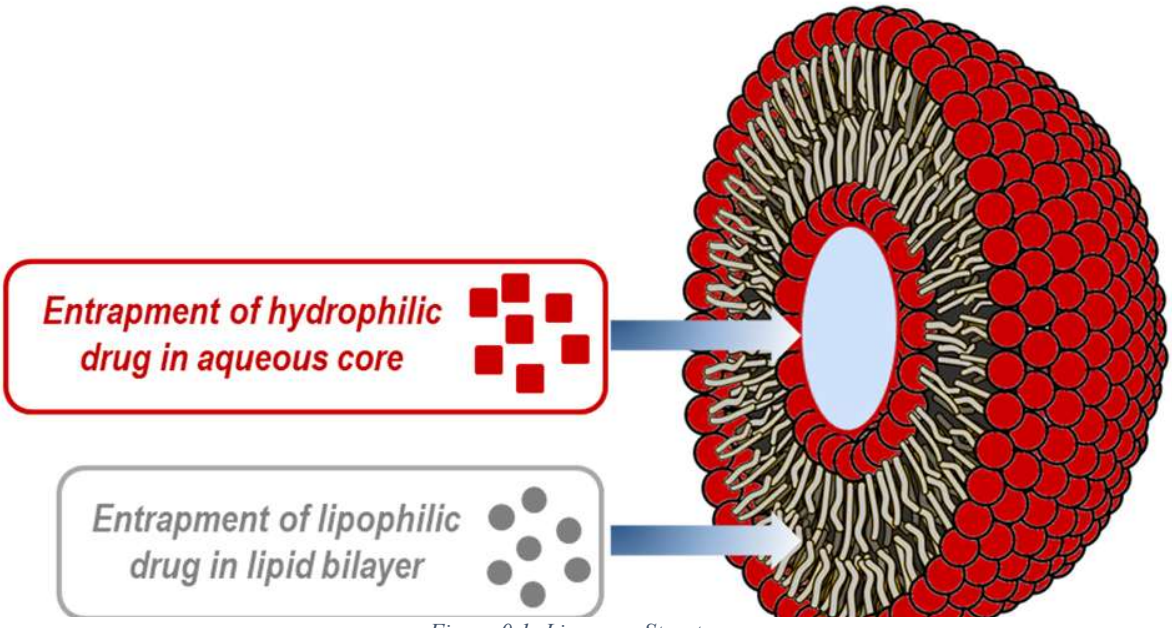

Figure 0.1: Liposome Structure

Taken from Anton Paar GmbH (2024)

which would be only locally delivered. Liposomes are retained by specific organs according to their size (Isanin, Rozenberg, Shcherbakov, & Kh, 1984). Hence, medication embedded in liposomes may be specifically delivered to the organ in need. Often, uncertain treatment is offered

to patients suffering from challenging medical issues, such as cancer, gene related diseases, cardiovascular diseases, neurological disorders, and so on. With the correct size, targeted drug delivery through liposomes is possible while reducing exposure to non-targeted tissues and cells, directly minimizing off-target side effects. In contrast, chemotherapy is widely used in cancer treatment but does not only target problematic cells and also kills healthy tissues in an attempt in targeting tumors (Weeks JC, 2012). Encapsulating drugs in liposomes may, in some cases, reduce toxicity, which plays a vital role in the prevention of targeting healthy tissues, since the liposome membrane acts as a barrier. It is important to note that side effects are not eliminated completely but are potentially reduced in drug delivery using liposomes.

On top of the great risk reduction, drug delivery treatments using liposomes could revolutionize drug management in the pharmaceutical industry, given that the main production restrictions are resolved (Sanket, Dhawan, Holm, & Perrie, 2020). The global liposome drug delivery market value is expected to grow significantly during this decade if the current growth trend maintains itself, according to Data Bridge Market Research.

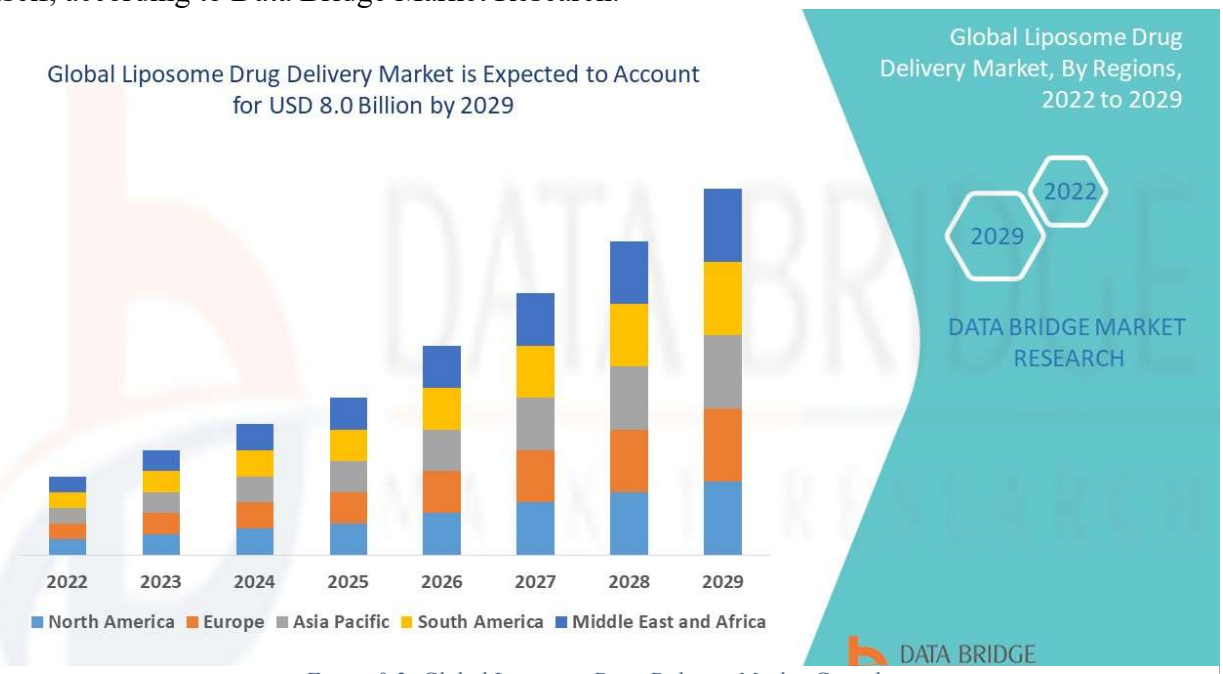

Figure 0.2: Global Liposome Drug Delivery Market Growth

This expectation in growth may directly be due to the applications associated with the production of liposomes. These vesicles serve a great purpose in medical treatments, the most common being tumor targeted therapy. In 2022, the global market size of cancer therapeutics alone was valued at USD $164 billion. Without considering other liposome applications, it is safe to say that the market size for liposome drug delivery will grow with the coming years (Bohr, Colombo, & Jensen, 2018).

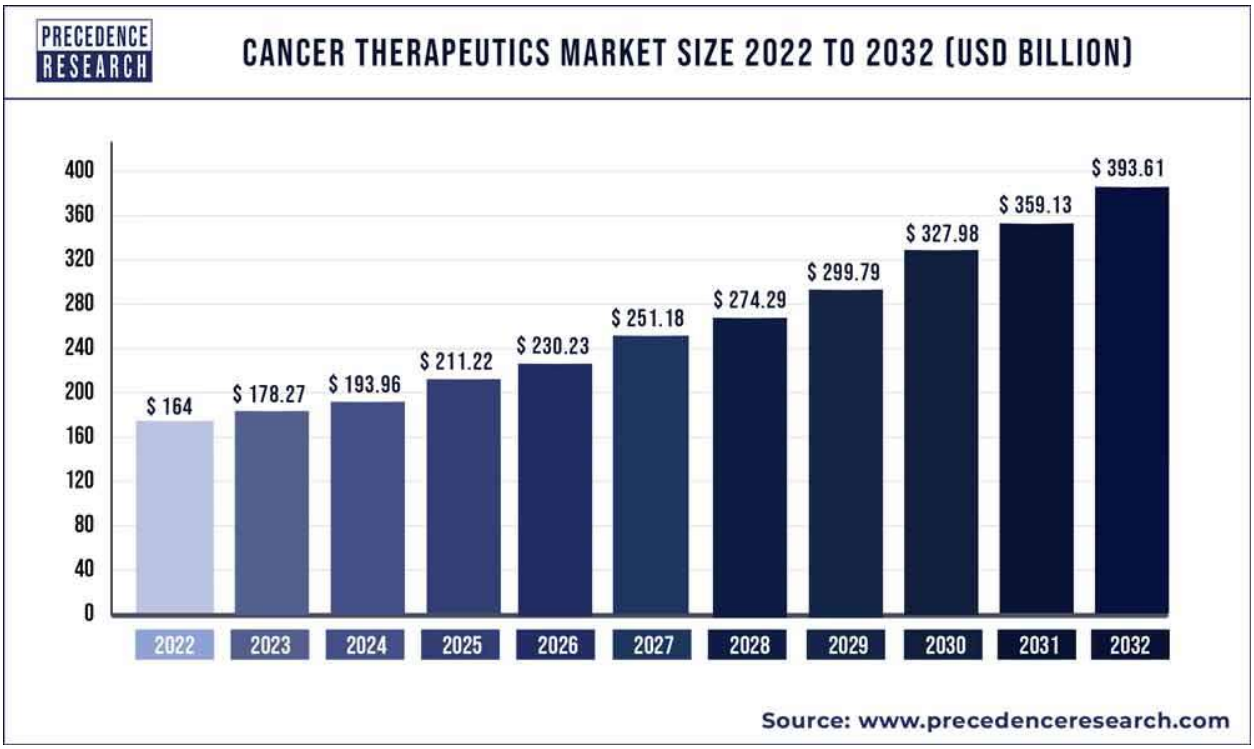

Figure 0.3: Global Cancer Therapeutics Market Size Growth

As research funds towards cancer treatment continue to grow, the development of new techniques in the field of microfluidics will follow the curve in an attempt to improve the efficiency of drug delivery but also reduce its costs related to microfabrication, production of liposomes and time consumed in production of liposomes.

One of the main research topics in the production of liposomes revolves around finding optimal ways to increase the output efficiently. Microfluidics allow reliable and stable production of

liposomes, but the process remains slow and the output insufficient for market demands. To increase the production output, there are a few different methods such as parallelization which can be achieved by using microfluidic arrays or high-throughput microfluidics.

As shown in Figure 0.4, an application of parallelization demonstrates how water and the solute solution are inserted into the microfluidic devices assembled in parallel for higher throughput. Parallelization increases production capacity by stacking multiple mixing channels in parallel, allowing more output. Another method is to increase the size of the microfluidic device to use milli-fluidic devices. By scaling up the device dimensions, a higher volume is allowed into the

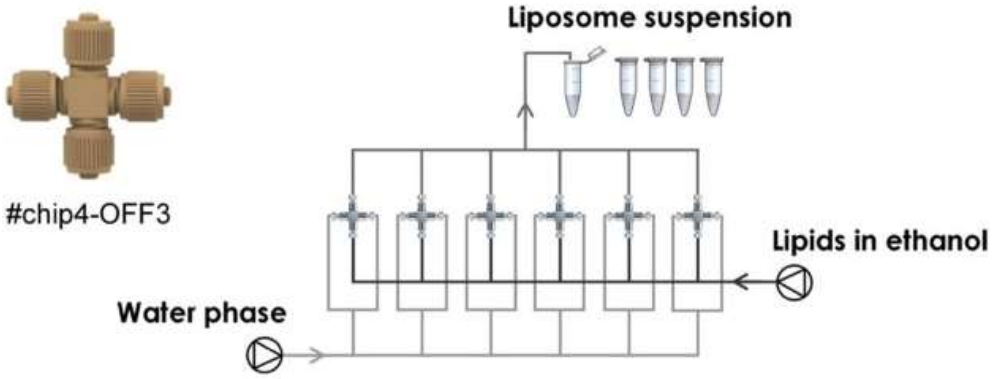

Figure 0.4: Parallelization Example in Microfluidics

Source: (Carugo, Bottaro, Owen, Stride, & Nastruzzi, 2016)

inlets and the mixing channel, therefore producing more liposomes (Michelon, Bernardes Oliveira, de Figueiredo Furtado, Gaziola de la Torre, & Lopes Cunha, 2017).

0.2 Problem Statement

Liposomes can be artificially prepared in the laboratory and are used in various fields of science and medicine for a variety of purposes, including drug delivery systems, gene therapy, and mRNA vaccines. Liposomes are advantageous in drug delivery because they can encapsulate drugs or

other substances within their aqueous core or lipid bilayers, allowing for targeted delivery and controlled release of the enclosed substance (Samad, Sultana, & Aqil, 2007).

The ability to modify the size, composition, and surface properties of liposomes makes them a versatile tool for researchers and a valuable technology in pharmaceutical and medical applications. Liposomes can encapsulate a variety of drugs while targeting specific cells or tissues, which is ideal for drug delivery. However, liposomes have a finite capacity and cannot deliver high doses of certain drugs, especially with the added difficulty of efficiently encapsulating the medication inside the liposome. At the same time, issues related to health can arise if the administered drugs are not quickly eliminated from the bloodstream by the body's immune system. On the flip side, there are also problematics related to production since the inability of filtering out toxins released during the process can damage the filters (Gregoriadis, 1995).

To benefit from a larger share of the market value of liposome drug delivery, it is imperative to increase production rates without compromising its size, while also taking in consideration health issues and production limitations. To solve this known conundrum, some factors must be taken into consideration. For microfluidic liposome production, a higher flow rate must be accommodated to generate higher production. Microfluidic devices must evolve and be replaced by devices with channels wide enough to allow more fluid. However, widening the microchannels might also result in increasing liposome size. This inconvenience can be limited by increasing the flow rate and maintaining a similar lipid concentration. The mixing of lipids with water must be done quickly and efficiently to achieve a production of smaller liposomes but in higher quantity. A relation exists for the size of liposomes with multiple factors such as TFR, FRR and lipid concentration, but their effects may be different when applied in milli-fluidics (Ruben Salazar, 2020).

The size of liposomes depends on its intended target during drug delivery. For that reason, it is important to factor in all variables that may impact this change. The ultimate objective would be to properly mix the necessary fluids in the right proportion in the production of liposomes in larger fluidic circuits. This would reduce costs enormously and increase production rate of medication.

0.3 Research Objectives

The importance of liposome production in the medical industry weighs enough to research new methods that would overcome the current limitations, which prevent its quicker adoption in the market. Small channels, such as the ones fabricated for microfluidic devices, can only host a low volumetric fluid flow rate, which drastically limits the production rate of liposomes. This problematic should hopefully be solved during this experiment by increasing the dimensions of the devices while maintaining similar vesicle sizes as the original microfluidic device tested in previous work. By increasing the channel size, the vesicle size might in consequence increase . However, the current hypothesis suggests otherwise.

0.4 Hypothesis

To avoid increasing the vesicle size when increasing the channel width, fluid characteristics should match the ones evaluated in the reference device. Therefore, it is believed that the diameter sizes of the liposomes measured from a milli-fluidic device should be the same as the output from a microfluidic device, given that the linear velocity inside the channels due to a proportional increase in TFR is the same while also keeping the concentration of diluted species constant.

0.5 Thesis Organization

The thesis includes 5 chapters and the supporting material of the present work. The content of the chapter is provided below.

Chapter 1 reviews literature and introduces the features of the liposomes. The different types of liposome structures are detailed, as well as the methods of production and their main application. The equipment required to produce liposomes are briefly described and their limitations.

Chapter 2 provides an in-depth description of the microfluidic device design by going over the different types of mixers, the behavior of fluid flow inside the channels, the methods of fabrication of such devices and the various forms they can take in terms of materials. The design process in COMSOL Multiphysics software is documented to create the physical model before reaching the numerical simulation modeling.

Chapter 3 presents the importance of numerical simulation and how the results are obtained. A comparison of the acquired data with the reference data is made and all simulation results are detailed.

Chapter 4 describes all experiments realized in the laboratory. The details include the fabrication of the device, setting up the test bench, measuring data and analyzing all observations.

Chapter 5 presents the conclusions of the works and suggests future directions of research in this field.

CHAPTER 1: LITERATURE REVIEW

1.1 Introduction

The history of liposomes dates back to the 1960s when British hematologist Alec D. Bangham discovered them while studying phospholipids. Liposomes are spherical vesicles with a lipid bilayer, initially observed as models for biological membranes. Their potential for drug delivery was recognized early on, leading to extensive research into their fabrication and applications. Fabrication methods evolved from simple hydration techniques to advanced methods like reverse-phase evaporation, ethanol injection, and microfluidics, enabling precise control over liposome size, charge, and drug encapsulation efficiency. In the 1970s and 1980s, liposomal research expanded, driven by the need for effective drug delivery systems that could enhance the therapeutic index of drugs, reduce toxicity, and improve pharmacokinetics. The first FDA-approved liposomal drug, Doxil, which stands for doxorubicin encapsulated in liposomes, marked a significant milestone in the 1990s, proving the clinical potential of liposomes. Today, liposomes are used in a wide range of applications, including targeted drug delivery, gene therapy, and vaccine delivery, as they can encapsulate both hydrophilic and hydrophobic drugs, protect them from degradation, and facilitate controlled release. They are also employed in cosmetics for improved skin delivery of active ingredients. The evolution of liposomes has been marked by continuous advancements in fabrication technologies and a growing understanding of their interactions with biological systems, paving the way for increasingly sophisticated and effective therapeutic applications (Lasic D. , 1996).

Liposomes have emerged as versatile carriers for drug delivery, offering significant promise in the pharmaceutical field due to their ability to encapsulate diverse therapeutic agents and deliver them to targeted sites within the body. These lipid-based vesicles possess a unique structural

characteristic, consisting of one or more concentric lipid bilayers enclosing an aqueous core, which makes them well-suited for encapsulating both hydrophobic and hydrophilic drugs. The versatile nature of liposomes has led to their widespread exploration in various biomedical applications, ranging from cancer therapy to drug delivery (Lasic, 1992).

Despite the remarkable potential of liposomes, their widespread clinical translation has been hindered by several challenges, one of them being the issue of low yield production. The production process for liposomes in microfluidic devices, which involves hydration of lipid films, is inherently time-consuming and labor-intensive. This limitation poses a significant bottleneck in the scalability and commercial viability of liposomal formulations, impeding their widespread adoption in clinical settings.

A comprehensive review of the existing literature reveals various strategies that have been explored to address the challenge of slow liposome production. These strategies encompass modifications to the lipid composition, optimization of manufacturing processes, and the development of novel production techniques aimed at enhancing the efficiency and throughput of liposome production. Additionally, advancements in microfluidic technology offer promising avenues for overcoming the limitations associated with traditional bulk production methods, enabling precise control over liposome size and uniformity while significantly reducing production timescales.

1.2 Liposome Structure

Liposomes can have different structural characteristics, depending on the application design factors such as the encapsulated volume, the desired amount of drug released, targeted delivery requirements and the nature of the encapsulated substance. The liposome structures can be divided

into four (4) categories: unilamellar (SUV), large unilamellar (LUV), multilamellar (MLV) and multivesicular vesicles (MVV) (Nsairat, et al., 2022).

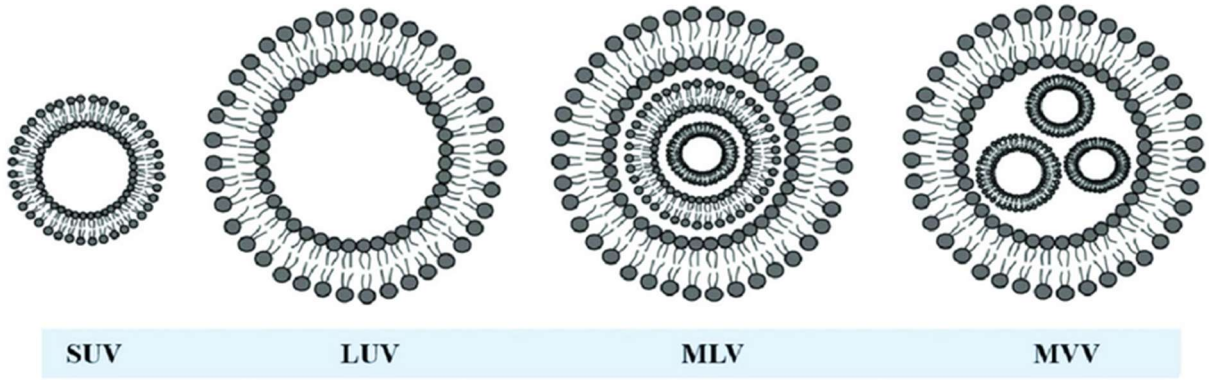

Figure 1.1: Difference between SUV, LUV, MLV and MVV Structures

Taken from Huang, L. & al. (2022)

1.2.1 Unilamellar Vesicles

Unilamellar vesicles consist of a single lipid bilayer surrounding an aqueous core. They are often used for drug delivery of hydrophobic and hydrophilic compounds. The simple structure allows the encapsulation of small molecules and can be designed for specific targeting of cells and tissues within the body. These vesicles can even be modified for the purpose of surface functionalization by coating the outer layer with biomolecules or polymers to achieve better results during drug delivery in terms of specific targeting of cells and tissues, stability and circulation time of liposomes in the bloodstream, drug release control, imaging and diagnostics, all while avoiding undesired interactions with other biological components (Moscho, Chiu, & Zare, 1996).

1.2.2 Large Unilamellar Vesicles

LUVs are required for drug delivery and research applications where larger vesicles are needed. In principle, they are similar to SUVs but are larger in size, allowing a higher volume of drug encapsulation. This means increased drug-carrying capacity compared to smaller vesicles. With a

larger liposome diameter, more disadvantages are observed as there is a reduction in efficiency regarding specific cell and tissue targeting while also limiting penetration. The reticuloendothelial system (RES) may reduce the circulation time of liposomes in the bloodstream by eliminating them in a faster manner. Also, it is more difficult to control the drug release kinetics. In the production aspect, issues may arise in stability since size distribution becomes more complex with larger vesicles as the encapsulation efficiency drops for certain substances, straying further from the objective of achieving uniformity (Moscho, Chiu, & Zare, 1996).

1.2.3 Multilamellar Vesicles

From Figure 1.1, it can be seen that MLVs differ in structure from the unilamellar vesicles due to the multiple lipid bilayers surrounding the aqueous core. This characteristic increases the available encapsulation space, providing a larger dosage when needed. In this case, the drug to be administered and carried inside the vesicle is released at a slower rate due to the multilayer structure (Bergenholtz & Wagner, 1996).

1.2.4 Multivesicular Vesicles

MVVs are specialized cellular structures, particularly found within endosomes and lysosomes, containing multiple smaller vesicles called ILVs. These ILVs, formed by the inward budding of the endosomal membrane, play crucial roles in cellular processes. MVVs are central to cellular communication, notably through the production of exosomes that mediate intercellular communication by transferring proteins, lipids, and nucleic acids between cells, influencing signal transduction pathways in recipient cells. They are also vital for waste disposal, aiding in the degradation and recycling of cellular components by delivering them to lysosomes for breakdown, and in removing damaged proteins and organelles to maintain cellular homeostasis. In medicine, MVVs are explored for drug delivery systems due to their natural ability to transport bioactive

molecules, and for targeted delivery by loading therapeutic agents for specific cells or tissues. Additionally, exosomes derived from MVVs are studied as biomarkers for various diseases, including cancer and neurodegenerative diseases, due to their specific molecular signatures. Typically, multivesicular bodies (MVBs) range from 100 to 1000 nanometers in diameter, while ILVs range from 30 to 100 nanometers (Betterelli Giuliano, Cvjetan, Ayache, & Walde, 2020).

1.3 Liposome Production

Similar to liposome structures, different production methods exist and are exploited based on the application design when considering size distribution, encapsulation efficiency, scalability and drug release kinetics. Each production method has its advantages and limitations. For example, extrusion is a common method to produce liposomes, which consists of extruding lipid mixtures through smalls pores, allowing good vesicle size control and polydispersity. However, this process requires specialized equipment which naturally increases production costs. Other methods may involve external excitation like the sonication method, which involves the application of high-frequency sound waves on lipid mixtures to form liposomes. This is one of the simpler production methods but only a small output can be realized while also generating heat and compromising size distribution (Patil & Jadhav, 2014).

Liposome production methods are suitable for certain design requirements, such as size control, scalability, encapsulation efficiency, and most importantly, reproducibility. Other factors may also come into play. No method is perfect, so compromising some factors becomes necessary to obtain the desired results. For instance, microfluidic liposome production allows precise control over fluid flow rates and mixing which enables better size distribution while ensuring high reproducibility. Microfluidic devices allow rapid mixing in a short distance while maintaining high encapsulating efficiency, resulting in satisfying liposome production. It is important to note that

microfluidic production can easily be scaled up, but some challenges may arise in terms of keeping the desired vesicle size and adapting the equipment to the changes in fluid dynamics (Lombardo & Kiselev, 2022).

1.3.1 Designing Microfluidic Devices

Microfluidic devices for liposome production should be designed with careful consideration of several key factors to achieve optimal performance and functionality. Firstly, the device geometry and layout must be tailored to accommodate the specific requirements of liposome formation processes, including lipid mixing, hydration, and encapsulation. This may involve designing microchannels, chambers, and mixing structures that facilitate efficient lipid bilayer formation and encapsulation of therapeutic agents. Secondly, material selection is crucial to ensure compatibility with lipids and biological components, as well as to minimize potential interference with liposome production processes. Biocompatible materials such as polydimethylsiloxane (PDMS), glass, or polymethyl methacrylate (PMMA) are commonly used for microfluidic device fabrication to prevent leaching or contamination of liposomal formulations. Based on the choice of material, a suitable fabrication process should be determined (Losey, Jackman, Firebaugh, Schmidt, & Jensen, 2002).

1.3.2 Manufacturing Microfluid Devices

Precision and specialized equipment are required to manufacture microfluidic devices. After coming up with an initial design, it is important to achieve the desired result for the purpose of reenacting theoretical simulation in an experiment. Different methods of manufacturing can be employed, ranging from glass etching, micromanufacturing or 3D printing. Since the micromanufacturing of a microfluidic device is a bottom-up process, a material must first be chosen for the substrate. In this case, PDMS will be used since it is transparent and easy to

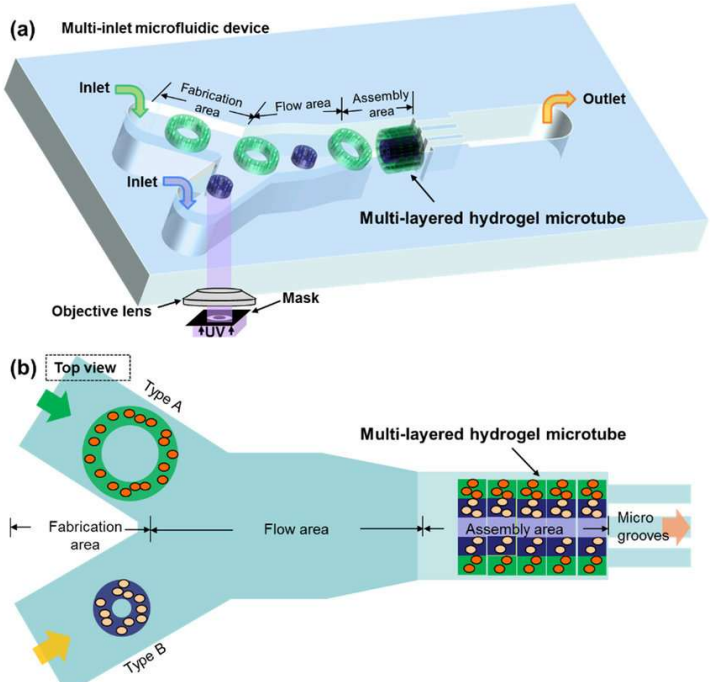

Figure 1.1.1: Photolithography on Microfluidic Device

Source: Tao Yue & al. (2019)

manipulate. This material will be used to form the microchannels of the device. Once the substrate is ready, a thin film, also referred to as a mask, is applied on the surface as part of the process of photolithography. This mask is used to block UV light and allows the removal of exposed material. This fabrication technique requires expensive equipment and can be quite complex. However, photolithography can achieve micron resolution even in large batches as this process is highly scalable. Alternatively, other fabrication techniques, such as etching or soft lithography, can be applied depending on the design. The device used to achieve this experiment was fabricated in a more cost-efficient way as dimensions were scaled up to test our theory. Microchannels were created on the substrate directly using micromachining. Half of the microchannel was done on one substrate and the other half on another, which were then merged to create the test channels. Evidently, surface treatment was required for this experiment to make sure that the test device was properly sealed but also to improve the inlets and mixing channel. Making sure that surfaces are

hydrophilic will lower the Reynold's number and promote a more laminar flow. It also prevents the formation of bubbles inside the channels while also improving biocompatibility (Losey, Jackman, Firebaugh, Schmidt, & Jensen, 2002).

1.4 Liposome Applications

Drug delivery remains the most popular application of liposomes. Its production is most commonly investigated to be applied in medical treatments, such as cancer treatment, antibiotic delivery, and even gene therapy. However, they are also useful for vaccine delivery, cosmetics, diagnostic imaging, nutrient delivery, etc. Their versatility is due to the capacity of encapsulating different compounds and targeting specific regions of the human cells and tissues (Barenholz, 2001).

1.4.1 Drug Delivery

Liposomes have garnered significant attention in the realm of drug delivery due to their unique structure and properties. Their ability to encapsulate both hydrophobic and hydrophilic drugs within their aqueous core or lipid bilayers makes them versatile carriers for a wide range of therapeutic agents. In drug delivery applications, liposomes serve as vehicles to transport drugs to specific target sites within the body, thereby enhancing their therapeutic efficacy while minimizing off-target effects and systemic toxicity. One of the key advantages of liposomal drug delivery is the ability to modify their surface properties, allowing for targeted delivery to particular tissues or cells through surface functionalization with ligands or antibodies that recognize specific receptors or antigens (Sharma & Sharma, 1997). This targeted approach enhances drug accumulation at the desired site, improving therapeutic outcomes and reducing adverse effects. Furthermore, liposomes can protect encapsulated drugs from degradation and clearance mechanisms in the body, prolonging their circulation time and enhancing their bioavailability. This property is particularly

advantageous for drugs with poor solubility or stability, enabling their efficient delivery to the intended site of action (Anwekar, Patel, & Singhai, 2011).

In addition to cancer and genetic disorders, liposomal drug delivery holds promise for the treatment of inflammatory diseases, such as rheumatoid arthritis and inflammatory bowel disease, by delivering anti-inflammatory agents to affected tissues.

1.4.2 Cancer Treatment

Liposomes are becoming integral in cancer treatment due to their unique ability to deliver therapeutic agents specifically to tumor sites while minimizing systemic toxicity. Chemotherapeutic drugs encapsulated within liposomes, such as doxorubicin and paclitaxel, benefit from enhanced accumulation in tumors through the enhanced permeability and retention (EPR) effect. This targeted delivery mechanism improves drug efficacy by increasing drug concentration at the tumor site, while reducing off-target effects on healthy tissues.

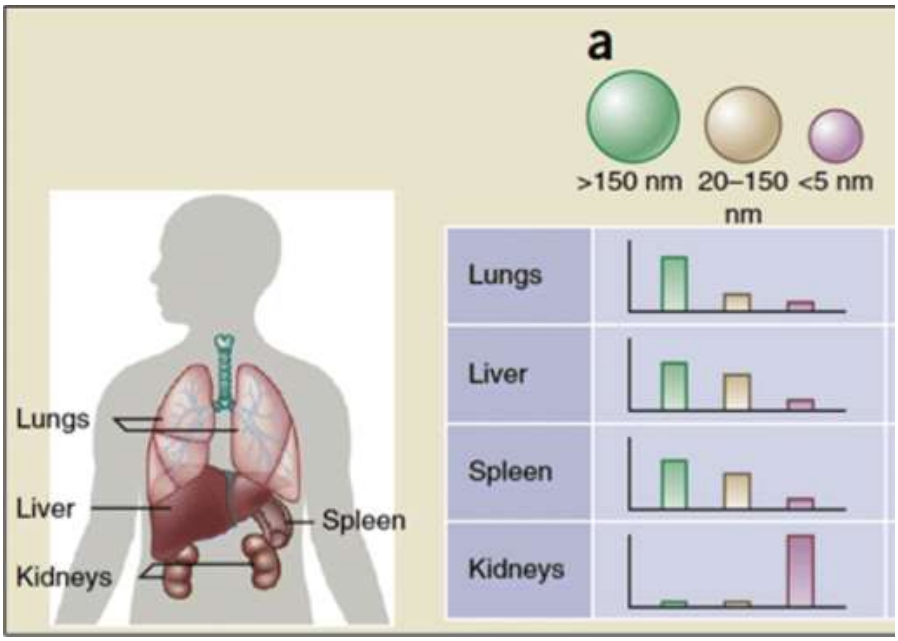

Figure 1.2: Targeted Organ based on Liposome Size

Source: (Rawal, Singh, & Amiji, 2019)

Figure 1.3 effectively shows the targeted organs based on the liposome sizes. Controlling liposome size is crucial during production when designing for drug delivery. In cancer research, targeting specific organs becomes a vital part of treating cancerous cells located in a specific area in the body.

The advantages of using liposomes in cancer treatment are manifold. Firstly, liposomal formulations protect encapsulated drugs from premature degradation and clearance in the bloodstream, prolonging their circulation time and enhancing bioavailability. Secondly, liposomes can be modified to display ligands or antibodies on their surface, facilitating targeted delivery to cancer cells expressing specific receptors or antigens. This targeted approach further enhances drug accumulation at tumor sites while minimizing exposure to healthy tissues. Additionally, liposomal formulations offer the potential to overcome drug resistance mechanisms commonly observed in cancer treatment, thereby improving treatment outcomes. Various types of cancer are treated using liposomal formulations, including breast cancer, ovarian cancer, lung cancer, and leukemia, among others (Pandey, Rani, & Agarwal , 2016).

1.4.3 Gene Therapy

Liposomes are increasingly utilized in gene therapy for their ability to efficiently deliver nucleic acid-based therapeutics, such as small interfering RNA (siRNA), messenger RNA (mRNA), and plasmid DNA, to target cells. In gene therapy, liposomes serve as carriers to protect nucleic acids from degradation and facilitate their uptake by cells, enabling modulation of gene expression for therapeutic purposes. One significant advantage of using liposomes in gene therapy is their ability to overcome biological barriers, such as cell membranes and endosomal compartments, which can hinder the delivery of nucleic acids. Liposomes can encapsulate nucleic acids and facilitate their transport across cellular barriers, improving their bioavailability and enhancing their therapeutic

efficacy. Moreover, liposomes offer flexibility in terms of surface modification, allowing for targeted delivery to specific cell types or tissues by functionalizing liposomal surfaces with ligands or antibodies that recognize cell surface receptors. This targeted approach increases the specificity of gene delivery, minimizing off-target effects and reducing systemic toxicity (Tseng & Huang, 1998).

In gene therapy, liposomes find applications across various diseases since they are particularly valuable for delivering nucleic acid-based therapeutics to target tissues or cells.

1.5 Production Limitations

While microfluidic devices offer promising advantages for the production of liposomes, several limitations slow their widespread adoption and scalability in industrial settings. Firstly, one of the primary challenges in microfluidic-based liposome production is achieving high throughput. Traditional bulk production methods allow for large-scale production, whereas microfluidic devices typically operate at much smaller scales, limiting their production rates. The microscale channels and chambers inherent to these devices impose constraints on flow rates and volumes, resulting in lower overall production yields compared to bulk methods (Carugo, Bottaro, Owen, Stride, & Nastruzzi, 2016). Scaling up microfluidic production to meet market demands without compromising the advantages of precise control and reproducibility remains a significant challenge that will be addressed in this research thesis.

Secondly, the fabrication and operation of microfluidic devices can be complex and require specialized expertise. Designing and fabricating microfluidic chips with precise geometries and surface properties suitable for liposome production demands expertise in microfabrication techniques such as photolithography, soft lithography, or micro-machining. The operation of microfluidic systems often involves intricate fluid handling and control mechanisms, including

precise regulation of flow rates, pressure, and temperature. This complexity may pose challenges in terms of system reliability, reproducibility, and maintenance (Christoffersson & Mandenius, 2019).

Thirdly, microfluidic-based liposome production may be susceptible to issues related to material compatibility and fouling. The materials used in microfluidic devices, such as polymers or glass, must be biocompatible and inert to avoid interference with liposome formation or drug encapsulation. The small dimensions of microfluidic channels increase the likelihood of fouling due to interactions between lipids, drug molecules, and channel surfaces, leading to inconsistent production and reduced efficiency over time (Carugo, Bottaro, Owen, Stride, & Nastruzzi, 2016).

1.6 From Microfluidics to Millifluidics

Upscaling a microfluidic device to a millifluidic mixing device can have effects on the size of liposomes through factors like TFR and FRR, but also the polydispersity index (PDI), and zeta potential of liposomes produced. Higher TFR generally leads to smaller liposome sizes in both methods. Specifically, in millifluidics, increasing the TFR decreased the liposome size significantly when applying a high FRR. In microfluidics, a similar trend is observed where increasing the TFR results in smaller liposomes, but the sizes vary depending on the FRR. As for the PDI, both methods demonstrate that a higher TFR tends to produce liposomes with lower dispersity, indicating more uniform size distribution. For example, at a TFR of 10 mL/min, the PDI in millifluidics was found to be around 0.07, whereas in microfluidics, it remained below 0.2 across various conditions. The liposome size decreased from 169 nm to 88 nm at a FRR of 20 when using a TFR of 10ml/min instead of 1ml/min. The zeta potential, which indicates the stability of the liposomes, showed that in both methods, liposomes remained stable over different TFRs and FRRs, although specific values varied with the lipid compositions used. Generally,

millifluidics produced liposomes with more consistent and therapeutically relevant sizes and dispersity compared to microfluidics, highlighting its potential for scalable and efficient liposome production (Yanar, Mosayyebi, Nastruzzi, Carugo, & Zhang, 2020).

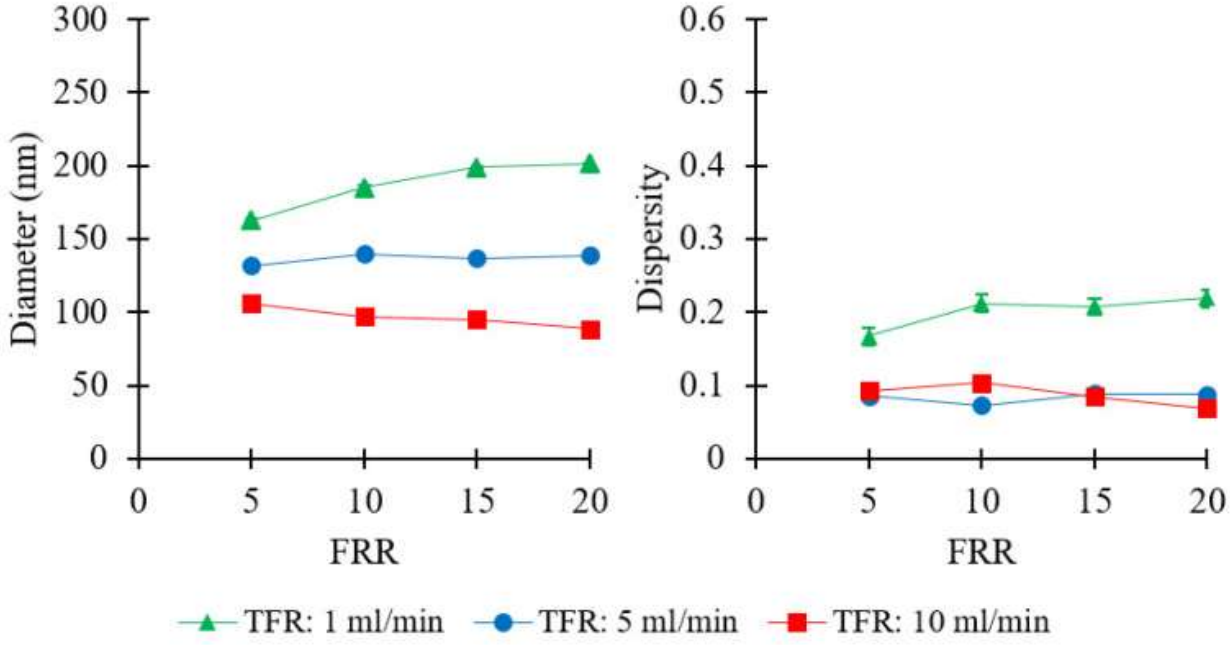

Figure 1.3: Example of Expected Results

Source: (Yanar, Mosayyebi, Nastruzzi, Carugo, & Zhang, 2020)

Figure 1.3 represents the results taken from that same study on the production of liposomes in millifluidics. The review of this article sets the expectations of what can be achieved in this experiment.

In the same referenced study, the mixing efficiency of microfluidic and millifluidic devices both theoretically and experimentally were studied for the production of liposomes. The microfluidic device typically uses a hydrodynamic focusing architecture where inlet channels meet at an angle, leading to the formation of laminar flow regimes that facilitate diffusion-driven mixing. In contrast, the millifluidic device incorporated a serpentine-like mixing channel that enhances mixing efficiency by increasing residence time and inducing secondary Dean flows. CFD

simulations indicated that the millifluidic device's serpentine channel design significantly improves mixing efficiency compared to straight channels due to these secondary flows. Theoretical models suggested that increasing the TFR and FRR enhances mixing efficiency in both devices, with more pronounced effects observed in the millifluidic system due to its design features. Experimental results corroborated these findings, showing that the millifluidic device achieved higher mixing efficiency and more consistent liposome production. Specifically, at higher TFRs, the millifluidic device produced liposomes with narrower size distributions and lower PDI values compared to the microfluidic device. Additionally, the millifluidic device demonstrated better scalability, maintaining high mixing efficiency and liposome quality across a broader range of flow conditions, which is advantageous for industrial-scale liposome production (Yanar, Mosayyebi, Nastruzzi, Carugo, & Zhang, 2020).

CHAPTER 2: MICROFLUIDIC DEVICE DESIGN

2.1 Introduction

In the context of liposome production, microfluidic devices present a promising platform for the precise engineering of liposomes with well-defined size distributions and compositions. The design of microfluidic devices involves intricate channel networks, where fluids are manipulated in laminar flow regimes to facilitate controlled mixing and encapsulation processes. One of the common designs employed in liposome production is the Y-shaped mixer, where two or more fluid streams are merged to induce rapid mixing and subsequent liposome formation. By leveraging the unique flow characteristics at the microscale, such as low Reynolds numbers and high surface-to-volume ratios, microfluidic devices enable the production of liposomes with uniform sizes ranging from tens to hundreds of nanometers. Moreover, the ability to precisely control parameters such as flow rates, lipid concentrations, and channel geometries allows for the customization of liposome properties, including size, membrane composition, and cargo encapsulation efficiency.

2.2 Design

During the design process of microfluidic devices, the inlet and mixing channels must be evaluated to eventually obtain laminar flow while ensuring a high mixing efficiency. The most common designs involve Y-shaped or T-shaped inlet channels. The Y-shaped inlet channel can be seen as an intermediate solution between a straight channel microfluidic device and a T-junction microfluidic device, as one uses a difference of 180 degrees between both inlet channels while the other has 0 degrees between both. The Y-channel microfluidic device would have an angle between both inlet channels. The value of the angle is an arbitrary value that can be chosen. In the case of this experiment, the angle was chosen to be 90 degrees. Also, the cross-section of the inlet channels was chosen to be rectangular while using a serpentine mixing channel. Other geometric

values, such as the length of the mixing channel and the inlet channels, had to be defined. The design process must also cover other factors such as the Reynold's number of the anticipated flow in the device, the dimensions of the cross-section of all channels, the technology to be used in the fabrication of the microfluidic devices, and all related performance limitations due to design choices (Lopez, Ocampo, Sánchez, & al., 2020).

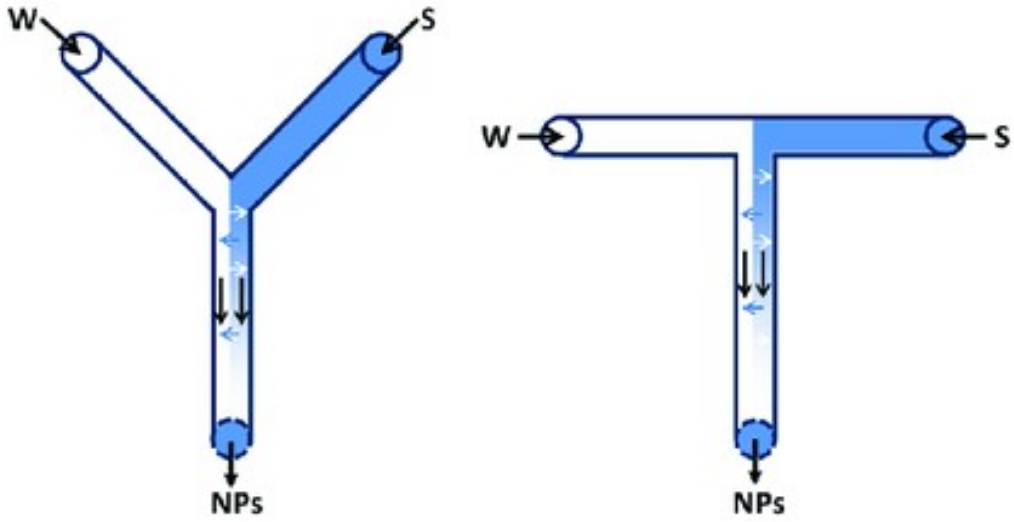

Figure 2.1: Y-Shaped Mixer and T-Shaped Mixer

Source: (Tao, Chow, & Zheng, 2018)

Figure 2.1 shows the visual representation of both the Y-shape mixer and the T-shaped mixer with 2 inlets and 1 outlet.

2.2.1 Mixers

There are two types of mixers, active and passive. Active mixers utilize external energy sources or mechanisms to induce fluid mixing. These energy sources can include electric fields, acoustic waves, magnetic fields, or pneumatic pressure. The active mixing process typically involves moving parts, such as pumps, valves, or actuators, which actively manipulate fluid flow or induce turbulence to promote mixing. Active mixers offer precise control over mixing parameters, such as mixing speed, duration, and intensity. This control allows for tailored mixing profiles to meet

specific application requirements. Additionally, active mixers are capable of achieving rapid and thorough mixing, making them suitable for applications requiring high mixing efficiency. However, active mixers may require external power sources and additional components, which can increase system complexity and cost. Maintenance and operation may also be more demanding due to the presence of moving parts. Despite these challenges, active mixers are versatile and can be adapted to various applications by adjusting the external energy input and system parameters.

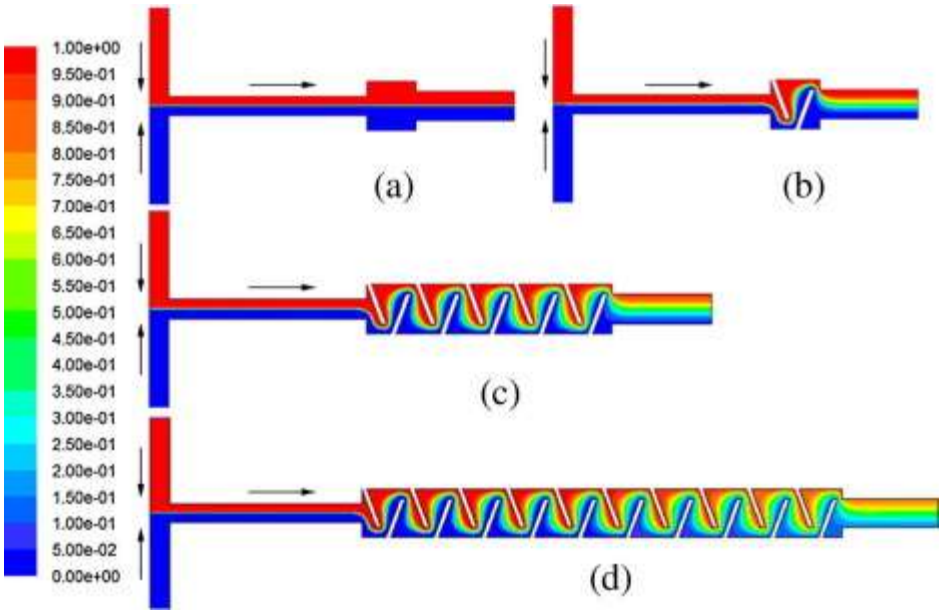

Figure 2.2: Examples of Passive Mixers

Source: (Lee, Wang, Liu, & Fu, 2016)

In contrast, passive mixers rely solely on the inherent fluid dynamics within microchannels to induce mixing. They do not require external energy input or moving parts to promote mixing. Figure 2.2 shows different examples of passive mixers, where the obstacles within the channel induce mixing due to pressure and shear stress. Passive mixers exploit phenomena such as diffusion, chaotic advection, and hydrodynamic focusing to achieve fluid mixing. Passive mixers are simpler in design and operation compared to active mixers. They do not require external energy sources or moving parts, resulting in reduced system complexity and potential points of failure.

However, passive mixers offer limited control over mixing parameters compared to active mixers. While the geometry of the mixer can be tailored to influence mixing behavior, the extent of control is generally less precise. Despite these limitations, passive mixers are more cost-effective than active mixers due to their simpler design and lower operational requirements. Simpler design facilitates the production of liposomes since the probability of wrongful operation is reduced. In essence, passive mixers are suitable for applications where precise control over mixing parameters is not critical (Giraldo, Bermudez, Torres, & al., 2021).

In our application, a combination of active and passive mixing is used to test our prototypes. The objective is to reach a high rate of mixing as quickly as possible to ensure optimal formation of liposomes. The active mixing process used is known as pump-driven mixers. The principle of pump-driven mixing involves the precise manipulation of fluid flow rates using pumps to induce mixing within microfluidic channels. By controlling the flow rates of individual fluid streams entering the microfluidic device through separate inlet channels, the fluids are forced to interact and mix within a main channel. This manipulation of flow rates allows for customized mixing profiles, where fluids of different compositions or concentrations can be efficiently homogenized.

Pump-driven mixers exhibit several distinctive characteristics that make them valuable tools for fluid mixing in microfluidic applications. Firstly, these mixers offer precise control over fluid flow rates, enabling better manipulation of mixing parameters such as flow velocity, mixing duration, and the ratio of fluid components. This high level of control allows for tailored mixing profiles, ensuring that desired mixing outcomes are achieved consistently. Moreover, pump-driven mixers are highly flexible and adaptable to various experimental setups and applications. The ability to independently adjust the flow rates of individual fluid streams provides the flexibility to customize mixing protocols according to specific experimental requirements. Pump-driven mixers can

accommodate a wide range of fluid viscosities and compositions, making them suitable for mixing diverse types of samples and reagents. Another key characteristic of pump-driven mixers is their high mixing efficiency. By actively manipulating fluid flow rates, these mixers can achieve rapid and thorough mixing of fluids, even in microscale channels. This high efficiency is particularly advantageous for applications requiring homogeneous mixing of small sample volumes or rapid reaction kinetics. This mixing method benefits our experiment since speed of mixing is studied based on scalability, meaning different flow rates and perhaps different mixing durations. The disadvantages of this type of mixing do not limit our experiment, as pump-driven mixing faces complexities if incorporated with valves or control systems (Jahn, Stavis, Hong, & al., 2010).

Figure 2.3: Peristaltic Pump by ANKO

Comparing peristaltic pumps with syringe pumps, both offer distinct advantages and disadvantages in the production of liposomes. Peristaltic pumps, visualized in Figure 2.3, are advantageous for their ability to provide a continuous flow of fluids, which is crucial for scaling up production. Their

gentle pumping action minimizes shear stress, helping to maintain the integrity of liposomes. Additionally, the ease of sterilizing or replacing tubing reduces the risk of contamination, and their flexibility allows them to handle a wide range of viscosities, making them suitable for various fluid types. This adaptability makes peristaltic pumps scalable for both small and large-scale production, reducing cross-contamination as the fluid only contacts the tubing. However, they can introduce pulsations in the flow, which might affect consistency, and their limited pressure capability restricts some production applications. Tubing wear is another concern, necessitating regular maintenance, and their accuracy in fluid delivery might not match that of syringe pumps, especially at very low flow rates.

Figure 2.4: Syringe Pump by Harvard Apparatus

On the other hand, syringe pumps, as shown in Figure 2.4, are known for their high precision in fluid delivery, which is essential for producing uniform liposomes. They offer excellent control over flow rates, ensuring reproducibility and minimal pulsation, which is crucial for consistency

in liposome production. Their operation generates minimal shear stress, thus protecting liposome integrity, and they are particularly advantageous for handling small volumes, making them ideal for small-scale production or research applications where precise dosing is required. However, syringe pumps are limited by their fixed volume capacity, necessitating frequent refills for large-scale production, which can be labor-intensive. Their scalability is also limited compared to peristaltic pumps, and they are more prone to introducing air bubbles into the system, which can affect liposome formation. Additionally, high-precision, low-pulsation syringe pumps can be more expensive (Byun, Abi-Samra, & Cho, 2013). In the case of this study, the fluid will be pumped directly into the Y-shaped inlet channels which join together in the main serpentine-shaped mixing channel.

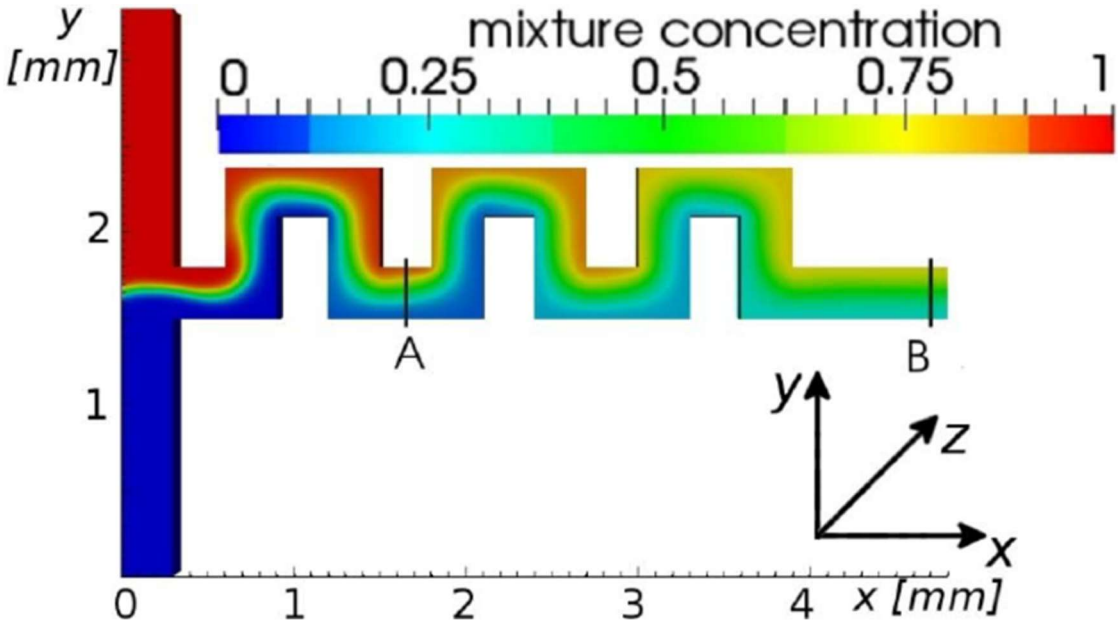

Figure 2.5: Serpentine Mixer

Source: (Malecha & Malecha, 2014)

Serpentine mixing, as seen in Figure 2.5, relies on the inherent fluid dynamics within a microchannel to induce mixing without the need for external energy sources or active manipulation. The principle of serpentine mixing involves designing the main channel with a winding or zigzagging geometry, often resembling the shape of a serpent or snake. As fluid streams

flow through this serpentine channel, they undergo repeated folding and stretching due to the channel's geometric features. This folding and stretching action generate chaotic advection, where fluid particles mix with each other as they circulate through the channel. By leveraging the convective flow patterns induced by the serpentine geometry, serpentine mixing achieves efficient and thorough mixing of fluids within microfluidic devices. Serpentine mixers possess several distinctive characteristics that make them advantageous for fluid mixing in microfluidic applications. Firstly, serpentine mixers offer efficient and thorough mixing of fluids within a relatively short channel length. The winding or zigzagging geometry of the main channel induces repeated folding and stretching of fluid streams as they flow through the microchannel. This complex flow pattern promotes chaotic advection, enhancing mixing efficiency without the need for external energy input or active manipulation. Serpentine mixers are relatively simple in design and operation compared to active mixers. They do not require additional components such as pumps or valves, making them easier to fabricate and integrate into microfluidic devices. This simplicity also reduces the risk of system failure and maintenance requirements. Serpentine mixers offer versatility in terms of their application. The mixing behavior of serpentine mixers can be influenced by adjusting parameters such as channel dimensions, curvature, and fluid flow rates. This flexibility offers the possibility to tailor mixing protocols to specific experimental requirements, making serpentine mixers suitable for a wide range of applications in areas such as chemical synthesis, biological assays, and drug delivery (Giraldo, Bermudez, Torres, & al., 2021).

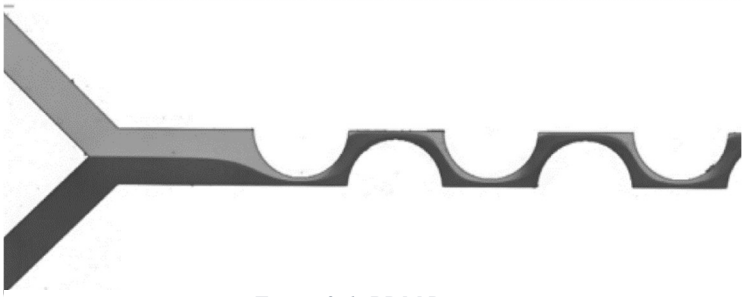

Figure 2.6: PDM Design

In this experiment, the design of the mixing device uses PDM, which is a technique to enhance mixing efficiency within the channels. This method involves the application of periodic pulsatile flows, where the fluid streams are alternately accelerated and decelerated. The resulting oscillatory motion, as described by Figure 2.6, disrupts the laminar flow regime, promoting better mixing through increased chaotic advection and interfacial area between the fluids (Ruben Salazar, 2020).

2.2.2 Fluid Flow

Microfluidic systems typically function within the confines of laminar flow due to their specific dimensions, resulting in a smooth flow of fluids. This is attributed to the prevalence of viscous forces over inertial forces, maintaining a consistent velocity throughout the liquid when boundary conditions remain constant. In contrast, turbulent flow is characterized by the supremacy of inertial forces, leading to random spatial and temporal motion, facilitating mass transport in multiple directions. The determination of laminar or turbulent flow is dictated by the Reynolds number, as defined in equation 2.1.

$$Re = \frac{\rho u D_H}{\mu} \tag{2.1}$$

Where u is the flow velocity, ρ is the fluid density, μ is dynamic viscosity, and D_H is the hydraulic diameter. The Reynolds number plays a crucial role in influencing mixing behavior within microfluidic devices. In systems where the Reynolds number is low, indicating laminar flow dominance, mixing primarily occurs through mechanisms such as molecular diffusion, chaotic advection, and Taylor Dispersion. However, as the Reynolds number increases, transitioning towards turbulent flow, mixing becomes more efficient due to enhanced convective mixing and increased turbulence (Yu, Lee , & Lee, 2009).

Taylor dispersion is a phenomenon observed in fluid dynamics, particularly in laminar flow conditions, where there is a gradient in the velocity profile across a fluid stream. It leads to the spreading out of solutes or particles carried within the fluid, contributing to mixing. Mathematically, Taylor dispersion can be described using the Taylor dispersion coefficient (D_t) which characterizes the rate of dispersion. The rate of dispersion can be calculated as in equation 2.2.

$$D_t = D_L + \frac{U^2\tau}{48L} \tag{2.2}$$

Where D_L is the longitudinal diffusion coefficient, U is the mean flow velocity, and τ is the characteristic time to travel the length L of the channel.

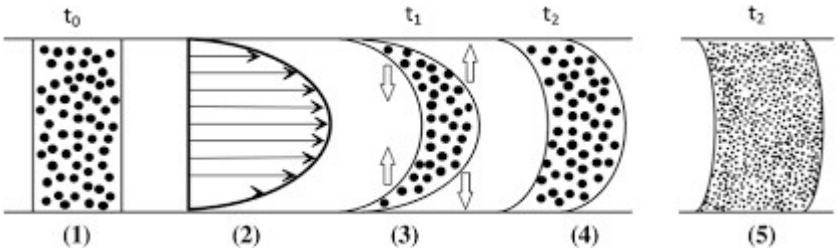

Figure 2.7: Taylor Dispersion Phenomenon

Source: (Donath, Kantzas, & Bryant, 2019)

The phenomenon, as represented in Figure 2.7, arises due to the variation in fluid velocity across the channel cross-section. As faster-moving fluid near the center of the channel overtakes slower-moving fluid near the walls, solutes or particles experience different velocities, leading to dispersion. This differential velocity causes a spreading effect, akin to a stretching or shearing of

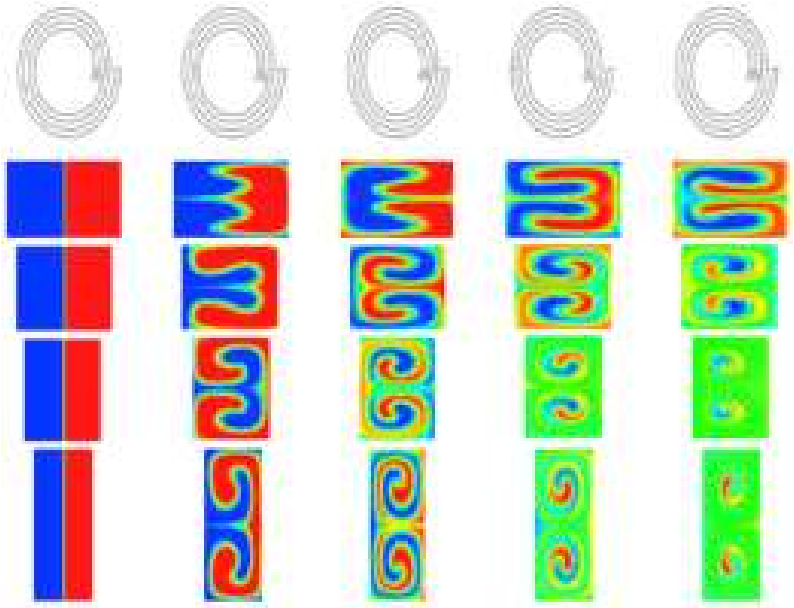

Figure 2.8: Mixing of Fluids due to Chaotic Advection

Source: (Vatankhah & Shamloo, 2018)

the solute band, resulting in enhanced mixing and dispersion of solutes across the channel (Ruben Salazar, 2020).

Chaotic advection, as visualized through virtual mixing process in Figure 2.8, occurs in fluid dynamics, characterized by irregular and unpredictable flow patterns that enhance mixing within a fluid system. It is particularly prominent in systems with complex geometries or under certain flow conditions, such as low Reynolds numbers. Chaotic advection arises due to the intricate interplay between advection, diffusion, and stretching of fluid elements within the flow field. It can be quantified using Dean's number (De), as defined in equation 2.3.

$$De = \frac{\tau_{flow}}{\tau_{diffusion}} \tag{2.3}$$

Where τ_{flow} represents the characteristic time scale associated with the flow dynamics, while $\tau_{diffusion}$ represents diffusion processes.

Similarly, another equation for the Dean number utilizing the Reynold's number previously calculated in equation 2.1 is described in equation 2.4.

$$De = Re\sqrt{\frac{D_H}{2R_c}} \tag{2.4}$$

Where D_H is the hydraulic diameter and R_c is the ratio of curvature.

In systems with low Dean numbers (De << 1), diffusion dominates over advection, resulting in minimal chaotic mixing. Conversely, at high Dean numbers (De >> 1), advection prevails over diffusion, leading to extensive chaotic mixing and enhanced dispersion of solutes or particles within the fluid (Ruben Salazar, 2020).

Active mixing techniques may often induce chaotic advection. However, the flow rate of the peristaltic pumps used in our experiment ensures laminar flow into the inlet channels. The intricate trajectories of our serpentine mixing channel introduce disturbances in the flow, which in turn leads to chaotic advection to optimize mixing efficiency.

When mixing water with an aqueous solution composed of lipids and ethanol, the specific characteristics of the fluids, such as their viscosities and densities, will influence the Reynolds number and subsequently affect mixing efficiency. The presence of lipids and ethanol may alter the fluid properties and enhance mixing through changes in interfacial tension, which can be described by the Marangoni effect. Due to laminar flow predominance, the majority of mixing within microfluidic setups is achieved through passive molecular diffusion and advection. Molecular diffusion refers to the random movement of molecules from regions of high concentration to those of lower concentration, a phenomenon known as Brownian motion

(Michelon, Bernardes Oliveira, de Figueiredo Furtado, Gaziola de la Torre, & Lopes Cunha, 2017). This process is detailed by Fick's first law, as presented in equation 2.5.

$$j = -D\frac{dc}{dx} \tag{2.5}$$

Where j is the diffusion flux, D is the diffusion coefficient, and dc/dx is the rate of change of the concentration. This equation takes a new form when dealing with spherical particles and would then be referred to as the Einstein-Stokes equation (2.6).

$$D = \frac{kT}{6\pi\mu} \tag{2.6}$$

Where k is the Boltzmann's constant, T refers to the absolute temperature in kelvins, R is the particle's radius and μ is the fluid viscosity.

2.2.3 Microfluidic Channels

To investigate the size of liposomes produced, a standard device was used as reference since previous tests were already performed. This reference device was tested several times. The microfluidic device consists of a Y-shaped mixer used as inlet channels that converge into a serpentine-shaped mixing channel. In essence, there are two (2) inlets and one (1) outlet. The geometric shape of the cross section is rectangular. The microchannels have a maximum width of 300 µm. The serpentine shape is created by equally spaced semicircular holes which have a radius of 260 µm. This would yield a narrow spacing of 40 µm in the mixing channel where maximum fluid velocity is observed. Two other devices were modeled and tested virtually in the Multiphysics COMSOL software solution for microfluidics. Due to computational limitations, the devices produced and those in simulation are not equal in dimensions, but the experiment remains valid as the results would help validate the same theory. In simulation, the dimensions were increased by

3 and 5 times while the physical devices were scaled up by 10 and 100 times. Evidently, the devices can no longer be called microfluidic devise, since the size has exceeded the definition of the word. This experiment uses the concept of microfluidics to try and solve the critical problem of underproduction by scaling up the size. In theory, scaling up the dimensions of the reference microfluidic device while maintaining pressure and fluid velocity by varying the flow rate would yield the same quality of liposomes in terms of vesicle diameter and zeta potential.

2.2.4 Fabrication Methods

There are different methods to manufacture microfluidic devices, whether it is through glass-etched channels, PDMS or even 3D printing. Microfluidic devices with glass-etched channels are fabricated through a series of precise steps involving photolithography and wet chemical etching techniques. Initially, a glass substrate, typically borosilicate or soda-lime glass, is cleaned thoroughly to remove any contaminants. A photoresist layer is then spin-coated onto the glass surface. A mask containing the desired channel patterns is aligned and exposed onto the photoresist layer using UV light. After exposure, the photoresist is developed to remove the areas exposed to UV light, leaving behind a patterned photoresist layer corresponding to the channel layout. Subsequently, the glass substrate undergoes wet chemical etching, where the exposed glass areas not protected by the developed photoresist are dissolved selectively. This etching process continues until the desired channel depth is achieved. Once the etching is complete, the remaining photoresist is stripped away, leaving behind precise glass-etched channels on the substrate. The substrate may undergo additional cleaning steps to ensure the removal of any residual photoresist or etchant residues. Finally, the glass substrate with the etched channels may be bonded with another glass layer or cover to enclose the channels and create a sealed microfluidic device. This

fabrication method offers high precision and reproducibility, enabling the creation of intricate channel geometries with excellent optical transparency (Patil & Jadhav, 2014).

Fabricating microfluidic devices using 3D printing involves additive manufacturing techniques to create intricate channel structures directly onto a substrate. The process typically begins with designing the desired channel layout using computer-aided design (CAD) software. This design is then converted into a digital file format compatible with 3D printing. During printing, a 3D printer deposits successive layers of material, such as thermoplastics or photopolymers, according to the digital design. Specialized 3D printing techniques, such as stereolithography (SLA) or digital light processing (DLP), enable high-resolution printing with feature sizes suitable for microfluidic applications. After printing, the fabricated device may undergo post-processing steps, such as cleaning and curing, to remove any residual support material and enhance structural integrity. In some cases, additional surface treatments, such as hydrophobic or hydrophilic coatings, may be applied to modify the channel properties and improve fluid flow control. One advantage of 3D printing for microfluidic device fabrication is its flexibility in creating complex and customizable channel geometries with minimal design constraints. This enables rapid prototyping and iteration of device designs tailored to specific research or application requirements. Additionally, 3D printing allows for the integration of functional components, such as valves and sensors, directly into the device structure, enhancing its functionality (Patil & Jadhav, 2014). While 3D printing offers advantages in rapid prototyping and customization, it is not always ideal for fabricating microfluidic devices due to several limitations. Most 3D printers lack the resolution and precision necessary for creating fine micro-scale features, leading to rough surfaces and inconsistent channel dimensions. Additionally, the limited range of available materials may not meet the biocompatibility and chemical resistance requirements of certain applications. The surface

roughness and potential structural weaknesses from the layer-by-layer construction can disrupt fluid flow and compromise device integrity. Furthermore, 3D printing is less efficient for mass production compared to traditional microfabrication methods, which can consistently produce high-quality devices in large quantities (Chen, et al., 2016).

Our microfluidic device was built with PDMS. Taking into consideration that some techniques may incur high costs, some processes were simplified to achieve the best result possible while remaining within a small budget. The microchannels were fabricated from Polydimethylsiloxane (PDMS) elastomer using a brass negative mold. The fabrication of the channel mold involved CNC micromachining, which required a minimal feature size constraint of 0.8mm. Features smaller than this threshold cannot be reliably manufactured in-house due to tool deflection and path deviations proportional to the feature sizes. Upon completion of the negative mold, the SYLGARD™ 184 Silicone Elastomer base and curing agent were mixed in a plastic tray with a 10:1 mass ratio. After mixing for 3 minutes, the PDMS mixture was degassed in a vacuum chamber for 15 minutes to remove trapped air bubbles. Subsequently, the PDMS was poured slowly onto the brass mold and then cured in a 55°C oven for over two hours to avoid undesired expansion of the brass. Once cooled, the cured PDMS was trimmed to correspond with the piece of glass with which it will be

assembled. At this stage of the process, the channels are open until closed during the final assembly.

To seal the open PDMS channels, oxygen plasma bonding was employed to adhere the PDMS structure to an optical glass sheet. The bonding process involves first covering both the glass sheet and PDMS chip with isopropanol, drying the glass surface with chem wipes, and heating it on a 100°C hot plate for 10 minutes. The PDMS surfaces were dried using compressed air, but can be also be dried with nitrogen. Subsequently, both the treated glass and PDMS surfaces underwent

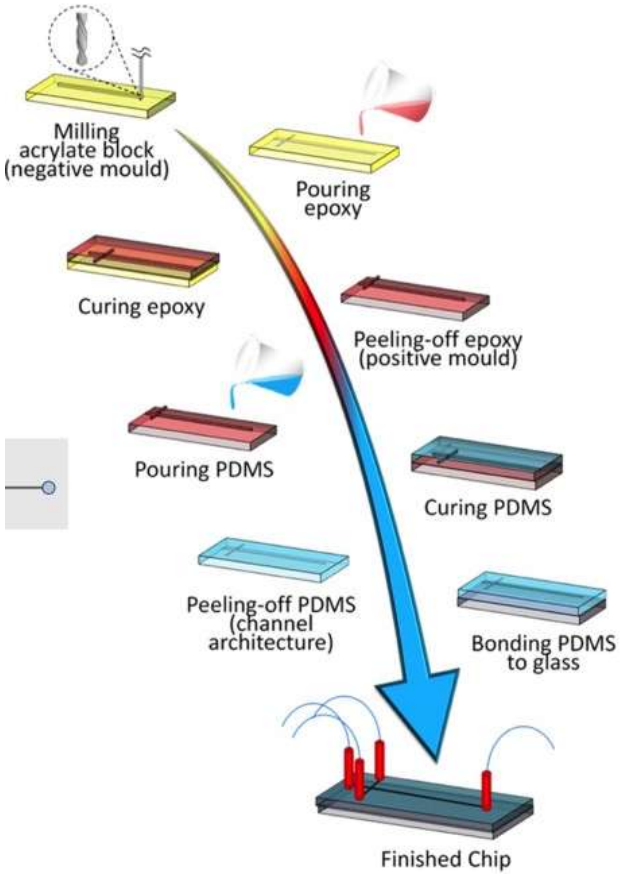

Figure 2.9: Fabrication Process of PDMS Microfluidic Device

Source: (Carugo, Bottaro, Owen, Stride, & Nastruzzi, 2016)

plasma treatment for one minute before being pressed together firmly for 20 seconds to initiate

bonding. The bonding process was then completed by placing the assembly in a 90°C oven for 10 minutes.

Oxygen plasma treatment is a crucial step in the fabrication of microfluidic devices, especially for achieving high-quality bonding between glass and polydimethylsiloxane (PDMS). This technique is widely used due to its ability to create strong, durable, and reliable bonds essential for the production of liposomes in microfluidic systems. The process begins by placing the glass and PDMS surfaces in a plasma chamber. Oxygen gas is introduced into the chamber, and an electrical field is applied to generate a low-pressure plasma. The oxygen plasma consists of highly reactive oxygen species, including ions, radicals, and UV photons, which interact with the surfaces of the materials. For PDMS, the oxygen plasma treatment modifies the surface by breaking the Si-CH3 bonds and introducing silanol (Si-OH) groups. This process effectively transforms the hydrophobic PDMS surface into a hydrophilic one. The presence of silanol groups increases the surface energy, promoting better wetting and adhesion properties. Similarly, the glass surface, which is primarily composed of silicon dioxide (SiO2), also undergoes activation, where the plasma treatment introduces additional hydroxyl (OH) groups. When the treated PDMS and glass surfaces are brought into contact, the hydroxyl groups on both surfaces interact to form strong covalent siloxane (Si-O-Si) bonds. This covalent bonding is essential for ensuring a robust, irreversible seal between the PDMS and glass, which is critical for the structural integrity of the microfluidic device. The high-quality bonding achieved through oxygen plasma treatment has several advantages. Firstly, it ensures that the microfluidic channels are leak-proof, which is vital for the precise control and manipulation of fluids within the device. Secondly, the strong bond prevents delamination under the mechanical and thermal stresses encountered during device operation. The enhanced surface properties facilitate the reliable and reproducible production of

liposomes, as the consistent surface chemistry ensures uniform flow and mixing conditions within the microfluidic channels (Lin & Chung , 2021).

The testing procedure comprises two main stages. Initially, the micromixer operates until the input reservoirs near depletion, after which the mixed fluid is gathered in an output reservoir. To assess the presence of liposomes, a zeta potential analyzer is utilized. This apparatus enables the measurement of zeta potential, indicative of the potential difference between the internal and external layers of liposomes. These results are then cross-referenced with established literature values to determine liposome presence or absence. Due to uncertainties in the channel geometry and fluid resistivity of the manufactured micromixer, its output and performance under specific input pressure and pump power settings may deviate from predictions. Thus, it is imperative to compare the device's performance with that of the COMSOL model. While direct measurement of fluid velocity, flow rate, and pressure in such small-scale devices may pose challenges, TFR can be readily assessed by measuring sample volume over a known time interval.

2.2.5 Performance and Limitations

Different types of limitations were encountered, whether it was during the modeling of the microfluidic device, the numerical simulation of fluid mixing, or the fabrication process. During the design stage, things went smoothly since the model was already predefined in previous work. The objective of the redesign was simply to scale up the physical model while ensuring that are dimensions respect the scale used. Complications arose when COMSOL software required more computational power during simulation of fluid mixing. Since the mesh size used was extremely fine and the overall volume of the device was getting bigger, it only meant that the mathematical load invoked by the resulting matrices made our computers run overtime. Extremely fine mesh is required to yield precise results in the concentration plots. No compromise was possible to ensure

the validity of our experiment. More information will be presented in the next chapter. The fabrication itself posed issues as unorthodox methods had to be employed to reduce costs while maintaining a high degree of reliability considering the pressure of the fluid flow inside the microchannels and the costly aqueous solution navigating through them. Leaks could, in fact, be quite costly. To ensure that all cracks were sealed, a water run was performed to identify all escape routes, which were later sealed. Micromachining of the brass mold required outsourcing as the tolerances were far too precise.

2.3 Physical Modeling

Prior to fabricating and testing the microfluidic device, producing the digital twin is crucial to understand the nature of our work, and has hence become a standard practice in the engineering design process nowadays. To recreate our prototype, COMSOL was used to first draw the 3D representation which would then serve for numerical modeling and simulation. Taking previous work as reference, the physical model was already drawn. However, it will be necessary to create new models similar to the original one, only scaled up in dimensions. This will allow for a proper comparison between the original microfluidic device and milli-fluidic devices, with the objective of creating similar sized and shaped liposome vesicles but in wider channels in the hopes of boosting productivity harmlessly. Setting up the foundation for numerical simulation will allow better understanding of mixing, which is a strong indicator for the formation of liposomes.

2.3.1 Reference Work

As mentioned, this experiment is based on previous work performed by Dr. Ruben Rodrigo Salazar and aims to understand if the production limitation of liposomes using microfluidic devices can be minimized. The initial design was copied and scaled up. This provides a great basis for data comparison.

The initial model is a Y-shaped mixer used for inlets and a serpentine-shaped mixer used as the main mixing channel. The dimensions of the cross-section are 300 µm and are square. The angle between both inlet channels is at 90°. The length of both mixing channels needs to be long enough to better evaluate the location where 90% mixing is achieved. The serpentine mixing channel was drawn with extruded half circles with radii of 260 µm. The center point of those circles corresponds with the top and bottom limit of the mixing channel The position of each circle alternates between the top and bottom limitation. Each circle on a single side is separated by a distance equivalent to 4 times the radius. An inlet flow of 18ml/h was used as the TFR and a FRR of 8.56 was defined between the water and the aqueous solution. A concentration of 1 mol/ml was used in that same solution. These parameters were used for the design of the physical model and for simulation purposes. All values used are based on multiple experiments which were documented in a previous paper (Ruben Salazar, 2020).

On top of the above parametrical values, computational parameters were also used for the purpose of generating similar simulation parameters, which were in turn used to validate the results of the upscaled models. The important parameter used in the study definition was the maximum and minimum mesh size. The mesh size defines the precision required in the calculation of the simulation results. Since the mesh lies between a range of values, the obtained data may have varied slightly from the original set but the differences are negligible as velocities and pressure results are the same. The mesh size is crucial for the concentration plot, which indicates the mixing efficiency throughout the serpentine mixer. The pressure and velocity values were used as references to ensure that the adjusted TFR would allow velocity and pressure to be the same in the enlarged devices. This is mandatory to validate the hypothesis that the speed of mixing when both fluids meet defines the size of the vesicles.

2.3.2 Geometry

The physical model was designed in the geometry module of COMSOL software solution. The 3D design would later be used to complete the study. As mentioned earlier, the channels have rectangular cross-sections. There are 3 iterations of the models. The reference has squares sides of 300 µm and a Y-shaped structure. The Y-shape refers to two inlet channels converging into main mixing channel. The width of the mixing channel is also 300 µm, but is height is adjusted to ensure smooth fluid mixing and avoid a higher pressure differential in this specific channel due to higher volumetric flow in a more restrictive space. The scaled models are 3 times and 5 times bigger, meaning that channel widths are at 900 µm and 1500 µm respectively.

2.3.3 Materials and Fluid

Once the 3D design is drawn, materials must be defined. The entire device is made out of PDMS and the only openings are at the 2 inlets and the 1 outlet (Ruben Salazar, 2020). The material has an impact on the simulation as surface roughness is an important factor when generating velocity gradient inside the channels, which in turn has an impact on the mixing efficiency. The fluid, which will be the main agent on which calculations are performed, will consist of a mix of water and an aqueous solution composed of cholesterol and alcohol. The output will yield a solution composed of liposomes. We are fortunate enough to have easy access to water, but the other chemicals and

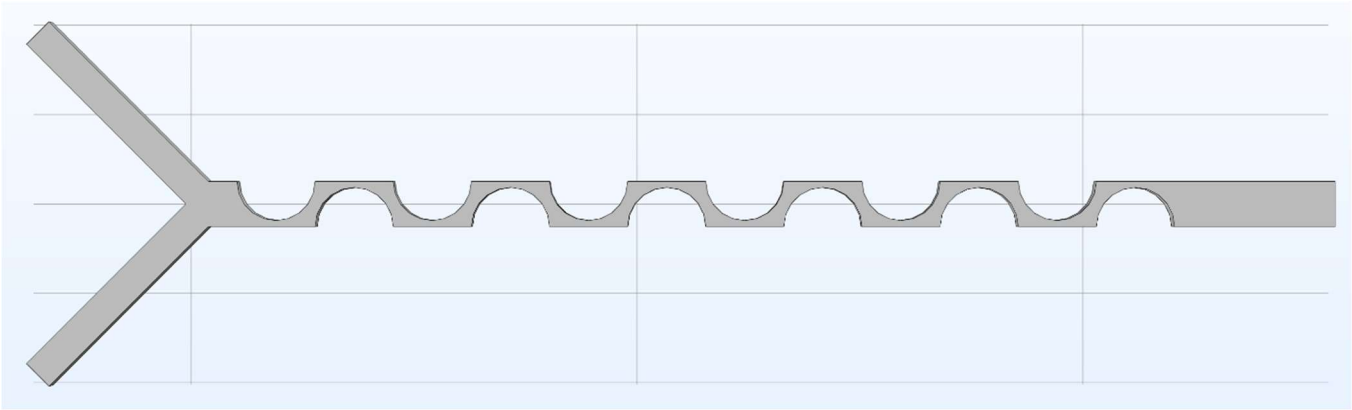

Figure 2.10: Geometry Design of Mixing Device

solutions had to be purchased. First, 1 gallon of food grade ethyl alcohol 200 proof (100%) was purchased from Lab Alley. Second, the rest of the necessary products were procured from Sigma Aldrich. Those include 1 gram of dihexadecyl phosphate, 1 gram of 1,2-dimysistoyl - sn-glycero-3-phosphocholine, 1 gram of cholesterol with a purity higher than 99%, and 1 liter of chloroform. One inlet would welcome the mixture of chemicals while the other inlet would allow water to be pumped in. Both inlets, as seen in Figure 2.10, join together in the main mixing channel, where the exposure of the mixture to water will force the sheets of fat to ball up into tiny spherical vesicles.

2.3.4 Expected Output

The expected results are aligned with the referenced work. During simulation, velocity and pressure gradients should remain about the same, as the output is calculated in a straightforward manner. However, the concentration plots are interesting and will enable to determine the mixing behavior under different conditions. Similarities would show that the experiment can be scaled

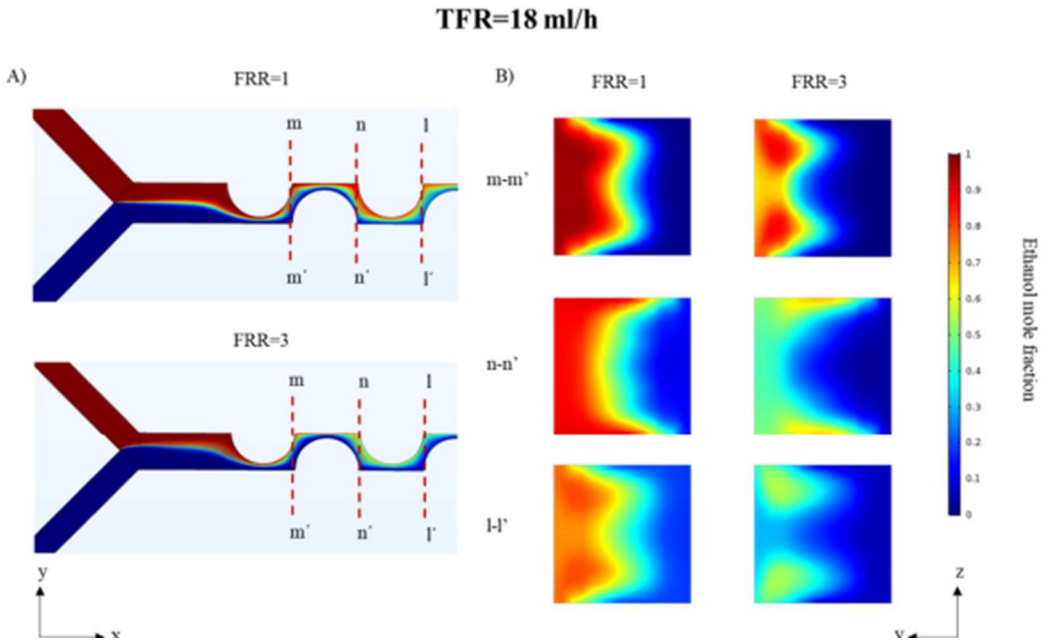

Figure 2.11: Expected Concentration Plot from COMSOL Multiphysics

and perhaps even produce liposomes of similar sizes, measured within the range of 52nm to 200nm. This data was taken directly from the reference research and can be found in Appendix 1.

Figure 2.2 shows the expected color gradient to be generated from the concentration plot in COMSOL Multiphysics. Similar simulation results would raise confidence in the ability of the milli-fluidic mixers to efficiently mix the ethylic solution with the aqueous solution. Then, the experiment would be validated through the measured size of liposomes produced from the scaled mixers.

The reference work also highlights that Dean flow dynamics-based micromixers are particularly suitable for liposome production due to their ability to generate fast and uniform mixing conditions, essential for producing liposomes with controlled size and homogeneity. These micromixers can overcome common issues associated with traditional micromixers, such as low productivity, fabrication challenges, clogging, agglomeration, and the presence of harmful solvent residues. By leveraging Dean vortices, these micromixers can achieve high production rates of nanosized liposomes, offering a simplified fabrication process that avoids complex three-dimensional structures. The research further shows that the proposed micromixer design can produce liposomes as small as 27 nm with production rates up to 41 mg/ml. The stability of these liposomes can last up to six months, which is crucial for their application in drug delivery systems. The study used numerical modeling and confocal imaging to investigate the mixing process, demonstrating the relationship between mixing efficiency and liposome properties (Ruben Salazar, 2020).

CHAPTER 3: NUMERICAL MODELING AND SIMULATION

3.1 Introduction

Once the physical model is configured, it would be pertinent to run virtual tests. By setting up the proper parameters, the computer begins tracing the fluid flow behavior by solving large matrices built by the equations governing over all interactions within the microfluidic channels. The power of simulation will allow us to solve the Navier-Stokes equation with defined boundary conditions of laminar fluid flow.

3.2 Numerical Modeling

Through the Microfluidics module of COMSOL Multiphysics 6.2, fluid properties are added to the geometry previously built. First, the Laminar Flow solver is added to the model, in which the fluid properties such as temperate, density and viscosity are defined. It also serves to define the cross-sections of the inlets, outlets and all rigid walls forming the microfluidic channels. On top of those definitions, the initial values are also necessary to define the boundary conditions of the differential equations representing the physical behavior of the fluid. Since laminar flow is predominant in our case, the software will automatically recognize a Reynold's number lower than 1000, and in consequence, solve the Navier-Stokes equation for incompressible and weakly compressible flows. Second, the Transport of Diluted Species interface is added to the model to represent the mixture of chemicals used as the solute. An initial concentration is defined and associated with an inlet. Once both fluids mix in the main channel, the concentration plot will show the change in concentration, indicating the mixing behavior.

3.2.1 Mixing Theory

In the context of this study, mixing involves the transport of diluted species to enhance uniformity. Specifically, in nanoprecipitation, mixing induces a transformation of lipids into liposomes by blending a low polarity organic solvent with a high polarity aqueous solvent. Micromixers adhere to the same underlying principles of physics as their macroscopic counterparts, albeit with dimensional scaling implications. Notably, factors such as surface area-to-volume ratio, surface tension, and diffusion exhibit nonlinear scaling. Microfluidic devices typically operate within laminar flow regimes due to their small dimensions, resulting in smooth fluid flow where viscous forces predominate over inertial forces. Consequently, the velocity remains constant over time given constant boundary conditions. At this scale, mixing primarily occurs through molecular diffusion, chaotic advection, and Taylor Dispersion. In contrast, turbulent flow is characterized by the prevalence of inertial forces, leading to random motion in both space and time, facilitating mass transport in all directions.

In this case, the numerical model behind the mixing of two fluids is characterized by the Navier-Stokes equation, since single-phase flow is used in the COMSOL software. With some parameters already predefined, the Navier Stokes equation (3.1) can be solved, assuming that a no-slip boundary condition is preconditioned and that the continuity equation (3.2) is respected.

$$\rho(u \cdot \nabla)u = \nabla \cdot [-pI + \mu(\nabla u + (\nabla u)^T)] + F \tag{3.1}$$

$$\rho\nabla \cdot (u) = 0 \tag{3.2}$$

Where ρ is the fluid density, u is the flow velocity, p is the pressure, μ is the dynamic viscosity, and F is the outer forces. The continuity boundary condition ensures that the pressure and mass flux are continuous (Ruben Salazar, 2020).

Mixing involves a combination of diffusion and convection processes to achieve homogeneity in a fluid system. In many mixing scenarios, both diffusion and convection act simultaneously and interactively to enhance the overall mixing efficiency. Diffusion facilitates the gradual blending of components on a molecular scale, while convection accelerates the transport of mixed fluid regions throughout the system. The combined effects of diffusion (equation 3.3) and convection (equation 3.4) enable the rapid and thorough homogenization of fluids, ensuring uniformity of composition and properties across the entire volume.

$$\nabla \cdot (-D\nabla c) + u \cdot \nabla c = R \tag{3.3}$$

$$N = -D\nabla c + uc \tag{3.4}$$

Where c is the diluted species concentration, D is the mutual diffusion coefficient between water and ethanol, R is the net volumetric source for the species, and N is the molar flux.

Efficient mixing of fluids is necessary for liposome formation as the kinetic properties are crucial to produce nanosized particles. The speed at which mixing occurs is controlled by the rate of change in polarity induced by the aqueous-organic solvent. The diffusion rates of both water and ethanol are required during fluid modeling for more accurate simulation. However, the results require interpretation to understand the mixing behavior of the fluids as they travel through the mixing channel. To validate if the concentration plots yielded good mixing results, calculations will be necessary using the simulated data to extract the mixing efficiency of the device's mixing channel.

First, the mixing efficiency will need to be calculated in order to understand the mixing time required to reach satisfactory levels. Typically, this range is from 90% to 95%. To evaluate the homogeneity of the mixed solution, it is first required to compute the intensity of segregation (I_S)

defined in equation 3.5, which will allow the calculation of the mixing efficiency (ME) defined in equation 3.6 (Danckwerts, 1952). Both equations can be found further in the chapter.

According to the reference work, a higher Dean number would suggest that the mixing process is optimal. The Dean number characterizes the of Dean vortices, which is the ratio between centrifugal forces and inertial forces. The Dean number can be described through equation 3.5 below.

$$De = Re\sqrt{\frac{D_H}{2R_C}} \tag{3.5}$$

Where D_H is the hydraulic diameter, Re is the Reynolds number, and Rc is the ratio of curvature.

Dean Flow Dynamics-based micromixers utilize curvilinear paths to generate Dean Vortices, while simultaneously incorporating microchannel size reductions to modulate flow speed and induce Taylor dispersion. The primary variables critical to the performance of this microfluidic device include the TFR, the radius and direction of the curvilinear paths, and the aspect ratio of the channels. It is essential to consider that the Dean number, which characterizes the intensity of Dean vortices, is directly proportional to the flow velocity. These factors influence the mixing efficiency and overall functionality of the micromixer.

3.2.2 Upscaling the Microfluidic Device

Changing the geometry sizes are not the only settings needed to be changed when simulating the same device but at a larger scale. In the objective of keeping linear velocity in the channels similar as in the model presented in the reference project, it will be necessary to increase the TFR as the linear velocity of the fluid depends solely on the flow rate and the surface area of the cross-section. When increasing the TFR to maintain the same linear velocity, an equation should be followed to

determine the appropriate value in recreating the same velocity gradient in the new enlarged device.

$$Q_1 = A \cdot v \tag{3.6}$$

$$A = b \cdot h \tag{3.7}$$

$$Q_2 = (x \cdot b \cdot x \cdot h) \cdot u \tag{3.8}$$

$$Q_2 = x^2 \cdot Q_1 \tag{3.9}$$

As shown in equation 3.8, the new TFR is calculated based on the scaling factor used to increase the geometric dimensions. Basing ourselves on the base model, the TFR used was 18ml/h, which was increased by 10 times and 25 times in the simulation models using scaling factors of 3.33 times and 5 times the values of each geometric dimension respectively. Equations 3.6 through 3.9 demonstrate how the new TFR values were calculated. Since the cross-section is rectangular, b and h were as the rectangular dimensions representing base and height, x was used as the scaling factor, u represents linear velocity, A is the surface area and Q is the flow rate.

On top of adjusting geometric dimensions and the TFR, it is also crucial to take in account the feasibility of the simulation with regards to the computer's capacity. Computer simulation relies on available RAM to conduct calculations. If higher precision is required, then the simulation will use more memory to complete the same task. In the simulation parameters, the user defines the precision of the simulation, which is defined through the mesh size. The precision was defined using a custom maximum and minimum element size, which would reduce the disparity between each mesh size used when calculating different iterations. This would increase precision drastically as opposed to the predefined mesh sizes. In our case, it was necessary to have a better understanding of the mixing efficiency through the concentration plots. For the velocity and

pressure gradients, this level of precision is not required. Some simulations did yield error messages due to insufficient RAM. The problem was encountered especially with larger devices when trying to solve the study using similar precision standards as the smaller devices. This made it impossible to evaluate the concentration plot of a device upscaled in cross-section area by 100 times. The simulation was then reduced to keep the surface area scaling factors at 10 times and 25 times. Although the same error was encountered with a scaling factor of 25, the precision was therefore reduced while keeping a similar range difference between the minimum and maximum element sizes.

3.2.3 Simulation Parameters

After upscaling all dimensions by a fixed factor, the geometry is rebuilt but conserves the same shape. Using COMSOL Multiphysics, concentration plots will be obtained by calculating the overall mixing efficiency. The precision of the results depends on the mesh size of the finite element being evaluated. Smaller mesh sizes will calculate the differences in data more frequently,

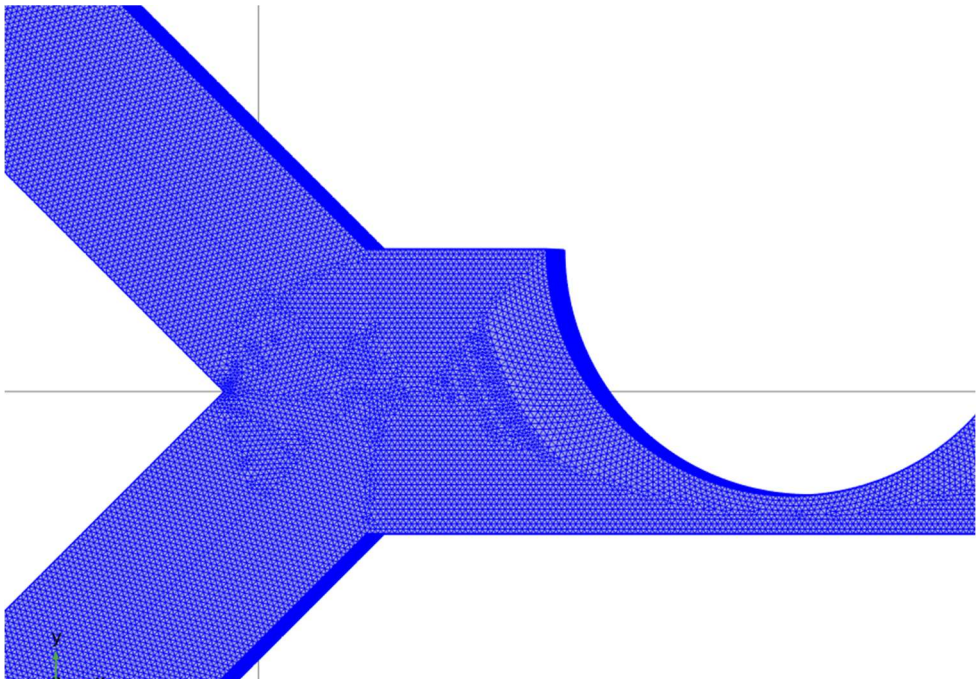

Figure 3.1: Mesh Size Used in Simulation

allowing higher precision in the final plot. However, this will cause the computer simulation to use more memory, which may cause a failure. Selecting a larger mesh size will compensate the accuracy of the results, which is an option that is simply not affordable.

The preset values for the mesh size, as seen in Figure 3.1, are in accordance with the level of precision needed in simulation. For each set of values, a minimum and maximum mesh size is defined, within which a mesh size will be used as basis for calculations, sometimes iterating multiple times with different mesh size values if complications arise. By default, the range defined

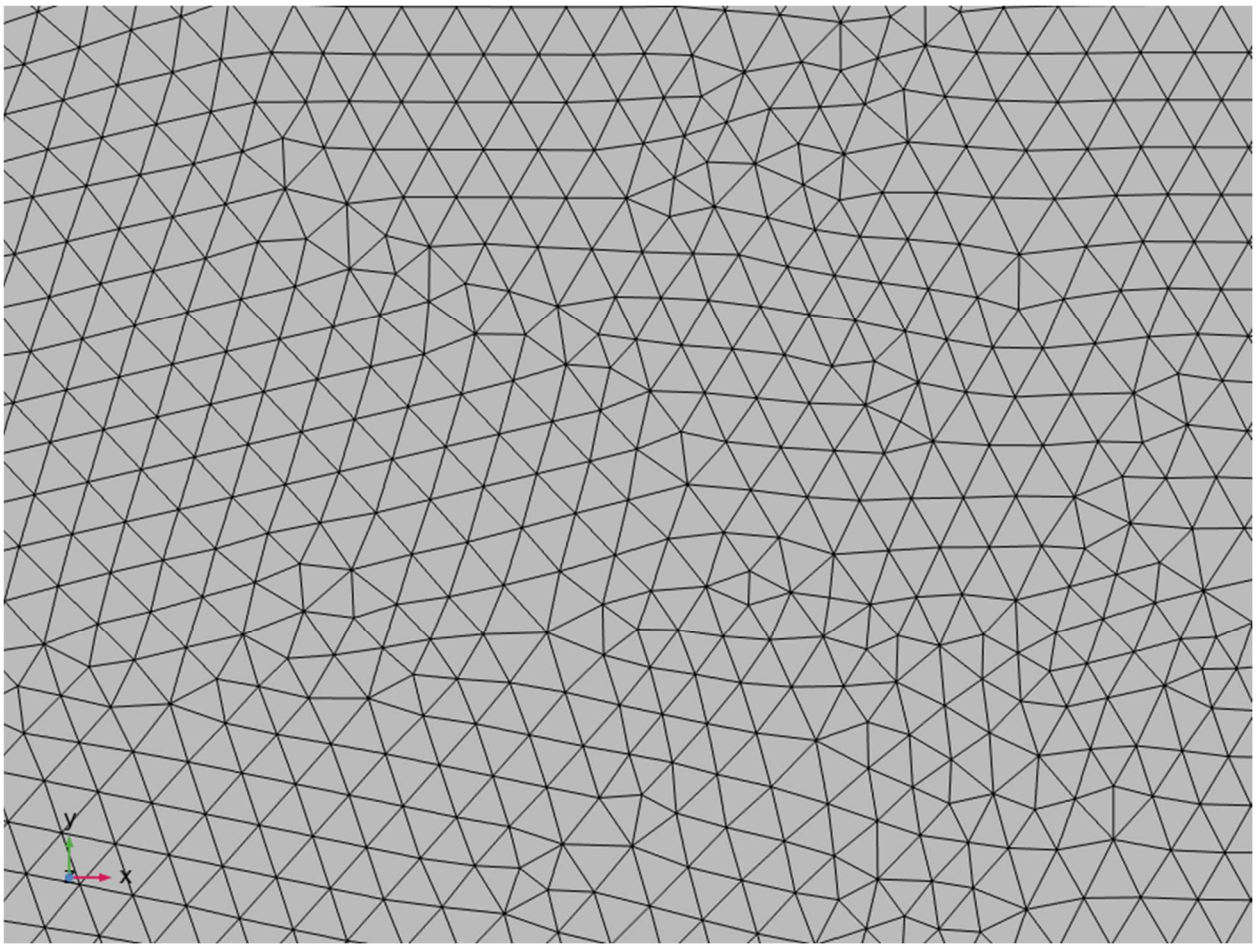

Figure 3.2: Zoomed-In View of Mesh Size

by the maximum and minimum mesh size is too large, which also yields unsatisfactory results even at the highest level of precision.

To solve this problematic, a custom range of mesh sizes will be defined. In the reference work, the maximum element size was set at 20E-6m and the minimum at 10E-6m (Ruben Salazar, 2020). These values were used in the original microfluidic device for the purpose of data acquisition through simulation. The same values were used when confirming our base model, as shown in Figure 3.2. After upscaling, the trial-and-error method was used to define a better range of element sizes since the prototype is now larger. A larger prototype means more calculation due to the higher number of elements in the matrix. The base model required over 77 hours of simulation time to yield results close to the reference model. After running the simulation on the upscaled models, the simulation time was used to evaluate the level of precision of the plot. Visually, it is also evident to realize if the concentration plot is lacking in detail. The trial-and-error method was used to achieve a similar simulation time, narrowly escaping failure. It is important to keep the element sizes consistent to avoid disparity in results between theoretical and experimental trials. Objectively, it is not possible to validate if the simulation is accurate other than simply trying the experiment, which was done by our peers.

The numerical simulation is specified for fluid dynamics and for all boundaries of the microfluidic device's body except for its inlets and outlets. Inlets allow the definition of ambient parameters such as temperature, but also differentiate between the water and diluted concentration solution. Each inlet has a concentration parameter when using the simulation model found in the transport of diluted species module within microfluidics. Realistically, the water would cause the alcohol and lipids mixture to react hydrophobically when exposed in the mixing channel, allowing the formation of liposomes. Analyzing the size of these vesicles will tell us the efficiency of the experiment. To do so, the variance of the data must be calculated to find the maximum efficiency (Danckwerts, 1952).

$$I_S = \frac{\sigma^2}{\sigma_{max}^2} \tag{3.10}$$

Where σ_{max}^2 is the maximum variance of concentration, and σ^2 is the variance of current concentration. The mixing efficiency ME is defined by:

$$ME = \left[1 - \sqrt{\frac{\sigma^2}{\sigma_0^2}}\right] \cdot 100 \tag{3.11}$$

Where σ^2 is the variance of the concentration in the tested cross-section, while σ_0^2 is the variance of the concentration in no mixing condition. The mixing efficiency ME is represented as a percentage, therefore indicating the mixing time required to achieve desired results.

3.3 Numerical Solution

After numerous trials, concentration plots were extracted after running the study. Concentration plots were the main interest in simulation results, while the velocity and pressure graph should remain constant for the purpose of validating simulation results in comparison with the reference work. The pressure gradient generated interest following the results it yielded. The velocity is calculated simply by taking the current flow rate and dividing it by the cross-sectional area at

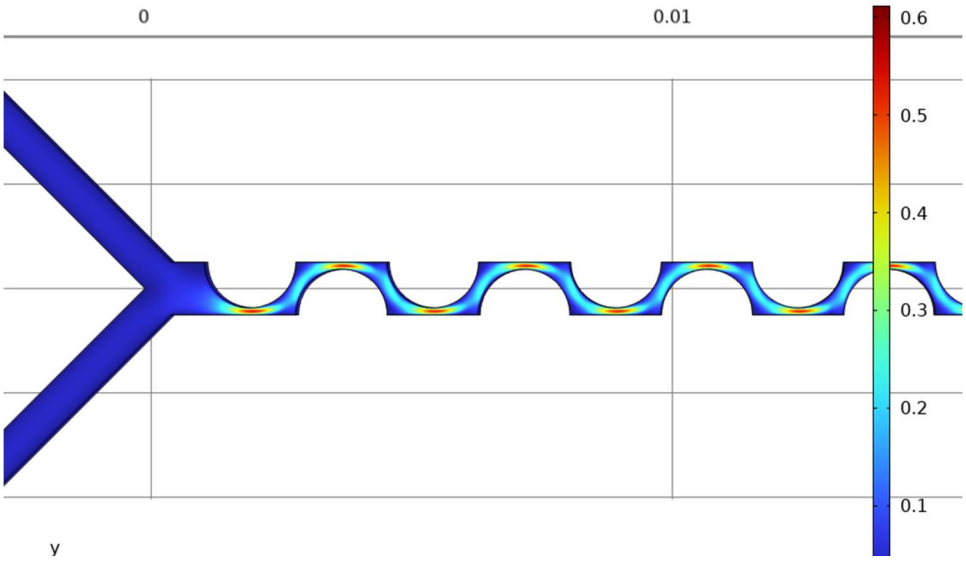

Figure 3.3: Velocity Gradient of 5:1 Model

different locations, as demonstrated in equation 3.6. This yields the velocity gradient, which would obviously lead to higher velocities in locations of smaller cross-sectional areas. The maximum linear velocity of the streamline is located closest to the longitudinal center line of each loop with a value approaching 0.7m/s.

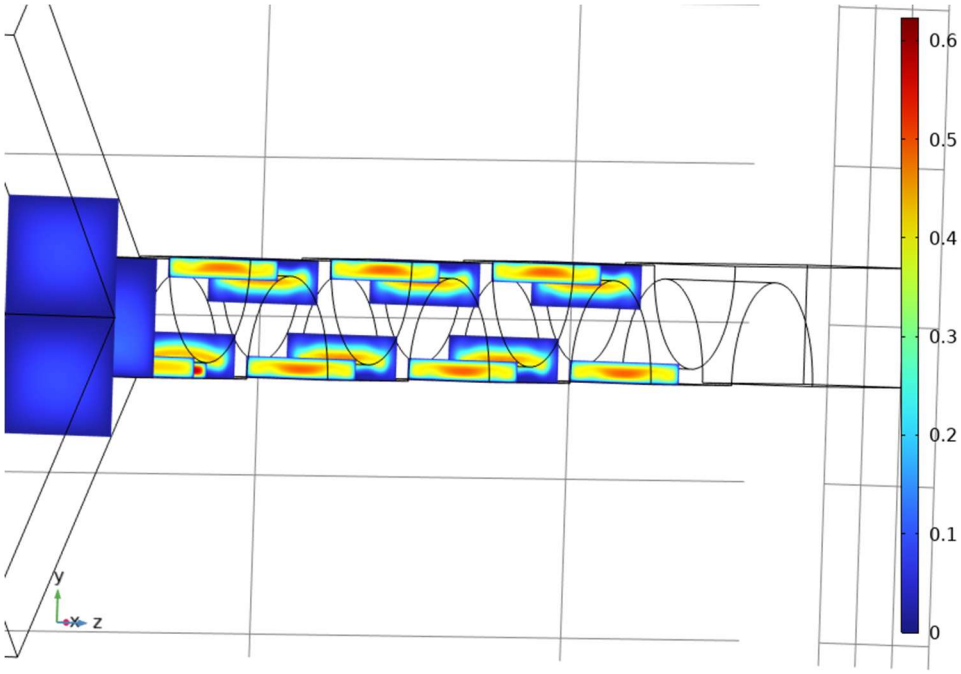

Figure 3.4: Cross-Section Color Gradient of Velocity Profile in 5x Model

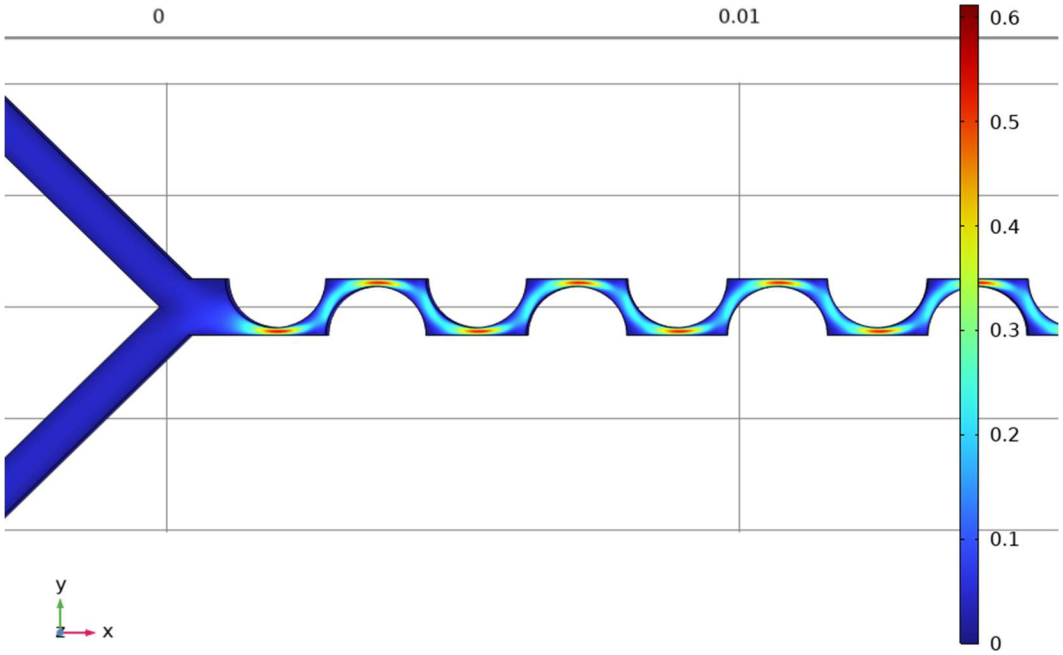

Figure 3.5: Velocity Gradient of 3.33:1 Model

As shown in figures 3.3 and 3.5, the velocity gradient remains similar to the reference work, ensuring that the grounds for comparison are solid. Figure 3.4 gives another perspective of the velocity profile by showing how fluid velocity changes within the cross-section. As the cross-section is wider, the minimum velocity is smaller and always located at the walls. Relating back to the hypothesis of the research, a link between velocity and liposome size are being evaluated. Since the reference work proved successful in creating nanosized vesicles under 40nm, it may be possible to recreate similar sized liposomes even if the mixing device was much larger. Theory states that bigger devices will in turn yield larger liposomes. However, perhaps adjusting other fluidic properties could reduce the significance that the device size plays on the results. On top of velocity pressure gradients were also used to maintain a similar environment within the confinements of the mixing device.

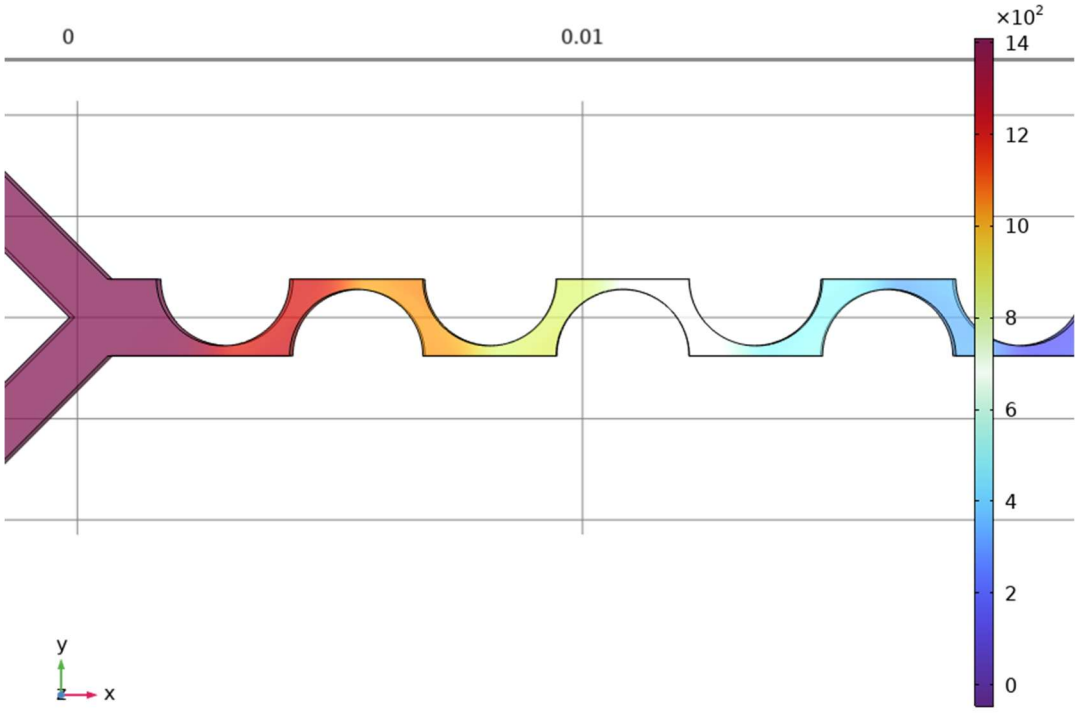

Figure 3.4: Pressure Gradient in Pa of 3.33:1 Model

As shown in figures 3.6 and 3.7, the pressure inside the mixing device decreases as the size of the device increases, even if the velocity remains constant from increasing the TFR. The maximum pressure in the model with a cross-sectional area upscaled by 10 times is nearing 2.5kPa while the

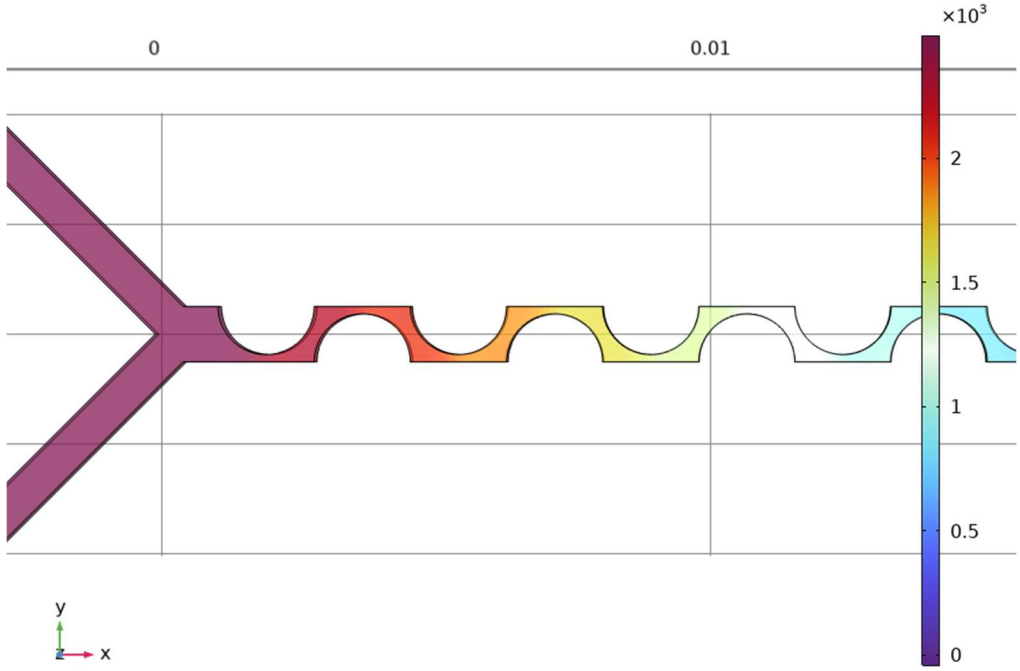

Figure 3.5: Pressure Gradient in Pa of 5:1 Model

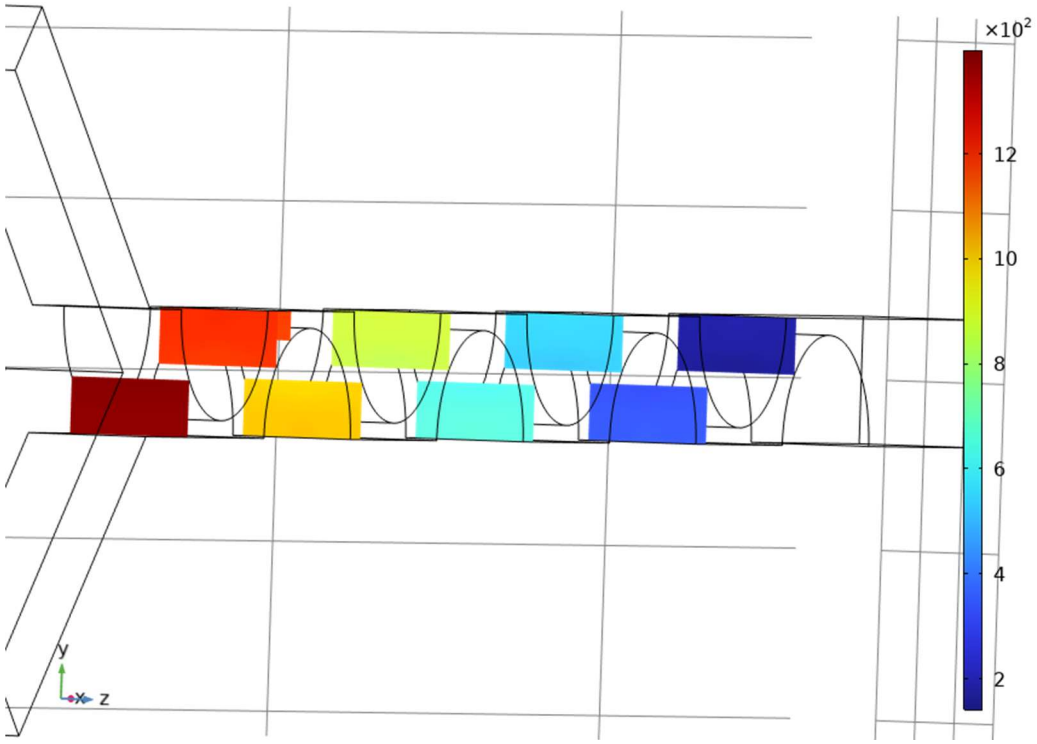

Figure 3.6: Cross-Section Color Gradient of Pressure Profile in 5x Model

model upscaled 25 times in cross-sectional area reaches 1.4 kPa in peak pressure. Values can be seen from the color gradient legend in each figure. Figure 3.8 shows how the pressure is applied inside the channel by simulating the pressure gradient from the cross-section view. From equation 3.3, the effects of diffusion in mixing relate pressure, as well as fluid velocity, to the time required to achieve homogeneity. In liposome formation, the time taken by the film of lipid to ball up directly impacts the size of the liposome diameter. Faster mixing will improve the chances for smaller liposomes. Since maximum pressure within the channels is going down as the device increases in size, it would then be necessary to increase the TFR to compensate for the lack of pressure, therefore a higher mixing efficiency quickly.

To ensure that the results obtained in simulation match with the ones contained in the reference work, it is insufficient to evaluate the data by the color gradient. At various intervals of the mixing channel, measurements were taken for every cross-section to calculate the variance and therefore,

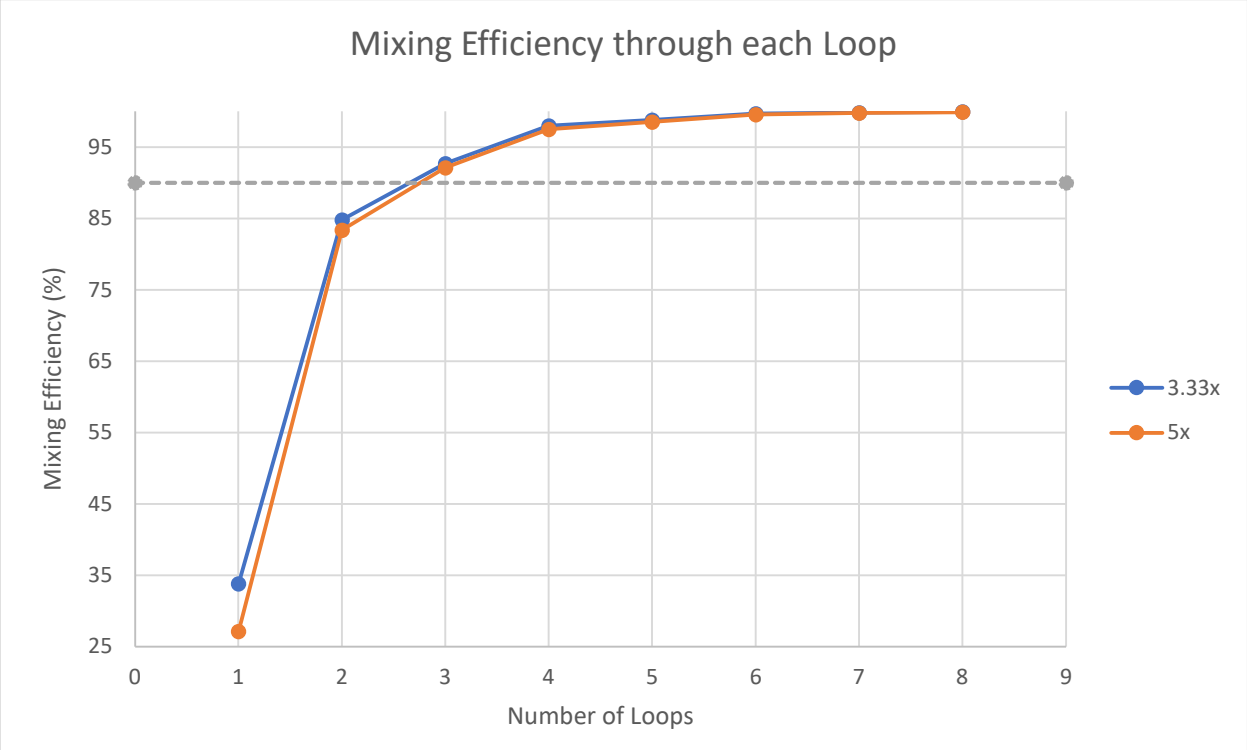

Figure 3.7: Mixing Efficiency Measured Across Each Loop

have a good approximation of the mixing efficiency as described in equations 3.10 and 3.11 respectively.

Figure 3.9 shows the mixing efficiency for both scaled models as basis for comparison with the reference model. The 90% mark indicates good mixing efficiency. By comparing the results with the reference work, it seems that the threshold of satisfactory mixing is reached earlier than in the microfluidic device. In the millifluidic device simulation, it requires 3 loops to achieve 90% mixing at a TFR of 180ml/h and 450ml/h for the 3.33x model and the 5x model respectively. The reference work shows an average minimum of 6 loops to reach the same mixing efficiency at a TFR of 18ml/h under various FRR conditions (Ruben Salazar, 2020). Data can be seen in Appendix 2, where the mixing is represented against time while plotting the measurements recorded at each loop.

3.4 Data Analysis and Reference Work

The results obtained during simulation in the reference work gives a hint on the validity of the design, but also helps to validate the new models. With the objective of producing similar sized

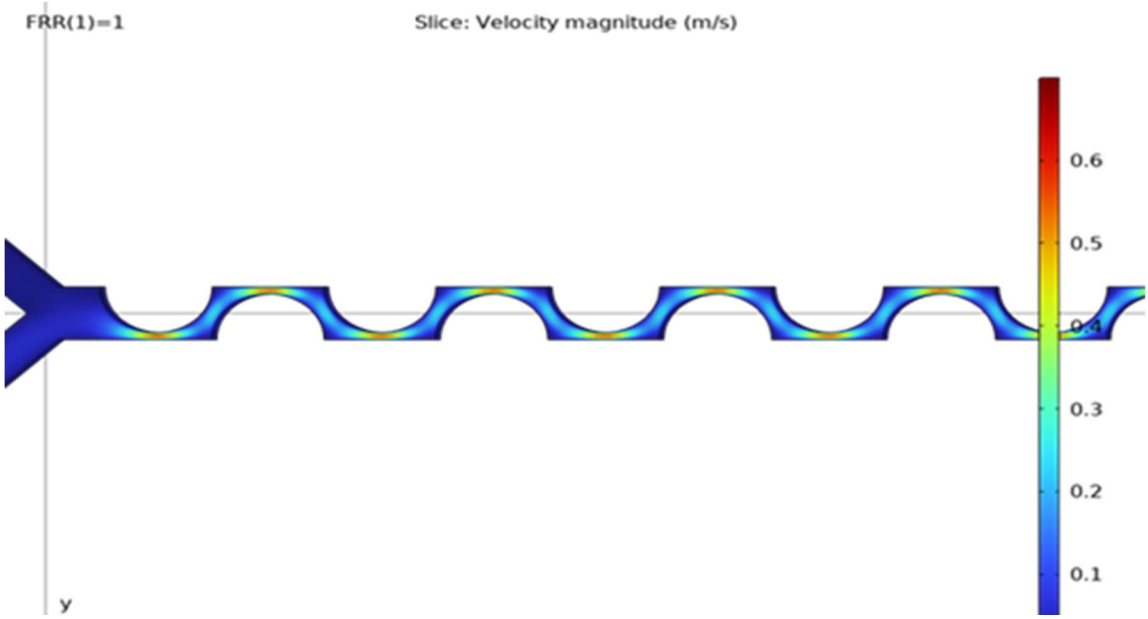

Figure 3.8: Velocity Gradient of Reference Work (1:1 Model)

liposomes at a higher rate, the same conditions must be achieved. Logically, it is crucial to match the velocity and pressure gradients of the new models to the ones obtained in the reference work (Ruben Salazar, 2020).

In this research, the theory states that velocity is the main parameter to test when forming liposomes in larger mixing devices. In the reference work, the velocity obtained from simulation resembles the plot generated in the upscaled models. Simultaneously, pressure gradients were plotted but were not the main focus of the experiment. However, if results show differences following testing, then conclusions could be drawn using the generated data. The pressure gradients of the upscaled models did show a drop in peak pressure as the size increased, but this observation was ignored to only validate the impact of fluid velocity on the diameter of the formed liposomes.

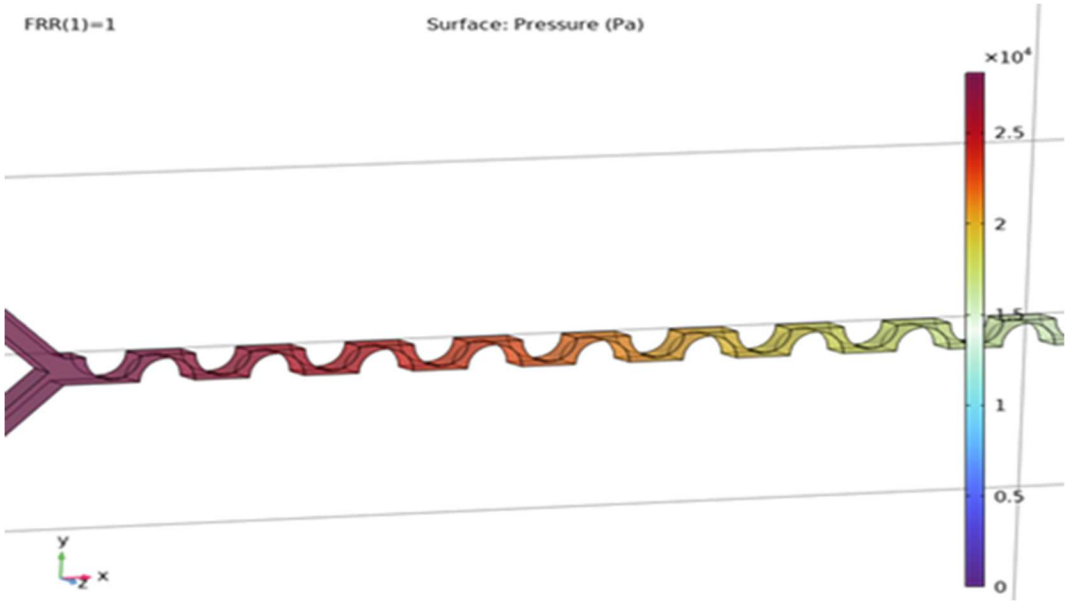

Figure 3.9: Pressure Gradient in Reference Work (1:1 model)

As shown in Figure 3.11, the peak pressure observed in the pressure gradient of the reference work is higher than 25kPa, which is over 10 times larger than the maximum pressure measured in the model with the cross-sectional area that is 10 times larger. Although this information will be kept

aside, it may be a good indicator for any variance in the experiment results. The gradients plotted in Figures 3.10 and 3.11 are important factors that directly influence the mixing results observed

in the concentration plot.

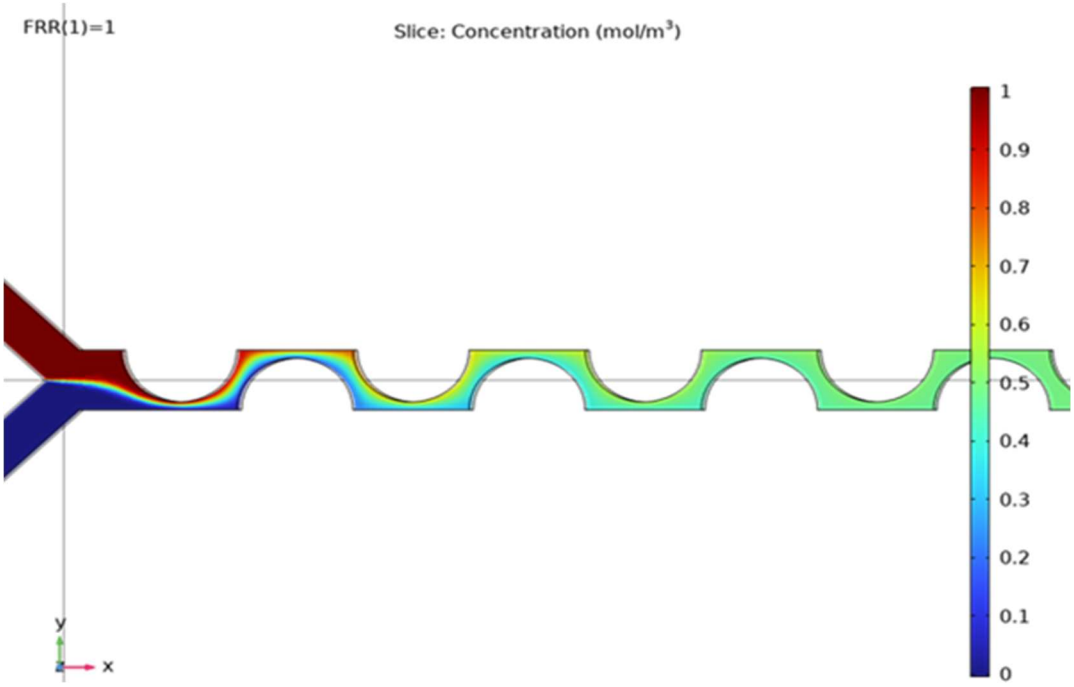

Figure 3.12: Concentration Plot of Reference Work (1:1 model)

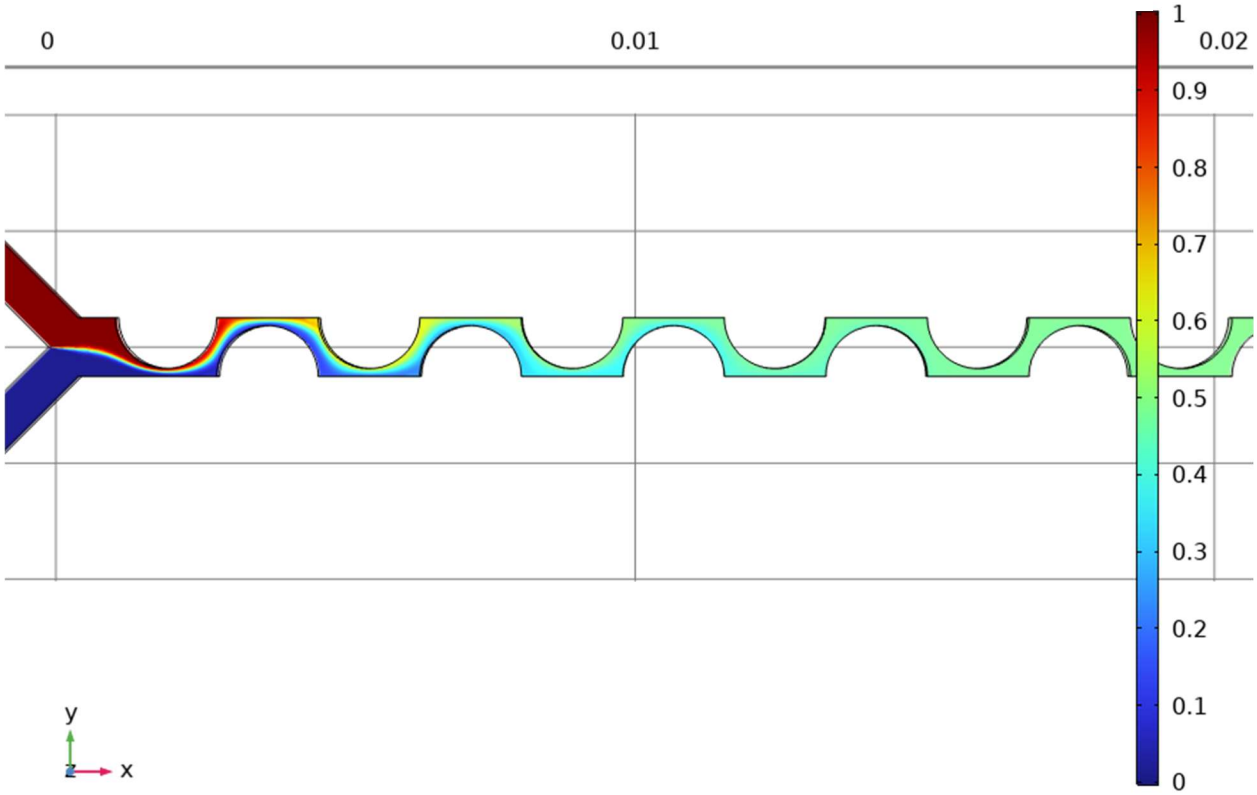

Figure 3.13: Concentration Plot of 3:33:1 Model

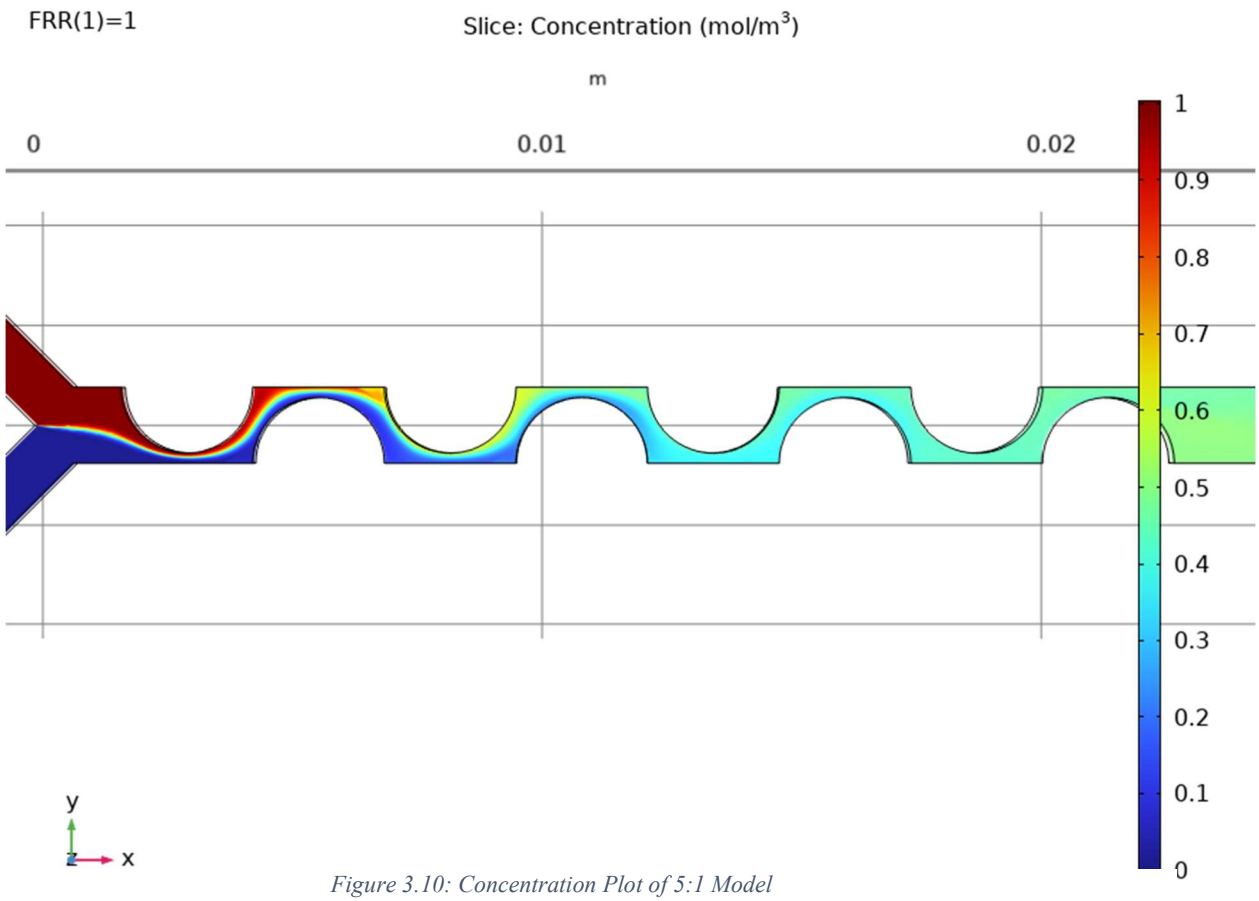

Figure 3.10: Concentration Plot of 5:1 Model

Referring to Figure 3.12, the color gradient shows the mixing behaviour throughout the mixing channel. At the 5th loop, the color becomes more uniform, suggesting sufficient mixing. It is not enough to visualize the plot to determine the mixing time, location and efficiency. Data must be exported and transformed, which was plotted in Figure 3.5. Figure 3.12 refers to the reference work, which is the model for the desired concentration plot in both upscaled models. Figures 3.13 and 3.14 represent the concentration plots of the 3.33:1 model and 5:1 model respectively. The concentration reaches equilibrium at 0.5 mol/m^3, as the FRR was computed only with a value of 1 and the concentration of the ethylic solution was 1 mol/m^3. Looking at the results for the first time, it may seem that there are little differences between each simulated model. However, results were evaluated and showcased in Figure 3.5, indicating great similarities between the recorded measurements in the reference work, which can also be found in Appendix 2. The positive results

observed in the numerical solution encourages the experimental mixing tests to evaluate if the liposomes produced in the upscaled devices would have similar sizes as the ones done in the microfluidic device as opposed to the milli-fluidic mixers.

With the data obtained from Figures 3.13 and 3.14, a comparison was made with the data extracted from Figure 3.12. At that point, the numerical simulation would be the indicator on whether mixing is possible and if the similarities between the upscaled models and the reference model were satisfying enough to conduct experimental tests to validate the hypothesis. From simulation, it was concluded that the mixing behavior in millifluidics seemed very close to what was presented in the reference, showing signs of hope for efficient mixing in a physical environment. The same number of loops were required to reach a uniform solution. From there, experimental testing would need to be organized to validate if the liposomes produced in the millifluidic device would also be similar to the ones examined in the reference work in terms of Z-Average, PDI and Zeta potential given that the linear velocity inside the channels are the same, as stated in the hypothesis.

CHAPTER 4: EXPERIMENTAL WORK, RESULTS AND ANALYSIS

4.1 Introduction

After collecting sufficient simulation data, the hardware needed to be tested for the purpose of validating the idea that linear velocity of fluid inside the mixing device's channel plays a crucial role in fabricating nanosized liposomes, more specifically a diameter ranging between 52nm to 200nm. To do so, a test bench was designed to apply the fabricated milli-fluidic mixers. The test bench includes two peristaltic pumps, 3 reservoirs, the milli-fluidic mixer and tubes to link all components. The fabrication of the milli-fluidic device was done using PDMS and analyzed using a digital microscope to evaluate the differences between the design and the prototype in case of errors during manufacturing.

4.2 Device Preparation

The microfluidic channels were fabricated from PDMS elastomer, which was cast onto a resin negative mold created using additive manufacturing. Once the negative mold was prepared, it was enclosed with four bounding walls constructed from Teflon and electrical tape layers. These walls were manufactured using SLA additive manufacturing with resin. The process of PDMS fabrication commenced with weighing and thoroughly mixing a Silicone Elastomer base and curing agent in a plastic tray for one minute. The ratio of base to curing agent was maintained at 10:1 by mass, adjusted according to the scale of the channels. After mixing, the PDMS mixture was poured slowly onto the mold, taking care to degas it in a vacuum chamber for 15 minutes to remove trapped air bubbles. The leak-free assembly of walls, mold, and tape prevented the liquid PDMS from escaping during its 48-hour air-curing phase. Upon complete curing, the PDMS was demolded, and reservoir holes were created using leather hole punching tools on a clean surface.

To facilitate hole cutting without cracks, dish soap was utilized as a lubricant, which was subsequently washed off, and the PDMS was air-dried.

Next, the PDMS piece shown in Figure 4.1, along with a precut glass piece, underwent oxygen plasma treatment to enhance chemical bonding. This involved placing them inside a treatment machine and manually pressing them together for 20 seconds. To maintain high bond quality, thorough cleaning of both glass and PDMS surfaces was crucial to avoid contamination. The microfluidic mixer assembly was then completed and integrated into the experimental setup. It required three tubes: one to supply deionized water from a beaker to the micromixer's reservoir via a peristaltic pump, another to supply lipids and ethanol mixture from another beaker to the micromixer's reservoir, and a third tube to transfer the mixed liposome solution from the micromixer to a collection beaker.

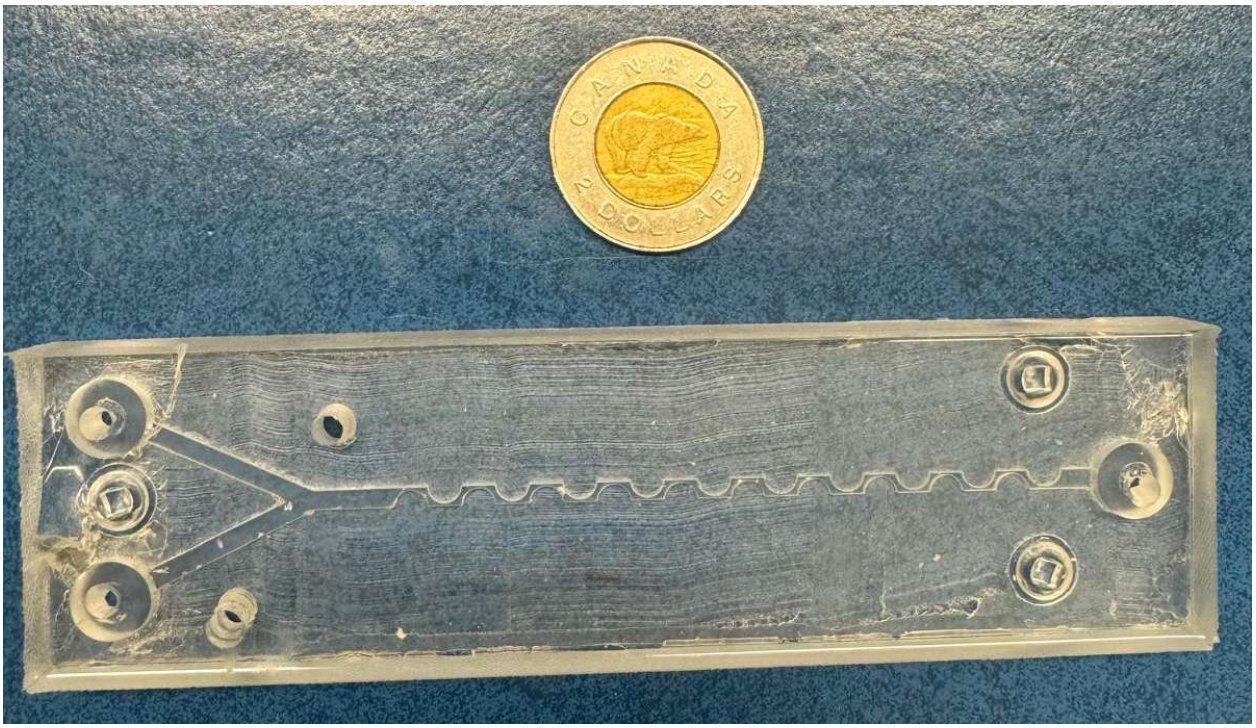

Figure 4.1: PDMS Millifluidic Device

Contrary to the simulation, the devices fabricated were upscaled by 2.75 times and 8.35 times to adapt to the manufacturing limitations. Even if the simulation was performed for different values,

there seems to be little to no difference in the mixing index shown in the previous chapter between both models. Thus, there remains confidence in the comparison of the simulation results with the experimental data to perform an overall assessment on the reproducibility of the reference work in enlarged devices.

During the pre-validation phase, the mixing devices had to be examined to ensure that they met the requirements for a trustworthy experiment. To do so, the devices were scrutinized under a digital microscope, more specifically the Keyence VHX-7000 model, which allowed the capture of high-resolution images of the mixing channels to inspect various data measurements. The data generated from the microscope would tell the story of the loops and their symmetry to reaffirm the validity of the manufacturing process. The straightness of the channel is important for proper comparison with the simulation results and the original work. A device with certain offsets could perturbate the results by influencing fluid velocity, shear stress or fluid flow. Figures 4.2 and 4.3 show the offsets of the centerline from the base line. Figure 4.2 shows the measurement of the minimum width in one of the periodic loops while also displaying visual information about the surface roughness. From the plotted data, differences can be assumed to be negligeable as similarities arose in the reference work. On top of verifying the consistency of the loops, it was also possible to measure the minimum opening inside the mixing channel, the converge of both inlet channels and even analyze the surface roughness at different locations. The level of zoom was adjusted to 5x, which allowed the extraction of quality images of the exposure area.

Tolerances for the negative molds were determined based on critical components of the mixers. Given that flow characteristics are influenced by the geometry of mixing channels and potential disturbances, these components were manufactured with increased tolerances. The finest tolerance

achievable was constrained by the 0.025mm resolution of the resin printer. Consequently, an inspection was conducted to verify the accuracy of the printing outcomes. Among the inspection

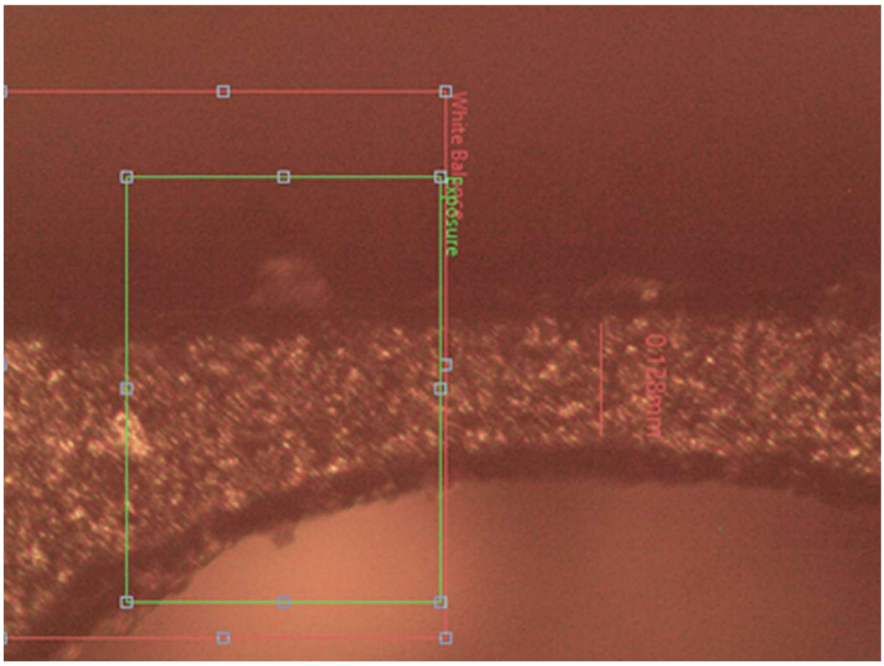

Figure 4.2: Minimum Width of Mixing Channel

findings, the most notable deviation from the original STL file was observed in the flatness of the prints. This warping issue was addressed by employing fasteners and a wooden brace, resulting in reduced warping to less than 0.13mm near the head screws and less than 0.25” at the edges. Other minor issues included slight bulging at the ends of disturbances, slight deviations in inlet angles, and increased surface roughness.

In Figures 4.3 and 4.4, the width inside the channels is measured with a digital microscope to verify that there no manufacturing errors in the structure. From Figure 4.3, there are disparities between each measurement of the periodic loops reaching up to 56µm, while the difference in the maximum and minimum values seen in Figure 4.4 is of 23µm. The error margin in the bigger device is much smaller. This can be due to manufacturing difficulties when dealing with distances of less than 1mm. The loops also seem to have some deformations in Figure 4.3, which is an

indication of a poor fabrication process and a big factor in the change of dimensions. Even though this will not affect the TFR, it will most definitely have an effect on the linear velocity in the loops, since they will be different from one to another, while also playing on the internal pressure and shear stress along the walls.

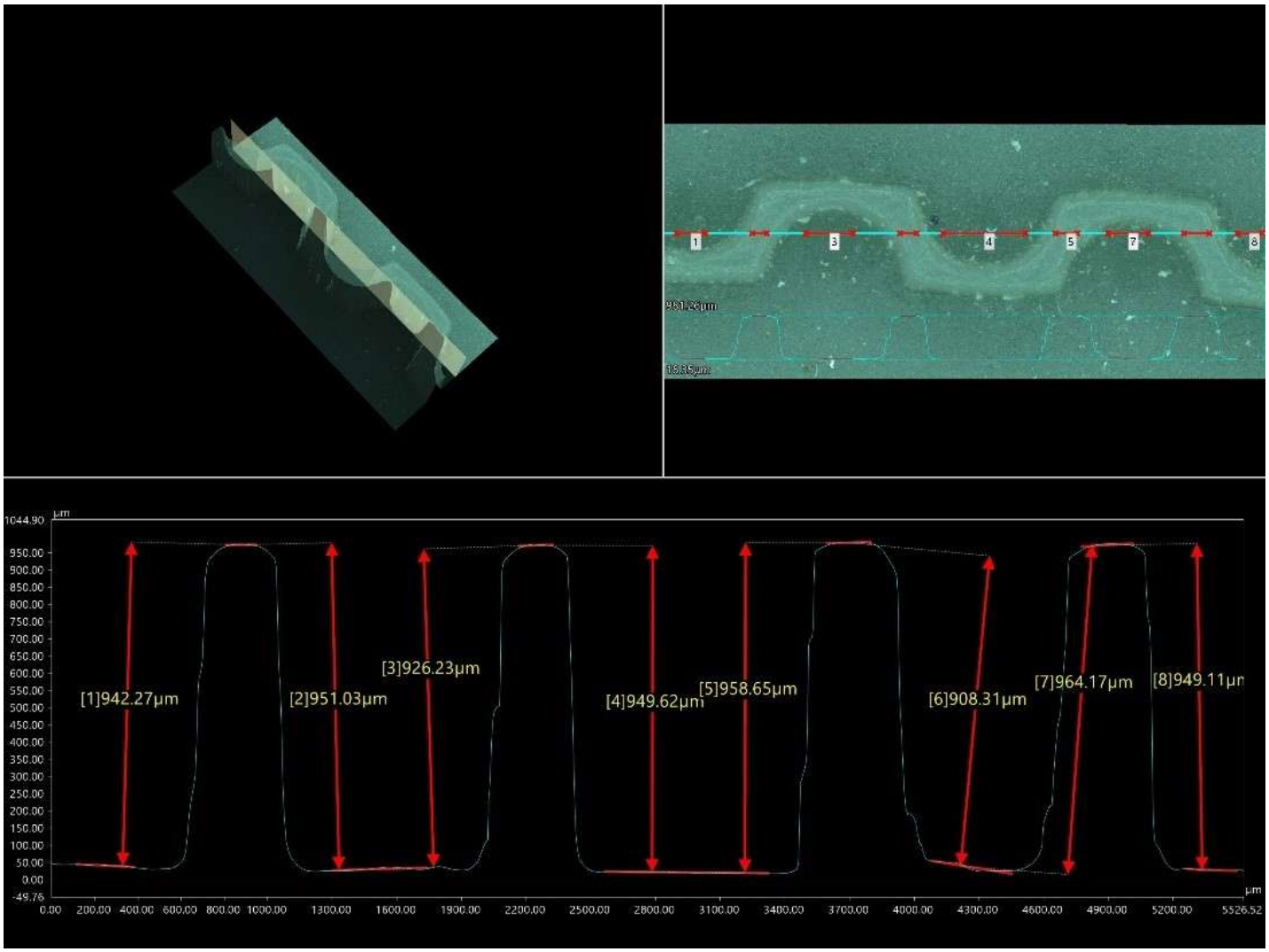

Figure 4.3: Inspection of 2.75x Mixer using VHX-7000 Digital Microscope

The inspection procedure employed a combination of calipers, micrometers, and microscope software to assess different aspects of the molds. Dimensions of significant size but with lower tolerance priorities were examined using a caliper with 0.01mm precision. More critical

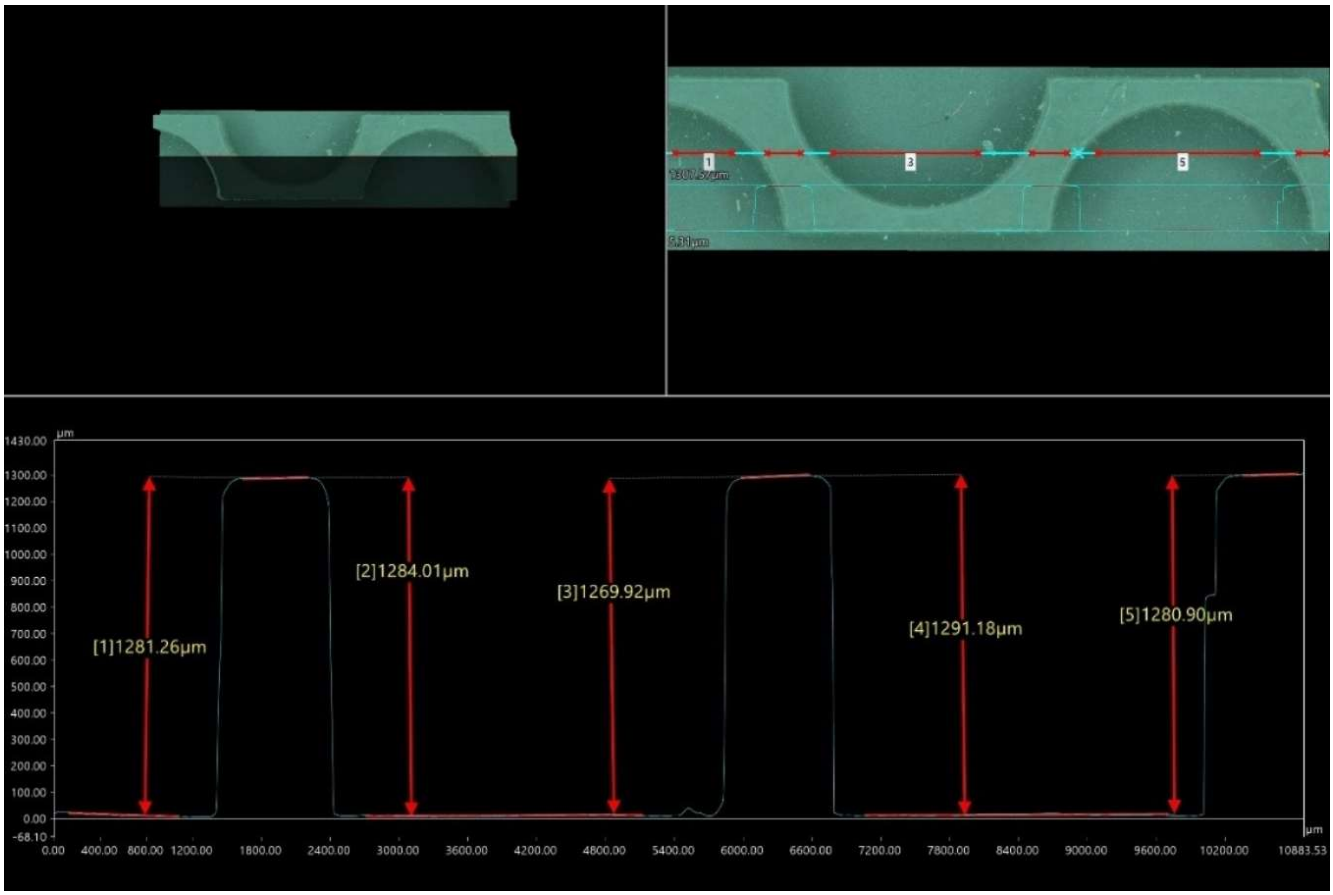

Figure 4.4: Inspection of 8.35x Mixer using VHX-7000 Digital Microscope

dimensions, which directly impacted flow characteristics and therefore demanded tighter tolerances, were measured with a micrometer offering 0.001mm precision. Key features requiring microscopic inspection, beyond the capability of manual tools, were analyzed using an electronic microscope equipped with AMscope software.

Following the inspection of the scaled-up PDMS and confirmation that all critical dimensions met specified tolerances, the team proceeded to validate the initial engineering analysis and design objectives. A subsequent phase involved re-evaluating the flow characteristics of the mixer to ensure several key aspects, such as verifying that the essential flow dynamics of the mixer closely approximate those of the reference device. Analysis of the predicted Reynolds number at nominal

TFR indicated laminar flow conditions while evaluation of the predicted Dean number at nominal TFR revealed values above 10, indicating the presence of Dean vortices.

Primary metrics included comparing maximum velocities in velocity fields, crucial for assessing similarity. These velocities typically occur at the narrowest points of channels, specifically at the crests of individual disturbances. Comparisons were made between their targeted maximum velocities and those predicted by COMSOL simulations using actual channel geometries, showing deviations from nominal dimensions with less than a 10% error as revealed in Table 4-1. An error margin of 10% is acceptable to perform the tests, but the error between the estimated velocity of both mixers is much higher, which makes it difficult to compare results.

Mixer	Target Velocity	Estimated Velocity	% Deviation
2.75x	1.21 m/s	1.09 m/s	-9.91 %
8.35x	1.21 m/s	1.32 m/s	9.09%

Table 4-1: Velocity Measured through Simulation and New Estimation

Also, calculations to estimate the Reynolds and Dean Numbers of both mixers were performed. Using approximations found in Table 4-1, new estimations were made and collected in Table 4-2 and Table 4-3.

De (Required)	De (Predicted)	Re (Required)	Re (Predicted)
>10	39.3	<2300	95.6

Table 4-2: Flow Characteristics of 2.75x Mixer

De (Required)	De (Predicted)	Re (Required)	Re (Predicted)
>10	225.5	<2300	615.2

Table 4-3: Flow Characteristics of 8.35x Mixer

Despite acknowledged challenges inherent to the resin printing process, all inspected components met the predefined tolerance criteria required for our purposes. To achieve even higher precision in molding, consideration of enhanced equipment or alternative machining techniques would be

necessary. Additionally, the inspection assumed that the results from the negative molds directly mirrored those of the final PDMS mixers, a reasonable assumption given that no material is lost during the curing process.

During validation, the setup was tested using only deionized water to verify proper functionality. Careful handling of components, adherence to clean workspace protocols, and operation within safe flow and pressure limits were crucial for the setup's reliability throughout the project duration. Following testing, the channels were slated for disposal. This comprehensive manufacturing process can be easily replicated by other research teams. If adapted for consumer use, other microchannel cleaning techniques would be essential for maintenance and reusability.

4.3 Testing and Validation

Testing encompassed three distinct phases, with the initial phase focused on pump characterization, particularly in the context of peristaltic pumps commonly used in milli-fluidic applications. The pumps employed included both 2.75x and 8.35x models. Each pump was integrated into the milli-fluidic circuit, where its performance was systematically evaluated. This involved setting the pumps to various gain levels and measuring the volume of fluid collected over specific time intervals. For each milli-fluidic mixer, this process was meticulously repeated three times to ensure consistency and accuracy in data collection. Subsequently, the collected data was analyzed to determine the flow rates corresponding to different pump gain settings. These findings were then graphed to establish a clear relationship between flow rate and pump gain, facilitating the derivation of a linear equation that quantitatively linked these variables.

In parallel with pump characterization, special attention was directed towards understanding the operational nuances of peristaltic pumps within the milli-fluidic environment. Peristaltic pumps, known for their gentle handling of fluids and precise control over flow rates, played a pivotal role

in the experimental setup. Their ability to deliver reliable and consistent flow rates across varying gain levels was crucial for the accuracy and reproducibility of the tests conducted. The integration of peristaltic pumps in milli-fluidic systems is notable for its capability to accommodate small volumes of fluids with minimal shear stress, which is vital for preserving the integrity of sensitive biological or chemical samples. This feature underscores their suitability for applications where precise fluid handling is required.

On top of the two peristaltic pumps, the design of the testing rig, as seen in Figure 4.5, included ¼" tubes that would connect two reservoirs containing to their respective pump, one containing water while the other holds the ethylic solution. From the pumps, tubes would feed each solution into their respective inlet within the milli-fluidic mixer where mixing would occur and output the solution containing the liposomes into a collector reservoir.

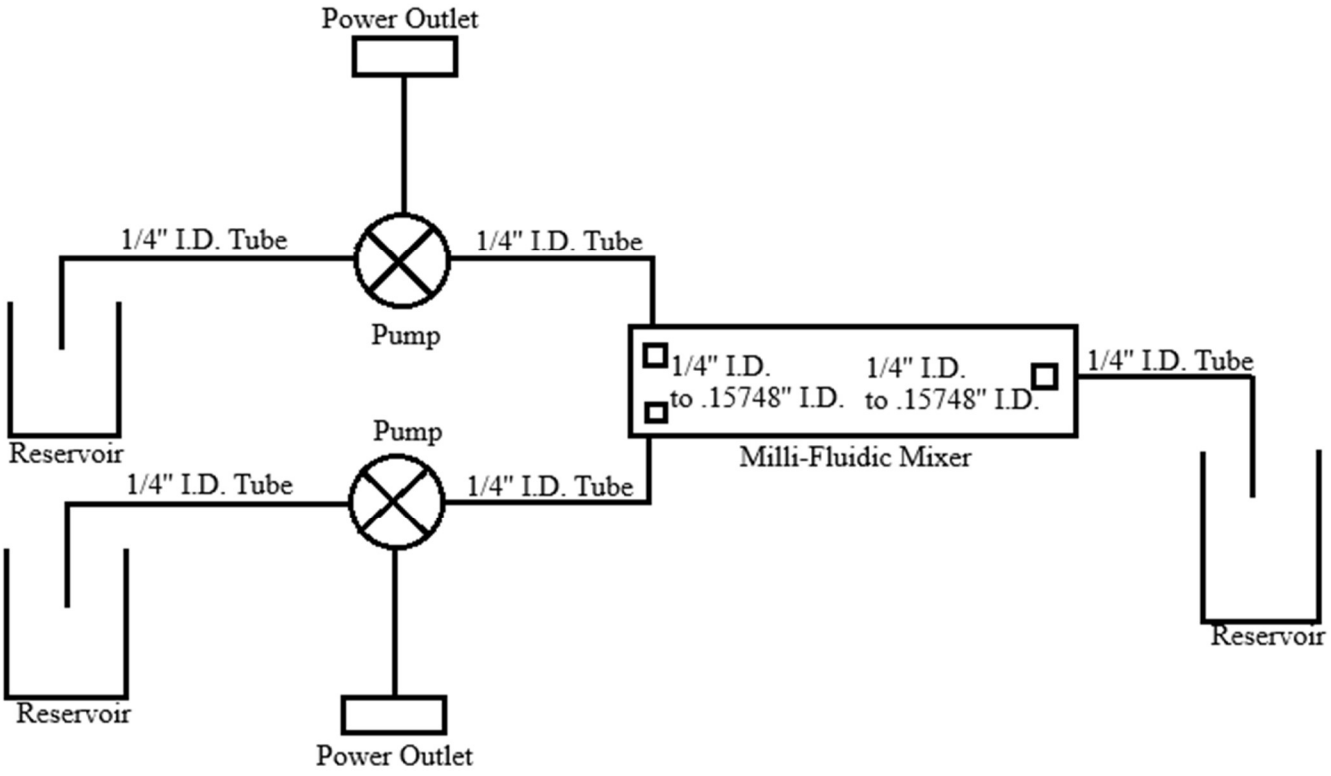

Figure 4.5: Design of Test Bench

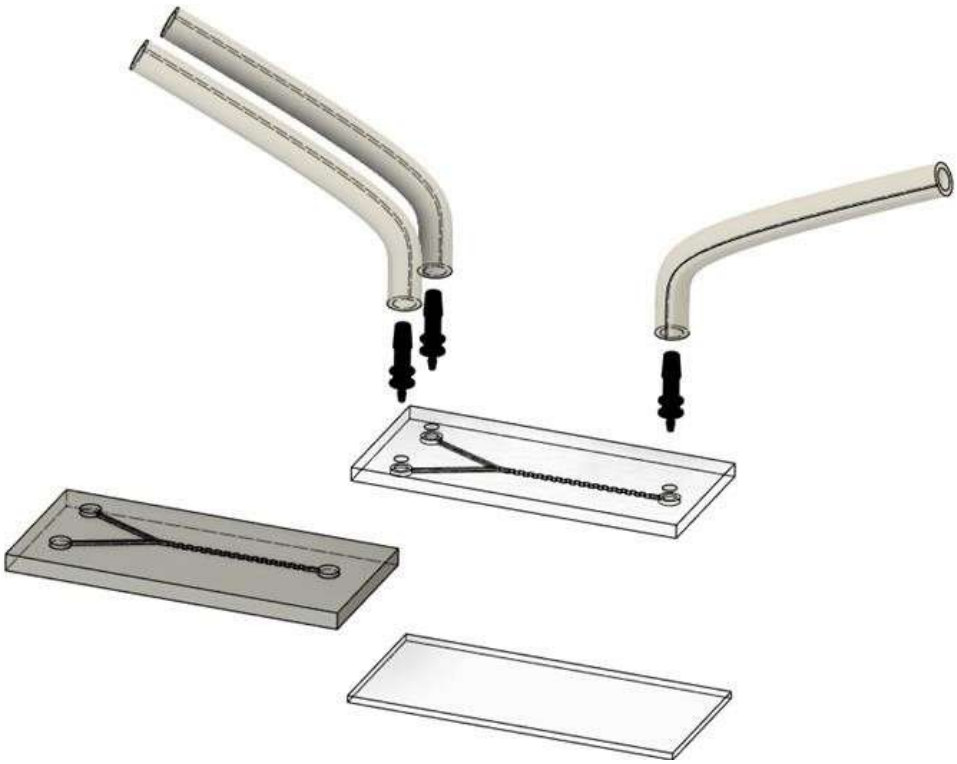

Figure 4.6: 3D Representation of Milli-Fluidic Mixer

The design of the millifluidic mixer represented in 3D can be seen in Figure 4.6, which shows an exploded view of the components connected to the millifluidic device. The tubing linked to and from the millifluidic device are connected to the pumps and collectors, as shown in the design represented by Figure 4.5. A picture of the entire testing setup was taken to be shown in Figure 4.8 and a better view of the connections on the millifluidic device can be seen in Figure 4.7.

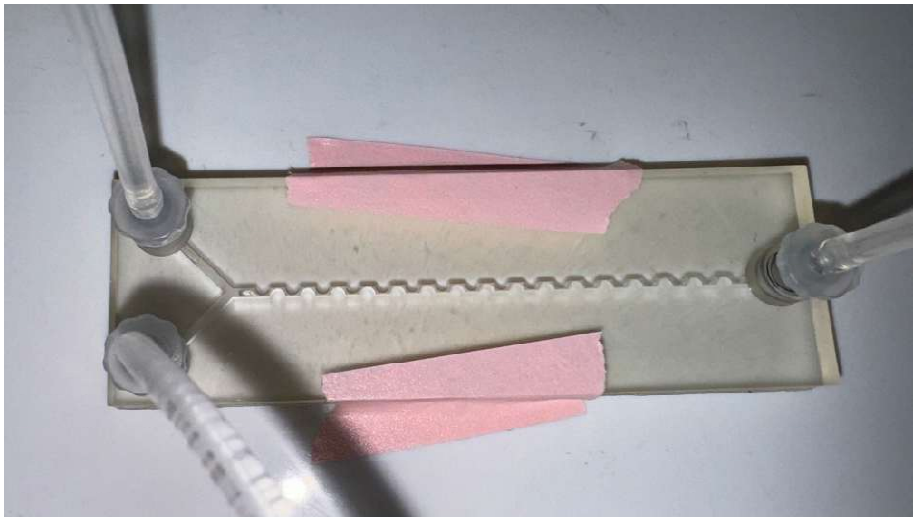

Figure 4.7: Tube Connections with Millifluidic Device

Figure 4.8 shows the visual representation of Figure 4.5. The millifluidic device had tube connections to its inlets and outlet to conduct the fluid to and from the components as shown by represented in Figure 4.7.

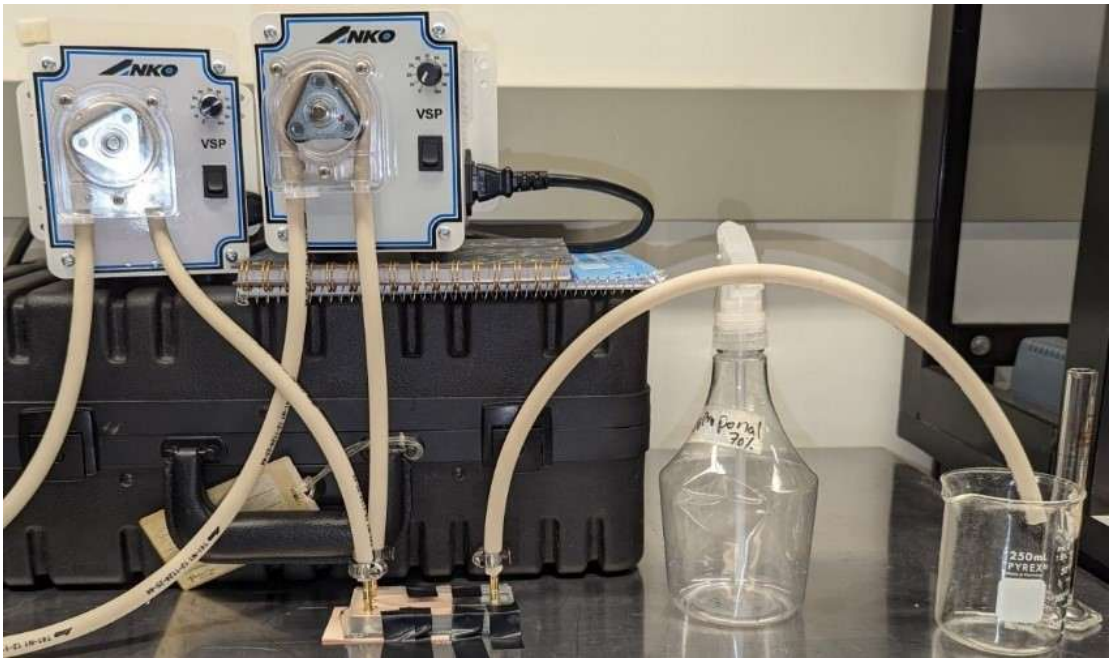

Figure 4.8 : Test Bench in Laboratory

By systematically characterizing and understanding the behavior of peristaltic pumps under controlled conditions, the team not only validated their operational parameters but also established a foundational understanding essential for subsequent phases of experimentation. This meticulous approach ensured that the pumps' performance met the demands of milli-fluidic applications, setting a reliable precedent for further investigation and development in the field.

To begin collecting measurements, the pumps first had to calibrated and tested to understand the volume of fluid pumped according to the power gain control while avoiding saturation. Table 4-4 shows measurements until 40% gain value, which was the maximum flow the smaller device could handle without increasing the pressure differential and causing the tubes to stretch.

Power [Gain Value]	Time Elapsed [s]	Fluid Volume Collected [mL]	Flow Rate [mL/s]	Flow Rate [mL/h]
15	207.54	7.2	0.0347	125
20	90.36	4.6	0.0509	183
30	48.33	6.0	0.124	447
40	38.72	6.4	0.165	595
50	-	-	-	-
60	-	-	-	-
70	-	-	-	-
80	-	-	-	-
90	-	-	-	-
100	-	-	-	-

Table 4-4: Trial Run on 2.75x Mixer

Power [Gain Value]	Time Elapsed [s]	Fluid Volume Collected [mL]	Flow Rate [mL/s]	Flow Rate [mL/h]
15	154.26	5.0	0.0324	117
20	74.84	6.0	0.0802	289
30	51.12	7.6	0.149	535
40	25.05	6.8	0.271	977
50	17.19	6.4	0.372	1340
60	13.57	6.8	0.501	1800
70	11.89	6.8	0.572	2060
80	10.61	7.0	0.660	2380
90	11.08	7.8	0.704	2530
100	10.00	7.2	0.720	2590

Table 4-5: Trial Run on 8.35x Mixer

The second phase focused on evaluating FRR to achieve specific TFR of 600 mL/h and 1800 mL/h for the 2.75x and 8.35x mixers, respectively. This step is crucial in microfluidics transitioning to milli-fluidics, where precise control over flow rates becomes increasingly critical. Dr. Salazar's thesis underscores the importance of these ratios in optimizing liposome production, testing ratios of 1, 2, 4, and 8 with varying outcomes. This comprehensive approach was driven by both pump capabilities and desired experimental results. Figures 4.9 and 4.10 show how the power gain value adjusted on the peristaltic pumps affected the total flow rates outputted by the same pumps. The

change of signal shows a relation that is not exactly linear, which may have led to inaccuracy recorded in Table 4-6 and Table 4-7.

In the realm of microfluidics, the transition to milli-fluidics necessitates meticulous testing of Flow Rate Ratios. These ratios dictate how fluids are mixed and delivered within microchannels,

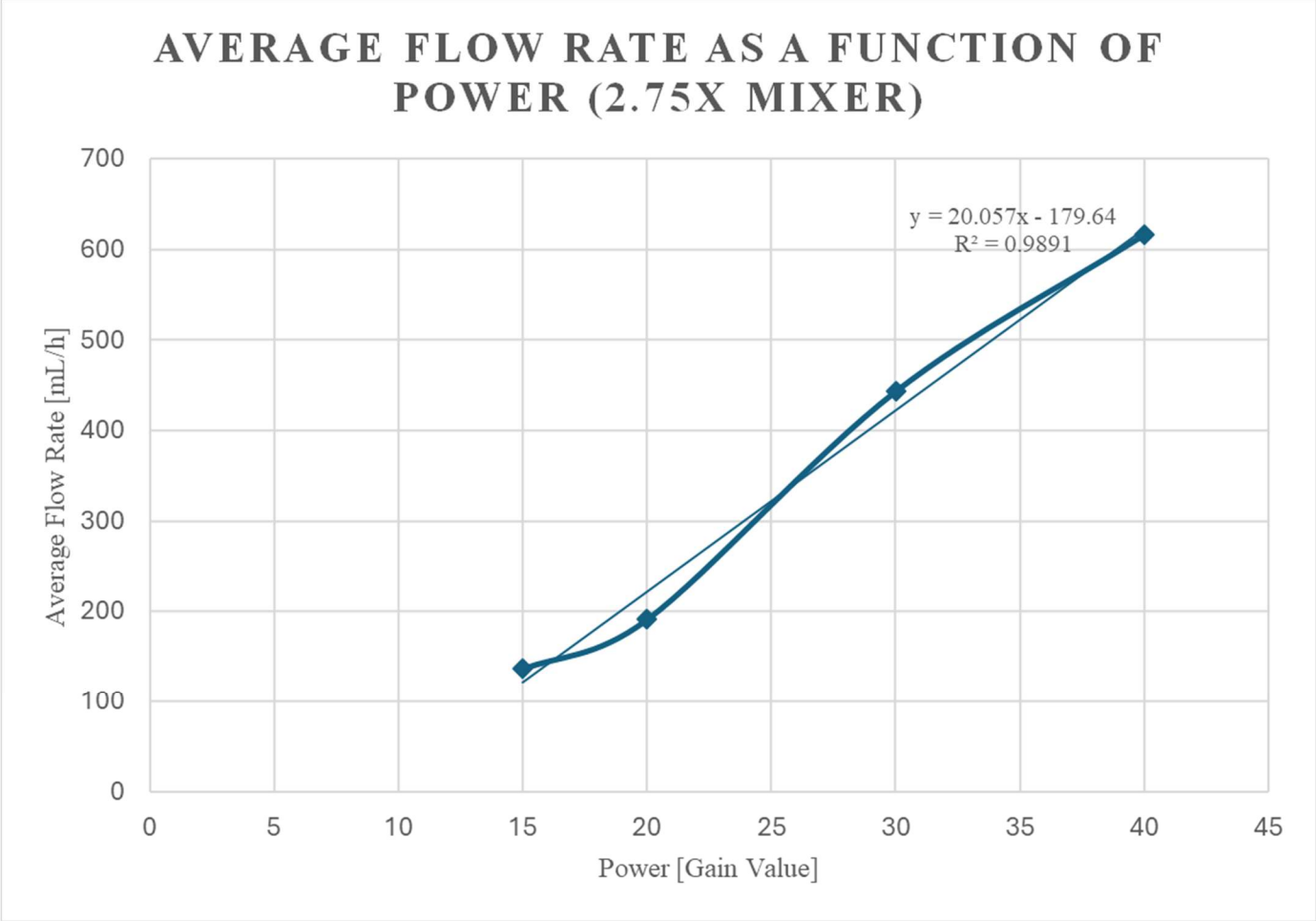

Figure 4.9 : Average Flow Rate Controlled by Power Gain in 2.75x Mixer

influencing processes such as particle encapsulation, droplet formation, and chemical reactions. Each ratio configuration impacts the overall flow dynamics and residence times of substances within the system, crucial for achieving reproducible experimental outcomes.

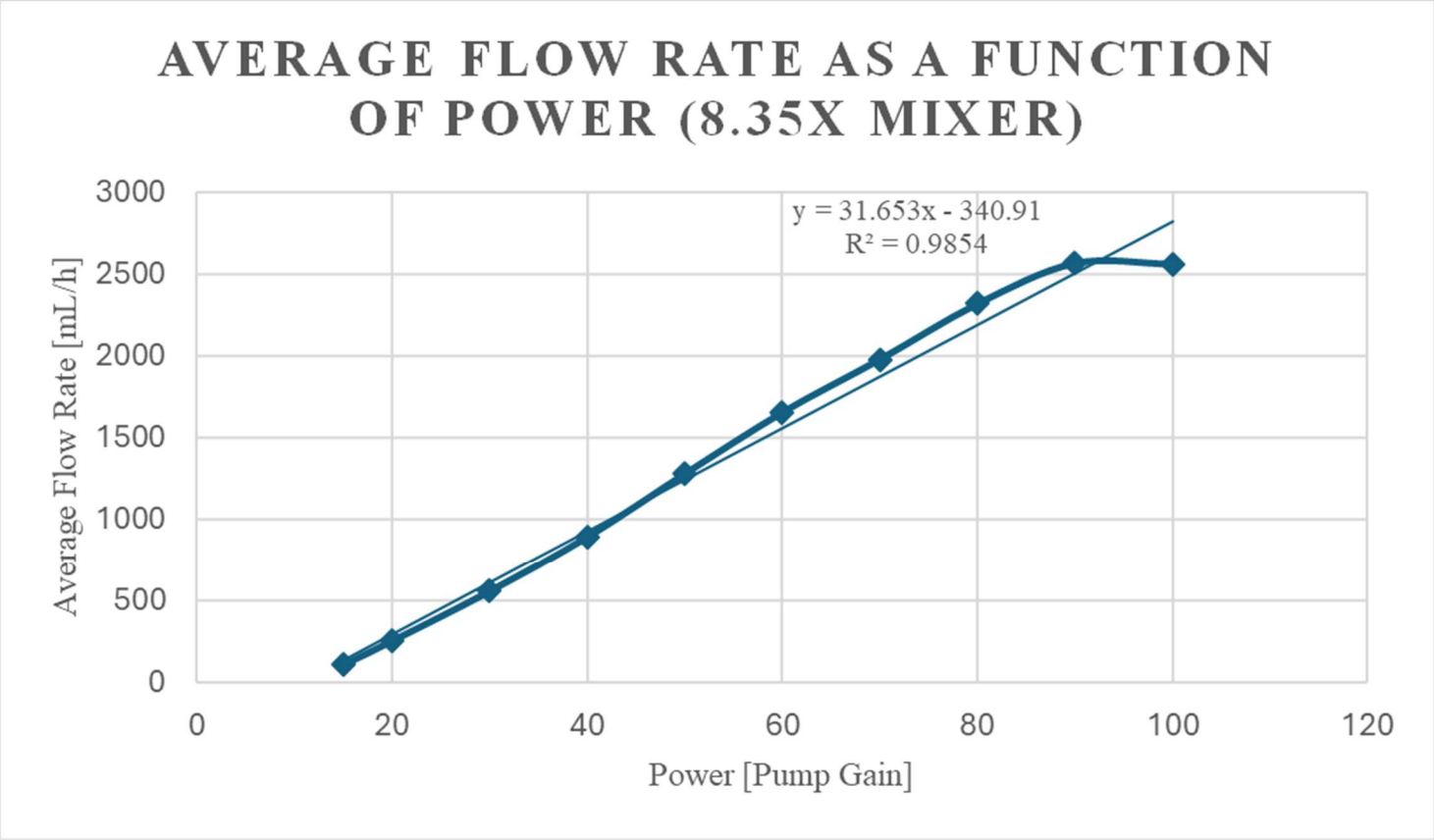

Figure 4.10: Average Flow Rate Controlled by Power Gain Value in 8.35x Mixer

Typically, experiments begin with a range of FRR to identify optimal conditions that yield the desired TFR while maintaining precise control over fluid delivery. This iterative process involves adjusting pump settings and observing how changes in ratios affect the performance metrics relevant to the specific application, whether it's drug delivery, biochemical assays, or material synthesis. For instance, in liposome production, where the encapsulation efficiency and size distribution of liposomes are critical factors, selecting the right Flow Rate Ratio ensures uniform mixing of lipid components and aqueous phases. The ability to fine-tune these ratios using peristaltic pumps allows the optimization of the process parameters and achieve consistent liposome characteristics across different experimental runs. Moreover, understanding the relationship between FRR and TFR is fundamental for scaling up microfluidic processes to milli-

fluidic levels. This scaling process involves not only increasing the volume throughput but also maintaining the precision and efficiency inherent to microfluidic systems.

Pump 1 Gain	Pump 2 Gain	FRR	Time Elapsed [s]	Fluid Volume Collected [mL]	Flow Rate [mL/s]	TFR [mL/h]	Error
39	39	1	19.53	8.9	0.456	1640	8.9
48	29	2	21.54	9.8	0.455	1640	9.0
56	22	4	15.85	8.2	0.517	1860	3.5
61	17	8	17.05	8	0.469	1690	6.2

Table 4-6:TFR Readings of Tests on 8.35x Mixer

Pump 1 Gain	Pump 2 Gain	FRR	Time Elapsed [s]	Fluid Volume Collected [mL]	Flow Rate [mL/s]	TFR [mL/h]	Error
24	24	1	52.23	7.5	0.144	517	13.8
28	18	2	62.57	8.2	0.131	472	21.4
32	15	4	55	7.6	0.138	498	17.1
36	12	8	68.44	8.2	0.120	431	28.1

Table 4-7: TFR Readings of Tests on 2.75x Mixer

In the third phase of testing, the focus shifted to verifying the mixing efficiency within the milli-fluidic mixers using dye visualization. This method involved assessing the mixing performance across various Flow Rate Ratios. Specifically, Flow Rate Ratios of 1, 2, 4, and 8 were examined, maintaining constant flow rates of 180 mL/h and 1800 mL/h per respective mixer size (representing ratios of 2.75x and 8.35x, respectively).

To conduct the test, two distinct colored dyes, blue and yellow, were introduced into each inlet of the mixers. The goal was to observe how well the mixing occurred within the device as the dyed

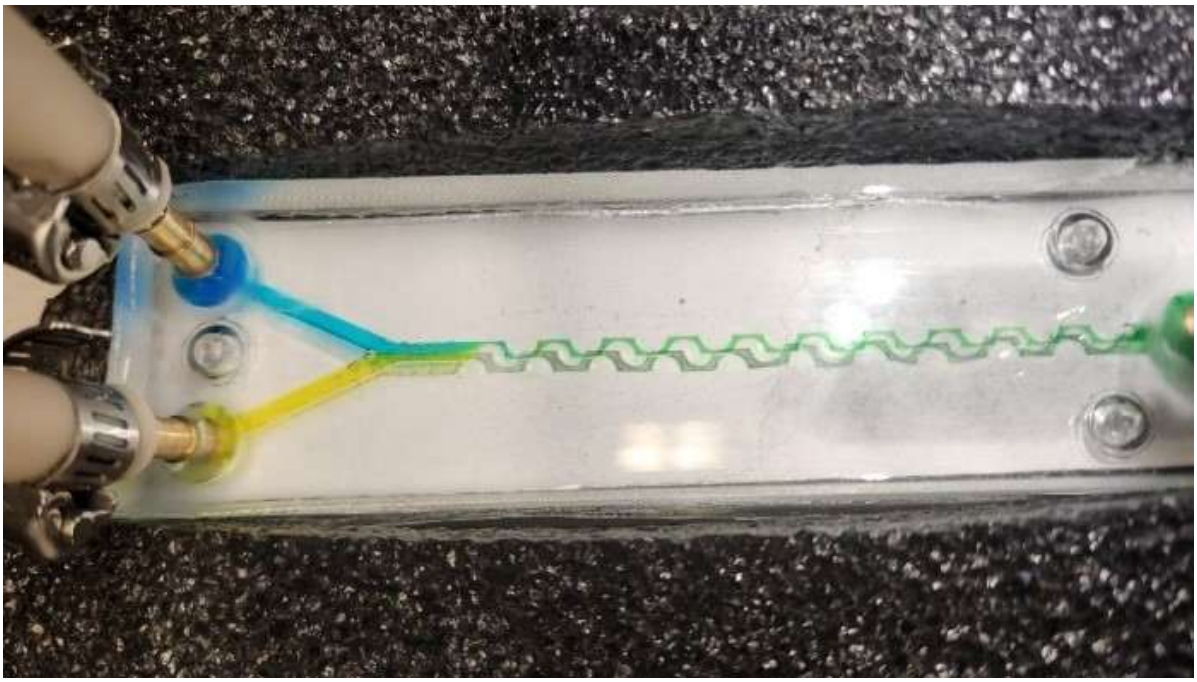

Figure 4.11: Mixing Test using Food-Grade Colorant

fluids interacted to give a mixed green solution. This approach allowed for a visual inspection of the mixing dynamics under controlled conditions. With this approach, it was possible to estimate if the number of periodic loops necessary to achieve satisfactory mixing was similar to the number found in simulation. Of course, it is hard to evaluate at the naked eye, but a clear distinction between the blue and yellow dyes can be observed in the first 2 loops, which means that good mixing was achieved starting at the 3rd loop as measured in the simulation. The choice of different dye colors served to enhance the clarity of the mixing process, enabling easier tracking and visualization of how the fluids blended within the mixers. By recording and closely observing the movement and blending patterns of the dyed fluids, it is possible to infer the effectiveness of mixing at various flow rate ratios. This methodological approach not only provided qualitative insights into the mixing behavior but also offered a comparative analysis across different operational conditions of the mixers.

From Figure 4.9, the milli-fluidic device can be seen undergoing preliminary testing using food grade colorant to ensure that mixing occurs as expected. Following successful trials, the mixing devices were applied as initially intended by running multiple trials at 180 ml/h, 600 ml/h and 1800 ml/h in both devices for FRR values of 1,3 and 5.

4.4 Results

Following the tests performed on both milli-fluidic mixers, the reservoir used to collect the output solution was sent for examination. Results yielded different characteristics of the solution and the liposomes produced, such as Zeta potential, liposome dimensions and PDI. All tests were performed at room temperature of 25°C.

Figure 4.12: Average Liposome Diameter Produced in 2.75x Mixer

The Z-average represents the average size of the produced liposomes under various experimental conditions.

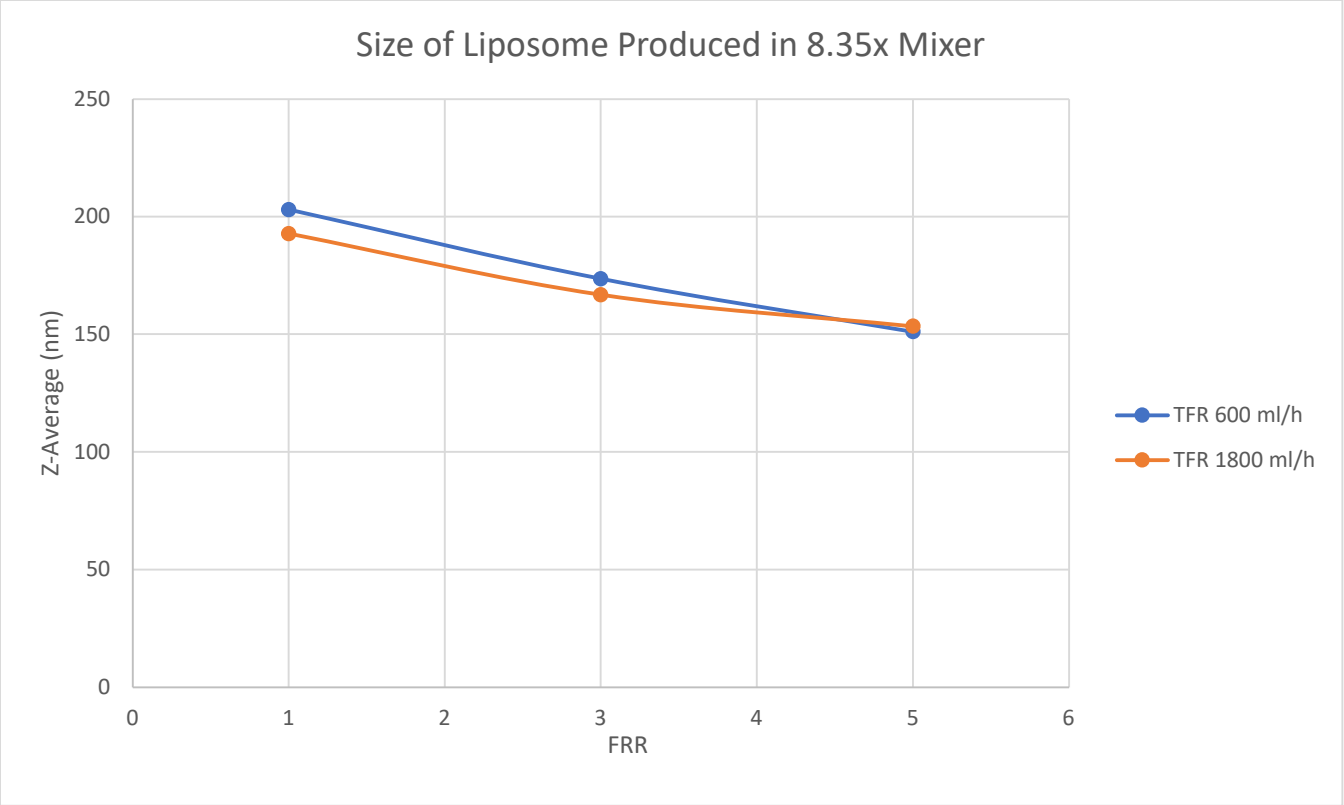

Figure 4.13: Average Liposome Diameter Produced in 8.35x Mixer

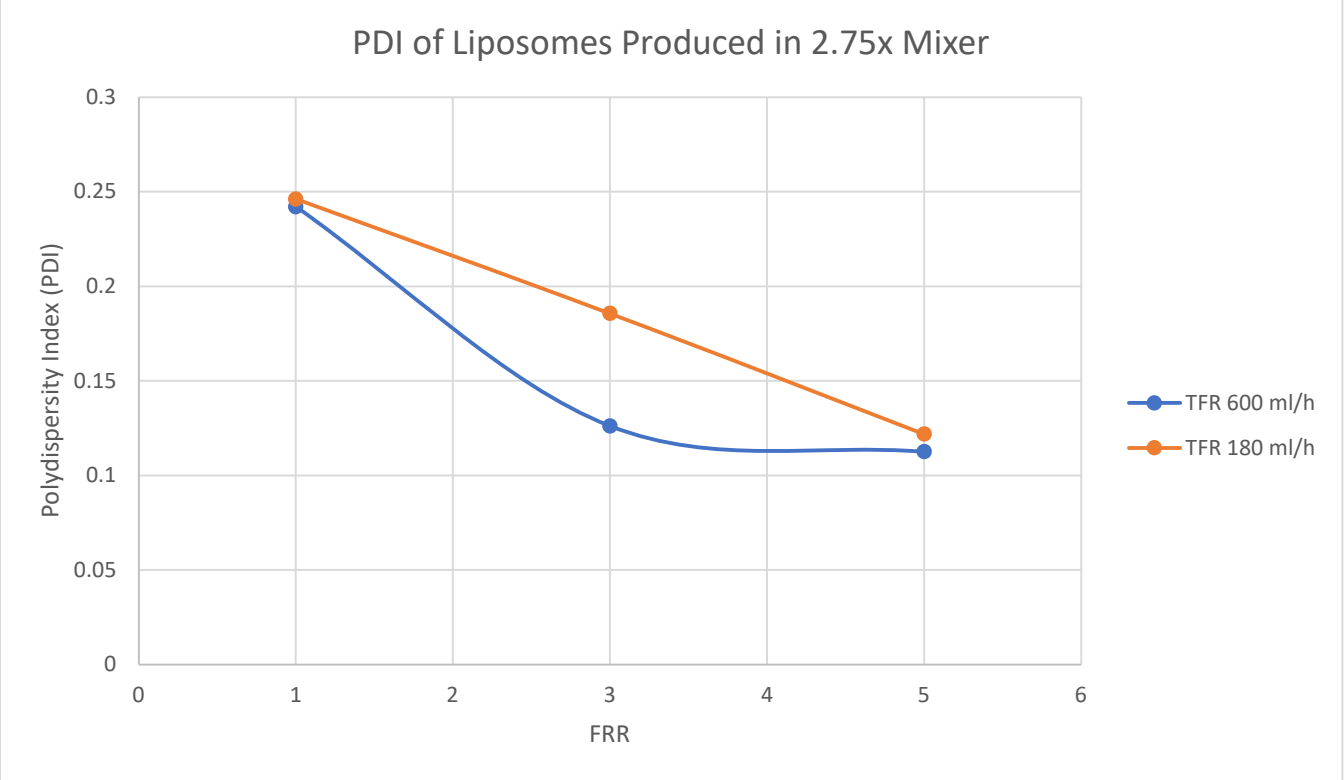

Figure 4.14: PDI of Liposomes Produced in 2.75x Mixer

Additionally, the Polydispersity Index (PDI) is a measure of the distribution of molecular mass in a given sample. For liposomes, it indicates the uniformity of their size distribution. The Zeta potential of the liposomes, measured in mV, refers to their ability of maintaining their structural integrity and size distribution over time and under various conditions. Typically, a value over 30mV and under -30mV ensure great stability and provide sufficient confidence that the encapsulated contents within the liposomes will not be lost (Ruben Salazar, 2020).

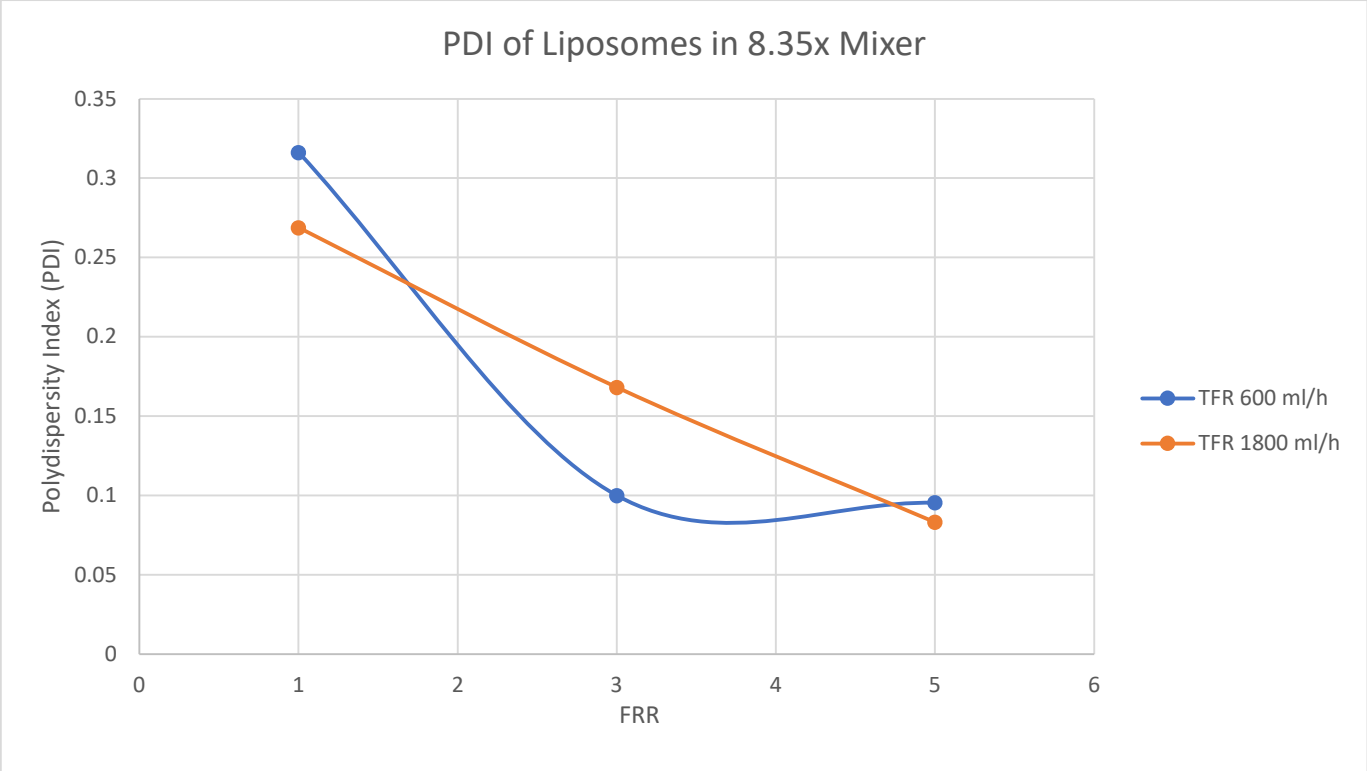

Figure 4.15: PDI of Liposomes Produced in 8.35x Mixer

All measurements were performed three times per sample. The values for liposome size, including Z-average and dispersity, as well as the surface charge indicated by zeta potential, were calculated by averaging the three measurements.

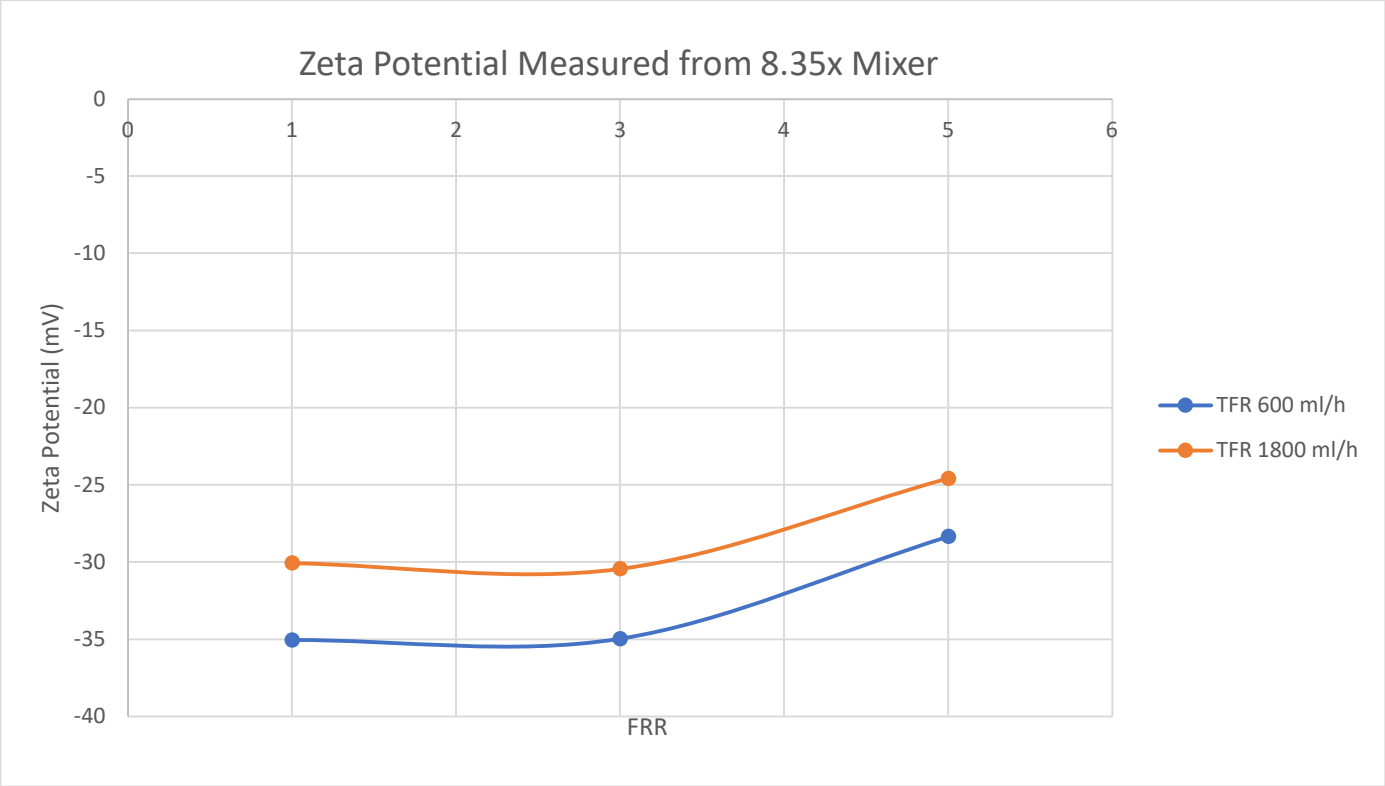

Figure 4.16: Zeta Potential of Solution Produced in 8.35x Mixer

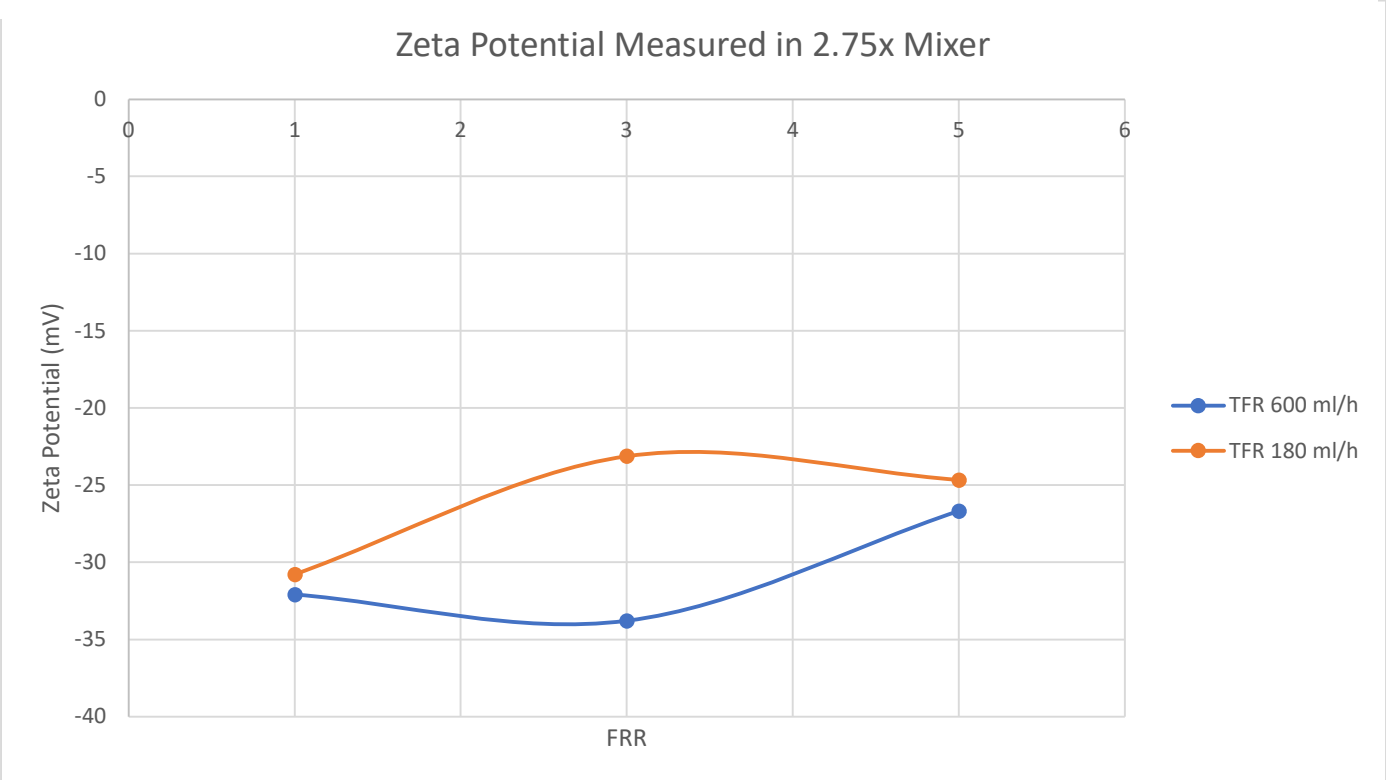

Figure 4.147: Zeta Potential of Solution Produced in 2.75x Mixer

Figures 4.12 and 4.13 show a linear downtrend in liposome diameter as the FRR increases. It seems that TFR also plays a role in ensuring the production of a small diameter. However, as the FRR increases, it seems that the contribution of TFR to that objective becomes negligeable.

The uniformity of the Z-average is measure by the PDI, which is a quality control parameter that describes how liposomes are monodispersed. A value closer to 0 shows better results, typically below 0.1, which is the case in Figures 4.14 and 4.15 at higher TFR and FRR values for both mixers. As the TFR is the same for both mixers, there seems more positive results in the 2.75x mixer, which may directly be related to the higher velocity and pressure within the device's channels.

In Figures 4.16 and 4.17, the plotted zeta potential shows different behavior when comparing both mixers. As the FRR increases, the zeta potential approaches 0 in both mixers. However, an increase in TFR benefits the zeta potential readings in the 2.75x mixer rather than the 8.35x mixer, indicating stronger electrostatic repulsion between particles under those conditions. A higher absolute value of zeta potential, typically higher than 30mV or lower than -30mV, means higher stability of the liposomes by ensuring dispersion and preventing aggregation (Ruben Salazar, 2020).

To validate the results measured in the laboratory, data obtained must be compared with the reference work and evaluate the margins between the two. Considering that testing conditions were not the same, there could be some improvements to eliminate sources of error.

4.5 Data Analysis

Results obtained from the experiments can be analyzed to validate the hypothesis. To do so, an extensive comparison between the work done and the reference study must be established to

understand where the data differs. That way, errors can easily be found and improvements noted down for later experiments.

4.5.1 Comparison with Reference Work

When looking back at the reference study, there are some factors that were used parametrically, but were not considered in this experiment in an effort of aligning the tests with the idea that linear velocity plays the most vital role in mixing efficiency. Those different factors would in turn have a direct effect on the Z-average, the PDI and the Zeta potential of the liposomes produced.

4.5.1.1 Z-Average of Liposomes

The reference experiment details the results for the Z-average of liposome sizes, focusing on how various production parameters influence the average particle size. The Z-average, or the mean hydrodynamic diameter of the liposome particles, was measured using DLS. A picture can be found in Appendix 3 of the measurements done using DLS. The study explored the impact of different TFR and FRR on the Z-average of the produced liposomes. The results showed that these flow parameters significantly affect the average size of the liposomes. Higher TFRs generally resulted in smaller liposomes due to the increased shear forces that facilitate the formation of smaller particles. Conversely, lower TFRs produced larger liposomes, indicating that the flow dynamics within the microfluidic device are a critical factor in controlling liposome size. The observed Z-average values for the liposomes ranged from approximately 60 nm to 150 nm, depending on the specific settings of the TFR, FRR, and lipid concentrations.

In comparison, the yielded results from the experiments done on both milli-fluidic devices show some similarities in the observations but with differences in the final range of measurements. Similarly, FRR and TFR affected the Z-average trend similarly where both the increase in TFR and FRR would decrease the diameter size of the liposomes. However, the average size of

liposomes produced in the milli-fluidic mixers vary between 150nm to 200nm. The minimum size produced is not close to what could have been achieved.

4.5.1.2 Polydispersity Index of Liposomes

PDI is a critical metric in liposome characterization, indicating the degree of homogeneity in particle size distribution within a sample. Lower PDI values denote more uniform particle sizes, which are essential for consistency and stability in applications such as drug delivery. The study reveals that TFR and FRR significantly affect the PDI of liposome samples. Higher TFRs generally result in lower PDI values, indicating more uniform liposome sizes. This outcome is due to the increased shear forces at higher flow rates, which promote the formation of liposomes with consistent sizes. In contrast, lower TFRs lead to higher PDI values, suggesting greater variability in liposome sizes. These findings highlight the importance of optimizing flow rates to achieve the desired uniformity in liposome production. The observed PDI values in the reference study range from approximately 0.1 to 0.3, depending on the specific settings of TFR, FRR, and lipid concentration. Values below 0.2 are generally considered indicative of monodisperse systems, while values above 0.3 suggest higher polydispersity and potential instability. Most optimized conditions yielded PDI values in the range of 0.1 to 0.2, indicating a narrow size distribution and high-quality liposome preparations (Ruben Salazar, 2020).

In the milli-fluidic devices, experiments show that the PDI ranges between 0.1 and 0.25 for the 2.75x mixer, while the PDI increases up to 0.3 in the 8.35x mixer. As mentioned in the reference thesis, the shear stress on the walls of the microchannels plays a key role in the consistency of liposomes' sizes, which is defined by the pressure within the device. For a larger mixing device, it is therefore normal to observe an increase in PDI.

4.5.1.3 Zeta Potential of Liposomes

Zeta potential was measured for various liposome samples to assess their stability in suspension. This measurement is crucial as it indicates the degree of electrostatic repulsion between similarly charged particles. High absolute zeta potential values, whether positive or negative, signify strong electrostatic repulsion, which is essential for maintaining stability by preventing particle aggregation. Stable dispersions are critical for ensuring the consistent performance and effectiveness of the liposomes in their intended applications. The measured zeta potential values for the liposome samples in the reference experiment were predominantly around -47 mV. This high negative value suggests robust electrostatic repulsion among the liposomes. Typically, zeta potential with an absolute value larger than 30mV indicate high electrostatic repulsion (Ruben Salazar, 2020).

In contrast with the results obtained from the larger mixers, the values of zeta potential obtained range from -25mV to -35mV, which indicates good stability. As shown in Figures 4-14 and 4-15, an increase in FRR typically affects the electrostatic potential measured by approaching values towards 0. Both figures indicate the same results, except for the behavior in TFR. It seems that increasing TFR also increases the zeta potential, until the limit is breached. This observation suggests an equilibrium point where the TFR value would be optimal to maximize the potential.

Evidently, there are large discrepancies between the experiments conducted on the upscaled models and the reference experimental results. For the sake of comparison, some parameters were not controlled to potentially affect the results, as opposed to the reference work. This was done purposely to focus on the effect of linear velocity within the channels.

4.5.2 Sources of Error

Following the comparison between this experiment and its reference, some sources of error have been noted down as potential for the error margin. It was observed that the peristaltic pumps had a significant margin of error between the TFR outputted and desired when adjusting the power control gain. Also, the reference work conducts a study to optimize liposome size by adjusting the concentration of lipids in the ethylic solution, which was not done in this case.

4.5.2.1 No Change in Lipid Concentration

In this study, evaluating the effects of linear velocity within the channels was the main focus. To increase the velocity and consequently the mixing time, the TFR was played with to conjugate he desired effect within the channels. Simultaneously, the FRR was also analyzed by adjusting the power gain control on the peristaltic pumps. Controlling both the TFR and FRR would have a direct effect on the velocity and pressure of the fluid within the devices' channels. The results obtained would then be compared with the reference work. However, some great differences were seen in some cases.

Since the lipid concentration was not modified in the ethylic solution prior to mixing, values of PDI and Z-Average were objectively worse in this experiment. The Z-Average, representing the mean hydrodynamic diameter of the liposomes, increases with higher lipid concentrations. This occurs because a greater amount of lipid material leads to the formation of larger liposomes. As more lipids are available, the vesicles can encapsulate more material, resulting in larger average sizes. Higher lipid concentrations also tend to increase the PDI values. PDI measures the uniformity of particle sizes within a sample, with lower values indicating more uniform sizes. An increase in lipid concentration can lead to a broader distribution of liposome sizes due to the

formation of a more varied population of vesicles, thereby increasing the PDI. This broader size distribution may reflect the presence of both larger aggregates and smaller liposomes.

4.5.2.2 Lack of Accuracy in Pumps

Adjusting the power gain control on the peristaltic proved to be hectic, as no matter how the knobs were adjusted, the TFR never seemed right. As shown in Table 4-7, the error margins are very high, typically over 20%, when comparing the desired TFR and the real output. In consequence, some results seemed to display bizarre trends, as the TFR and FRR are crucial to the proper realization of the experiment. As stated in the reference work, higher TFRs are associated with smaller Z-average values and lower PDI. Increased flow rates enhance shear forces, leading to the formation of smaller liposomes. Without proper control over the direct output of the pump into the inlet, some fluid would be lost in the rotational displacement of the pump, thus accounting for the marginal error calculated.

Additionally, since silicon tubes were used in the test setup, some losses may have played a part in the error margins. When using peristaltic pumps, losses in silicone tubes can be significant due to factors like wear and tear from continuous compression, chemical compatibility issues, and the effects of flow rate and pressure. The constant mechanical action can lead to material fatigue, and the pulsatile nature of peristaltic pumps can introduce additional stress, potentially causing microcracks or leaks over time. Ensuring chemical compatibility between the fluid and the tubing material prevents premature degradation, and operating the pump within recommended flow rate and pressure ranges minimizes stress on the tubes. Additionally, employing pulse dampeners can reduce pulsation and extend tube life. By addressing these factors, the efficiency and reliability of peristaltic pumps can be maintained, even in demanding applications. The low cost of silicon tubes remains the only advantage of its usage (Bahal & Romansky, 2002).

CONCLUSION

Summary

In conclusion, numerical simulation was performed in COMSOL Multiphysics to investigate the hypothesis that velocity inside the channels would result in quicker mixing time between the ethylic and aqueous solutions when mixing and produce nanosized liposomes similar to the ones fabricated in the reference work. Following good simulation results, the equipment and materials were purchased, which allowed the fabrication of the milli-fluidic mixers and setting up the testing rig. During testing, some problems were encountered with calibrating the power gain controls of the peristaltic pumps, which resulted in large deviations from the desired TFR output. Simulation results were confirmed prior to testing by running trials using food grade colorant in order to validate the mixing plots that were obtained. Following the experiment, the output solution was collected and analyzed in laboratory using DLS to measure Z-Average and PDI. It was found that the Z-Average ranged between 150nm to 200nm for the liposomes fabricated in both the 2.75x and 8.35x mixers. The lower values would correspond to higher FRR and, in some cases higher TFR, which contributed to minimizing the liposome diameter. Also, PDI values ranged between 0.3 and 0.1 with values dispersed evenly, while the Zeta Potential ranged between -25mV and -35mV. The reference experiments should Zeta Potential of -47mV, PDI ranging between 0.1 and 0.2 with a Z-Average of 52nm to 200nm. Objectively, the results obtained in the reference experiments are better for many reasons, such as better equipment during testing and the use of alternative methods to affect the final results like modifying the lipids concentration in the ethylic solution. In comparison with the reference work, the values obtained are not satisfactory, but do help understand that the project is feasible under certain conditions.

Future Work

To improve the overall results, numerical simulation in COMSOL Multiphysics should focus on achieving similar or higher pressure than what was extracted in the reference project. Focusing on pressure would simultaneously increase the TFR and therefore also increasing linear velocity of the fluid within the channel. In fact, a higher pressure would induce higher shear stress along the walls, which was proven to help reduce the Z-Average.

It would be relevant to calibrate the pumps in a manner minimizing the error margins of TFR between the desired and outputted value by finely tuning the power control gain. Although, some of the blame could be put on the silicon tubes, which would in turn need to be replaced with higher quality tubing in an effort to reduce losses. This would create a better testing environment, allowing proper evaluation of the different factors that influence the size of liposomes during their production while also recording the true weight they hold.

References

Anwekar, H., Patel, S., & Singhai, A. (2011). Liposome- as drug carriers. Bhopal: International Journal of Pharmacy & Life Sciences.

Bahal, S., & Romansky, J. (2002). *Spalling and Sorption of Tubing for Peristaltic Pumps.* Pharmaceutical Development and Technology.

Barenholz, Y. (2001). *Liposome application: problems and prospects.* Jerusalem: The Hebrew University.

Bergenholtz, J., & Wagner, N. (1996). *Formation of AOT/Brine Multilamellar Vesicles.* American Chemical Society.

Betterelli Giuliano, C., Cvjetan, N., Ayache, J., & Walde, P. (2020). *Multivesicular Vesicles: Preparation and Applications.* European Chemical Societies Publishing.

Bohr, A., Colombo, S., & Jensen, H. (2018). *Future of microfluidics in research and in the market.* Copenhagen: University of Copenhagen.

Byun, C., Abi-Samra, K., & Cho, Y.-K. (2013). *Pumps for microfluidic cell culture.* Electrophoresis.

Carugo, D., Bottaro, E., Owen, J., Stride, E., & Nastruzzi, C. (2016). Liposome production by microfluidics: potential and limiting factors. Nature Communications.

Chen, C., Mehl, B., Munshi, A., Townsend, A., Spence, D., & Martin, R. (2016). *3D-printed Microfluidic Devices: Fabrication, Advantages and Limitations—a Mini Review.* Anal Methods.

Christoffersson , J., & Mandenius, C.-F. (2019). *Fabrication of a Microfluidic Cell Culture Device Using Photolithographic and Soft Lithographic Techniques.* Linköping: Linköping University.

Danckwerts, P. V. (1952). *The definition and measurement of some characteristics of mixtures.* Applied Scientific Research.

Donath, A., Kantzas, A., & Bryant, S. (2019). *Opportunities for Particles and Particle Suspensions to Experience Enhanced Transport in Porous Media: A Review.* Transport in Porous Media.

Giraldo, K. A., Bermudez, J. S., Torres, C. E., & al., &. (2021). *Microfluidics for Multiphase Mixing and Liposomal Encapsulation of Nanobioconjugates: Passive vs. Acoustic Systems.* Bogota: Universidad de Los Andes.

Gregoriadis, G. (1995). *Engineering liposomes for drug delivery: progress and problems.* London: University of London.

Isanin, N., Rozenberg, O., Shcherbakov, L., & Kh, K. (1984). *Comparative organ distribution of various sizes of liposomes during their intravenous administration.* PMID: 6710935.

Jahn, A., Stavis, S. M., Hong, J. S., & al., &. (2010). *Microfluidic Mixing and the Formation of Nanoscale Lipid Vesicles.* American Chemical Society.

Lasic, D. (1992). Liposomes. Sigma Xi, The Scientific Research Honor Society.

Lasic, D. (1996). *Introduction On the History of Liposomes.* CRC Press.

Lee, C.-Y., Wang, W.-T., Liu, C.-C., & Fu, L.-M. (2016). *Passive mixers in microfluidic systems: A review.* Pingtung: National Pingtung University of Science and Technology.

Lin, L., & Chung , C.-K. (2021). *PDMS Microfabrication and Design for Microfluidics and Sustainable Energy Application.* Tainan: National Cheng Kung University.

Lombardo, D., & Kiselev, M. (2022). *Methods of Liposomes Preparation: Formation and Control Factors of Versatile Nanocarriers for Biomedical and Nanomedicine Application.*

Lopez, R. R., Ocampo, I., Sánchez, L.-M., & al., &. (2020). *Surface Response Based Modeling of Liposome Characteristics in a Periodic Disturbance Mixer.* Montreal.

Losey, M. W., Jackman, R. J., Firebaugh, S. L., Schmidt, M. A., & Jensen, K. (2002). *Design and fabrication of microfluidic devices for multiphase mixing and reaction.* Journal of Microelectromechanical Systems.

Malecha, Z., & Malecha, K. (2014). *Numerical Analysis Of Mixing Under Low And High Frequency Pulsations At Serpentine Micromixers.* Chemical and Process Engineering.

Michelon, M., Bernardes Oliveira, D., de Figueiredo Furtado, G., Gaziola de la Torre, L., & Lopes Cunha, R. (2017). *High-throughput continuous production of liposomes using hydrodynamic flow-focusing microfluidic devices.* University of Campinas.

Moscho, A., Chiu, D., & Zare, R. (1996). *Rapid preparation of giant unilamellar vesicles.* Stanford University.

Nsairat, H., Khater, D., Sayed, U., Odeh, F., Al Bawab, A., & Alshaer, W. (2022). Liposomes: structure, composition, types, and clinical applications. Amman: Elsevier Ltd.

Pandey, H., Rani, R., & Agarwal , V. (2016). *Liposome and Their Applications in Cancer Therapy.* Sam Higginbottom Institute of Agriculture Technology & Sciences.

Patil, Y. P., & Jadhav, S. (2014). Novel methods for liposome preparation. Mumbai: Elsevier Ireland Ltd.

Rawal, M., Singh, A., & Amiji, M. (2019). *Quality-by-Design Concepts to Improve Nanotechnology-Based Drug Development.* Pharmaceutical Research.

Ruben Salazar, R. (2020). *Controlled Liposome Production using Micromixers Based on Dean Flow Dynamics.* Montreal: École de Technologie Supérieure Université du Québec.

Samad, A., Sultana, Y., & Aqil, M. (2007). Liposomal Drug Delivery Systems: An Update Review. Bentham Science Publishers.

Sanket, S., Dhawan, V., Holm, R., & Perrie, Y. (2020). *Liposomes: Advancements and innovation in the manufacturing process.* Bombay College of Pharmacy.

Sharma, A., & Sharma, U. S. (1997). Liposomes in Drug Delivery: Progress and Limitations. Buffalo: Elsevier Ireland Ltd.

Tao, J., Chow, S., & Zheng, Y. (2018). *Application of Flash Nanoprecipitation to Fabricate Poorly Water-soluble Drug Nanoparticles.* Acta Pharmaceutica Sinica.

Tseng, W.-C., & Huang, L. (1998). *Liposome-based gene therapy.* Pittsburgh: University of Pittsburgh School of Medicine.

Vatankhah, P., & Shamloo, A. (2018). *Parametric study on mixing process in an in-plane spiral micromixer utilizing chaotic advection.* Analytica Chimica Acta.

Weeks JC, C. P. (2012). *Patients' expectations about effects of chemotherapy for advanced cancer.* PMID: 23094723.

Yanar, F., Mosayyebi, A., Nastruzzi, C., Carugo, D., & Zhang, X. (2020). *Continuous-Flow Production of Liposomes with a Millireactor under Varying Fluidic Conditions.* Pharmaceutics.

Yu, B., Lee , R., & Lee, L. (2009). *Microfluidic Methods for Production of Liposomes.* Columbus: The Ohio State University.

APPENDIX

Appendix 1: Liposomes Observed under TEM Microscopy

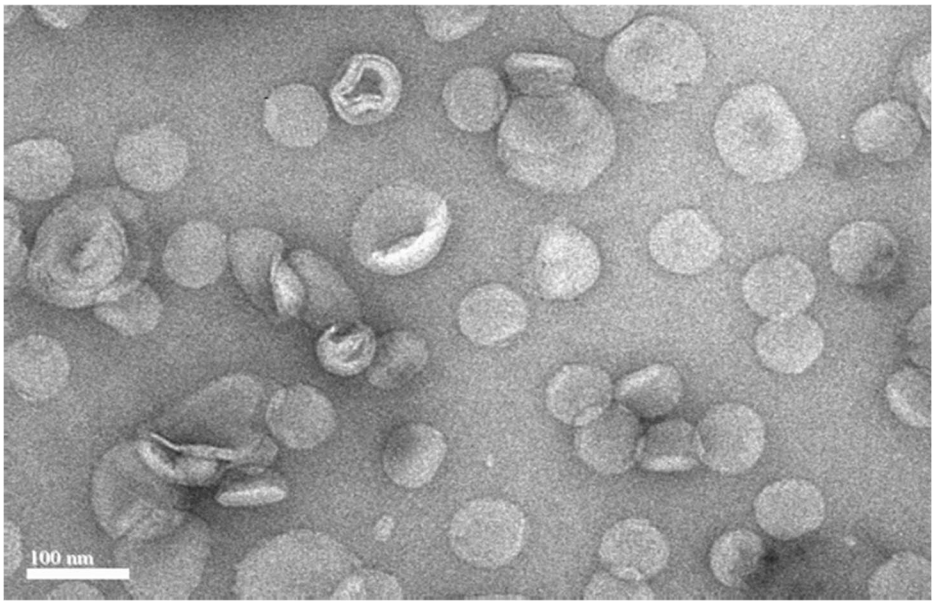

This image was taken from the reference work (Ruben Salazar, 2020).

Appendix 2: Mixing Efficiency Calculated in Reference Work

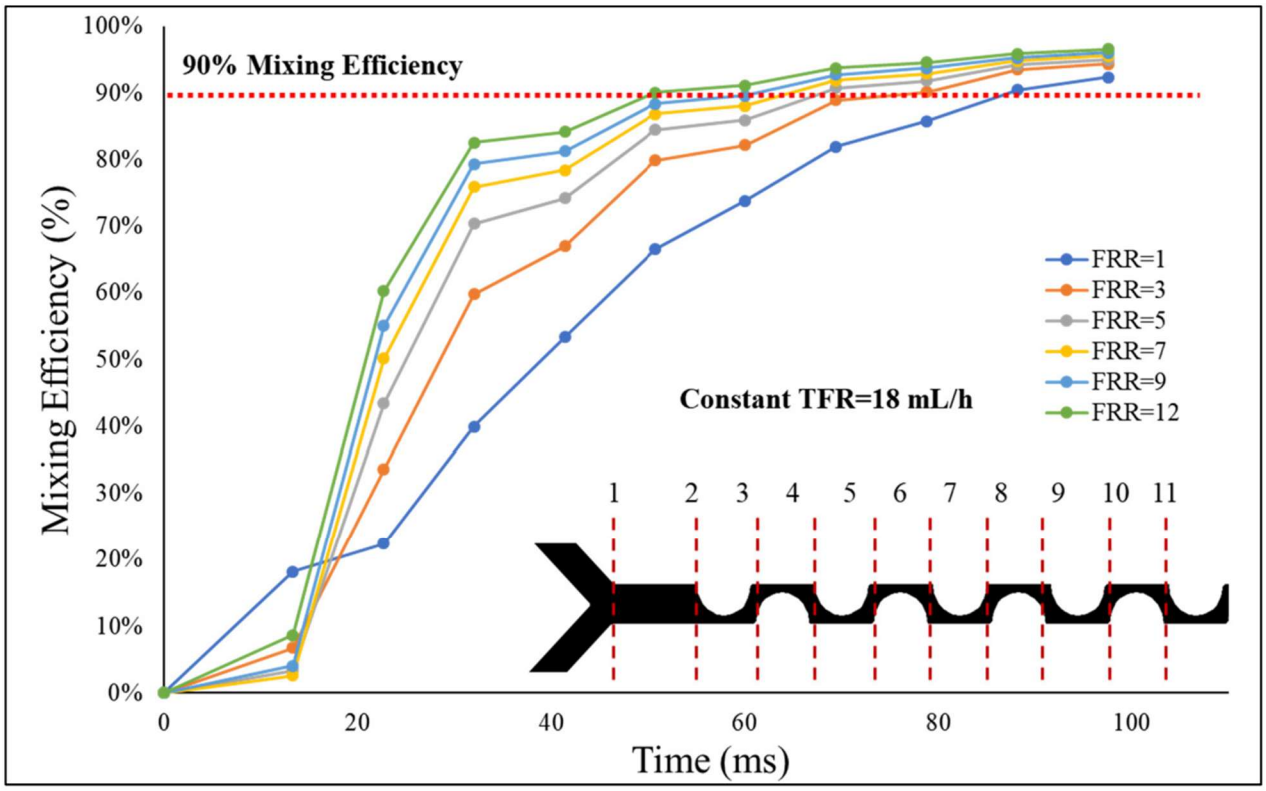

Appendix 3: Dynamic Light Scattering